Appendix 1

M. Rebei, A. Mahun, Z. Walterová, O. Trhlíková, R. K. Donato, H. Beneš, VOC-free tricomponent reaction platform for epoxy network formation mediated by a recyclable ionic liquid, *Polym. Chem.,* 13 (2022) 5380–5388.

Polymer Chemistry

ROYAL SOCIETY OF CHEMISTRY

PAPER

View Article Online
View Journal | View Issue

Cite this: *Polym. Chem.*, 2022, **13**, 5380

VOC-free tricomponent reaction platform for epoxy network formation mediated by a recyclable ionic liquid†

Marwa Rebei,[a] Andrii Mahun,[a] Zuzana Walterová,[a] Olga Trhlíková,[a] Ricardo K. Donato *[a,b] and Hynek Beneš *[a]

Herein we propose a simple, volatile organic solvent (VOC)-free tricomponent reaction platform for the stoichiometric step-growth polymerization between diepoxy resins and dicarboxylic acid in an imidazolium IL medium. The established epoxy resin diglycidyl ether of bisphenol A (DGEBA), as well as the bio-based diglycidyl ether of methyl hydroquinone (DGEMHQ), were used as epoxy sources, while bio-sourced succinic acid was used as the binding building block in this reaction platform performed under mild conditions (T = 80–120 °C). Moreover, no co-solvents, co-catalysts or conventional polymerization initiators were used in our platform as the IL acted as both solvent and initiator/catalyst, and as no direct residue was produced, this concept fully complies with most of the 12 principles of green chemistry. In addition, post-reaction IL-recyclability was studied to further prove the sustainability and cost-effectivity of this platform. The ring-opening of DGEBA and DGEMHQ was followed by FTIR analysis and confirmed with NMR, showing a full consumption of the oxirane ring within 3 to 5 h of reaction. Also, MALDI-TOF mass spectrometry was used for the detection of the intermediates formed in different reaction steps to define the initiation mechanism. Finally, crosslinking and network structure of the optimized solid epoxy materials were characterized using dynamic-mechanical and thermogravimetric analysis.

Received 8th August 2022,
Accepted 19th August 2022

DOI: 10.1039/d2py01031c

rsc.li/polymers

Introduction

Epoxy thermosets find applications in many industrial fields such as coatings, electronics, and composites due to their excellent thermo-mechanical properties, reduced flammability, and good resistance to chemical and environmental degradation.[1–6] Ring opening of epoxides proceeds *via* two different types of mechanism: an electrophilic attack on the oxirane ring oxygen atom or a nucleophilic attack on its carbon atom.[7] However, the molecules used for this task are usually limited to a handful and predominated by nitrogen compounds such as polyamines, polyamides, and polycarbamides.[8,9] Consequently, even the efforts to obtain bio-based alternatives to crosslinkers are highly focused on this class of compounds.[10]

A more sustainable alternative to this issue is the use of crosslinkers based on functional groups such as carboxylates and alcohols, as they are amongst the most abundant groups in nature.[11–13] This vastly increases the access to alternative bio-based monomers as polymer building blocks. However, due to their low reactivity/selectivity, they mostly rely on high temperature and moisture-sensitive processes such as polycondensation.[14] Nevertheless, acidic compounds have been recognized as curing agents/crosslinkers for many commercial resins, such as Bisphenol A diglycidyl ether (DGEBA), and other natural-based epoxies resins,[15–17] but they still rely on the application of catalysts such as organometallic compounds,[16] triethyl benzyl ammonium chloride[4] and other amine-based compounds,[13,18,19] especially imidazole-based compounds.[20,21] However, besides the many technical issues of applying catalysts on an industrial scale, most of these petroleum-based catalysts/hardeners are effective only at high temperatures and have many serious environmental issues associated with their disposal.[3,15]

In this context, ionic liquids (ILs) are effective multifunctional additives for epoxy materials, bringing together their excellent physicochemical properties, such as low flammability, negligible vapour pressure, low melting temperature, and low viscosity, and their tuneable property upon changing the anion/cation combinations.[22,23] Moreover, some ILs are "green solvents", used as a medium for polymerization reactions, as

[a]*Institute of Macromolecular Chemistry, Czech Academy of Sciences, Heyrovského nám. 2, Prague 6, 162 06, Czech Republic. E-mail: benesh@imc.cas.cz*
[b]*National University of Singapore, Center for Advanced 2D Materials, Singapore 117546, Singapore. E-mail: donato@nus.edu.sg*

†Electronic supplementary information (ESI) available. See DOI: https://doi.org/10.1039/d2py01031c

polymer plasticizers, or as stabilizing agents ensuring the miscibility and homogeneity between the epoxy resin and the crosslinker.[24] For the oxirane ring opening, imidazolium[24–26] and phosphonium-based[27,28] ILs were found to be the most promising. They are used in epoxy homopolymerisation without an external curing agent,[29] working as latent hardeners[24] and crosslinking the epoxy network even in complex systems such as ternary mixtures with thermoplastic polymers.[30]

Moreover, we have recently demonstrated that carboxylic acid-functionalized imidazolium ILs have a self-catalytic behaviour, allowing fast and selective reaction with epoxy groups under mild conditions.[31]

More importantly, in the same study, we have also noticed that this catalytical behaviour is present both when the carboxylic group is within the IL structure (referred to as intramolecular mechanism) or with an exogenous carboxylic source (referred to as intermolecular mechanism).[31] Considering that in this work we exploit in detail the latter intermolecular mechanism for a tricomponent epoxy resin/dicarboxylic acid/IL system. Due to the abundance of bio-sourced carboxylic acids and epoxy resins and the vast number of combinations of components allowed by this platform, we believe it presents a unique approach to producing epoxy materials with adaptable properties driven by specific application requirements. This reaction platform uses imidazolium IL (1-butyl-3-methylimidazolium chloride) as an all-in-one (solvent, initiator/catalyst and compatibilizer) reaction media for the step-growth of copolymers based on epoxy and carboxylic acid building blocks. As a proof-of-concept, we investigate the curing reaction of both petroleum-based and vanillin-based epoxy resins with a natural-based dicarboxylic acid (succinic acid) in the presence of imidazolium-based ILs. Moreover, this platform allows IL's recycling, further improving its sustainability and cost-effectiveness.

Experimental

Materials and methods

Bisphenol A diglycidyl ether is noted as DGEBA (D.E.R 332, Dow Chemical Company, 357 g mol^{-1}) with an epoxy equivalent weight of 179 g mol^{-1}. Succinic acid (118.09 g mol^{-1}) and activated charcoal were purchased from Sigma Aldrich and used as received. The IL 1-butyl-3-methylimidazolium chloride (99%, Iolitech, 174.67 g mol^{-1}) is purified using the active charcoal method described in the literature 32 and is measured by ^{1}H NMR to check its purity (see ESI, Fig. S1†). 1-Butyl-3-methylimidazolium bis(trifluoromethylsulfonyl) imide (419.36 g mol^{-1}) and 1-butyl-3-methylimidazolium methanesulfonate (234.32 g mol^{-1}) were purchased from Sigma Aldrich and used without further treatment. For the synthesis of the bio-based epoxy, 2-methoxyhydroquinone (97%, Alfa aesar, 140.14 g mol^{-1}), triethyl benzyl ammonium chloride (TEBAC, 99%, Aldrich, 227.77 g mol^{-1}), and epichlorohydrin (Aldrich, 92.52 g mol^{-1}) were used as received.

Fourier transmission infrared spectroscopy (FTIR) measurements of the obtained samples were performed using a Spectrum 100 spectrometer (PerkinElmer) equipped with a mercury–cadmium–telluride (MCT) detector and universal ATR (attenuated total reflectance) accessory with a diamond prism. The spectra were averaged over 32 scans with a selected resolution of 4 cm^{-1}. The disappearance of the peak at 915 cm^{-1} is followed during the reaction as it is attributed to the C–O stretching of the oxirane group.[31] The quantification of the progress of the polymerization reaction is calculated using the area of the epoxy band at 915 cm^{-1} related to the area of the reference band at 1507 cm^{-1}, attributed to the aromatic ring 34. The conversion of the epoxy group is calculated according to the following equation[35,36]

$$\alpha(\%) = [(A_0 - A_t)/A_0] \times 100 \quad (1)$$

where A_0 is the area ratio ($A915/A1507$) at curing time t = 0 h and A_t is the area ratio ($A915/A1507$) at the curing time t.

Matrix-assisted laser desorption ionization-time of flight (MALDI-TOF) mass spectra were obtained with an UltrafleXtreme (Bruker Daltonics, Bremen, Germany) in the positive ion reflectron mode. The spectra were the sum of 25 000 shots with a DPSS, Nd:YAG laser (355 nm, 2000 Hz). Delayed extraction and external calibration were used. The samples were prepared by the dried droplet method: solutions of the sample (10 mg mL^{-1}) and DHB (2,5-dihydroxybenzoic acid; Sigma–Aldrich, 98%, 20 mg mL^{-1}) as a matrix in DMSO (methyl sulfoxide, Sigma–Aldrich, spectrophotometric grade, 99.9%) were mixed in the volume ratio 4 : 20. 1 μL of the mixture was deposited on the ground-steel target plate. The drop was dried in an ambient atmosphere.

Nuclear Magnetic Resonance (NMR) ^{1}H and ^{13}C NMR spectra were recorded using Bruker Avance III 600 spectrometer operating at 600.2 MHz for ^{1}H and 150.9 MHz for ^{13}C. All samples were dissolved in DMSO-d_6 at 295 K. ^{1}H NMR spectra were acquired by applying a 90° pulse (width = 18 μs) with a 10 s recycle delay and 32 scans. For recording ^{13}C NMR spectra, 14 μs 90° pulse was used with 10 s recycle delay and 7168 scans. High-power proton decoupling (inverse-gated mode) was used for removing ^{1}H–^{13}C interactions. The chemical shifts are relative to TMS using hexamethyldisiloxane (HMDSO, 0.05 ppm from TMS in ^{1}H spectra, and 2.0 ppm from TMS in ^{13}C spectra) as an internal standard.

Dynamic-mechanical and thermal analysis (DMTA) of the cured epoxy samples was measured on an ARES G2 rheometer (TA Instruments). The temperature dependence of complex shear modulus (G^*) was determined on rectangular samples (20 × 10 × 2 mm) using oscillatory shear deformation (0.1% strain) at 1 Hz frequency from 0 °C to 200 °C at a temperature ramp rate of 3 °C min^{-1}. The main transition temperature (T_α) was determined as the tan δ peak maximum.

Thermogravimetric analysis (TGA) was carried out with a thermogravimetric analyzer Pyris 1 TGA (PerkinElmer). A sample of *ca.* 5 mg was heated from 30 °C to 600 °C at a heating rate of 10 °C min^{-1} in nitrogen flow (25 cm^3 min^{-1}).

Synthesis of bio-based epoxy resin (DGEMHQ)

The 2,2′-[(2-methoxy-1,4-phenylene)bis(oxymethylene)]bis (oxirane) (DGEMHQ) was synthesized following the method mentioned in the literature with few adaptations.[33] The epoxy equivalent weight of DGEMHQ is determined to be 153.51 g mol^{-1}, with a yield of reaction of 84.24%. The details of the synthesis of DGEMHQ, as well as its FTIR, ^{1}H and ^{13}C NMR spectra that confirmed the formation of functional groups in the final product, are described in ESI (Fig. S2–S4†). The bio-based epoxy monomer was also analysed by GC/MS and structures present in the monomer are shown in ESI (Fig. S5†).

Curing of epoxy resins

The chemical structures of epoxy resins (DGEBA and DGEMHQ), ILs and dicarboxylic acid used in this work are summarized in Fig. 1a. First, succinic acid (SA) and IL were mixed for 30 min at 80 °C under an N_2 atmosphere. After SA solubilization, epoxy resin (DGEBA or DGEMHQ) was added to the mixture (the reaction beginning). Immediately after adding the epoxy resin, a biphasic mixture was formed. The mixing/reaction steps of the tricomponent system DGEBA/SA/BMImCl are shown in Fig. 1b. The molar ratios of epoxy resin/SA/IL = 1/1/1.6 was considered ideal for the reaction as they were based on the solubility limits of both the epoxy resin and dicarboxylic acid towards BMImCl, and the avoidance of gel formation at the reaction temperature.

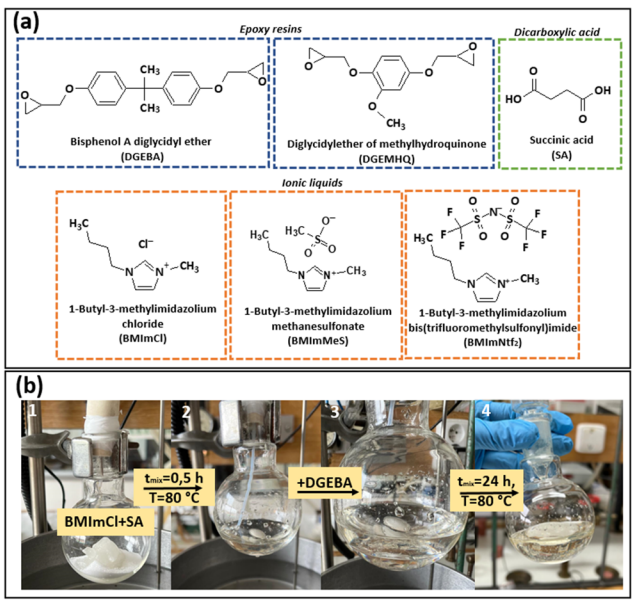

Fig. 1 (a) Chemical structures of epoxy resins, ILs, and dicarboxylic acid used in this work. (b) Experimental steps of the tricomponent DGEBA/SA/BMImCl system. These steps prove the homogeneity of the system due to the addition of BMImCl, which acts here as the solvent. It is important to mention that the transparent homogeneous mixture is already formed after *ca.* 10 min of mixing of all components at 80 °C (photo not shown here). The final product (the mixture after 24 h, photo 4) looks visually similar to the mixture after *ca.* 10 min but has a much higher viscosity and a gel-like structure.

Ionic liquid recycling

The IL-recycling from the mixture DGEBA/SA/BMImCl, after the step-growth reaction, was performed to better understand the system's sustainability and cost-effectiveness. A large-scale DGEBA/SA/BMImCl reaction is performed, where 12 g of BMImCl is mixed with 5 g of SA and 14.31 g of DGEBA for 24 h under an N_2 atmosphere, producing 31.05 g of product (Fig. 1b). After 24 h, the reaction mixture was diluted with distilled water under ultrasound to better solubilize the IL. Then, the mixture was subjected to filtration and the solution containing water and BMImCl is dried in a rotary evaporator under a vacuum. A transparent yellowish viscous liquid was obtained and characterized by FTIR and ^{1}H NMR to confirm the purity of the recycled BMImCl.

Results and discussion

Previously, we have described in detail the self-catalytic reaction mechanism for Brønsted-acidic ILs and monofunctional epoxide groups under solvent-free and mild conditions.[31] Besides observing a robust reaction of these ILs with epoxides *via* intramolecular catalysis, since the IL was bearing both a reacting group (carboxylate) and the catalyst/initiator (cation and anion), this reaction also occurred *via* an intermolecular approach (reactant and catalyst/initiator in different molecules).[31] Thus, here we exploit this intermolecular mechanism using difunctional epoxide and dicarboxylic acid, allowing for polymerization and/or crosslinking reactions and following both the evolution of the epoxide ring-opening and the step-growth mechanism between epoxides and carboxylic acids.

Epoxide ring-opening mechanism investigation

Initially, bicomponent systems, DGEBA/SA (IL-free, Fig. 2, route 1) and DGEBA/BMImCl (dicarboxylic acid-free, Fig. 2, route 2) are performed to study individual roles of dicarboxylic acid and ILs during the epoxy polymerization. The FTIR spectra of the DGEBA/SA mixture show the presence of the epoxy band (at 915 cm^{-1})[34,37] even after 24 h of heating at 80 °C (Fig. 2, route 1) which proves that SA alone is not able to react with DGEBA under such mild conditions without a catalyst. This complies with the literature that shows that the epoxy/acid reaction is mainly initiated by amines, imidazole, pyridine derivatives, or organic catalysts at temperatures above 80 °C.[38–40]

In contrast, the DGEBA/BMImCl system (without SA, Fig. 2, route 2) shows a colour change from transparent yellow to dark red during heating at 80 °C, which indicates the increase in aromaticity and average molecular weight.[41] Slight consumption of epoxy groups is confirmed *via* FTIR (Fig. 2, route 2) for system DGEBA/BMImCl. Also, the formation of carbonyl groups C=O is confirmed (band at 1738 cm^{-1}, Fig. S6†) and is related to the epoxy ring-opening and formation of ether groups initiated by BMImCl.[24,26,42] The carbonyl group formation during the epoxy/imidazolium IL reaction has been previously demonstrated as the result of the imidazolium rings

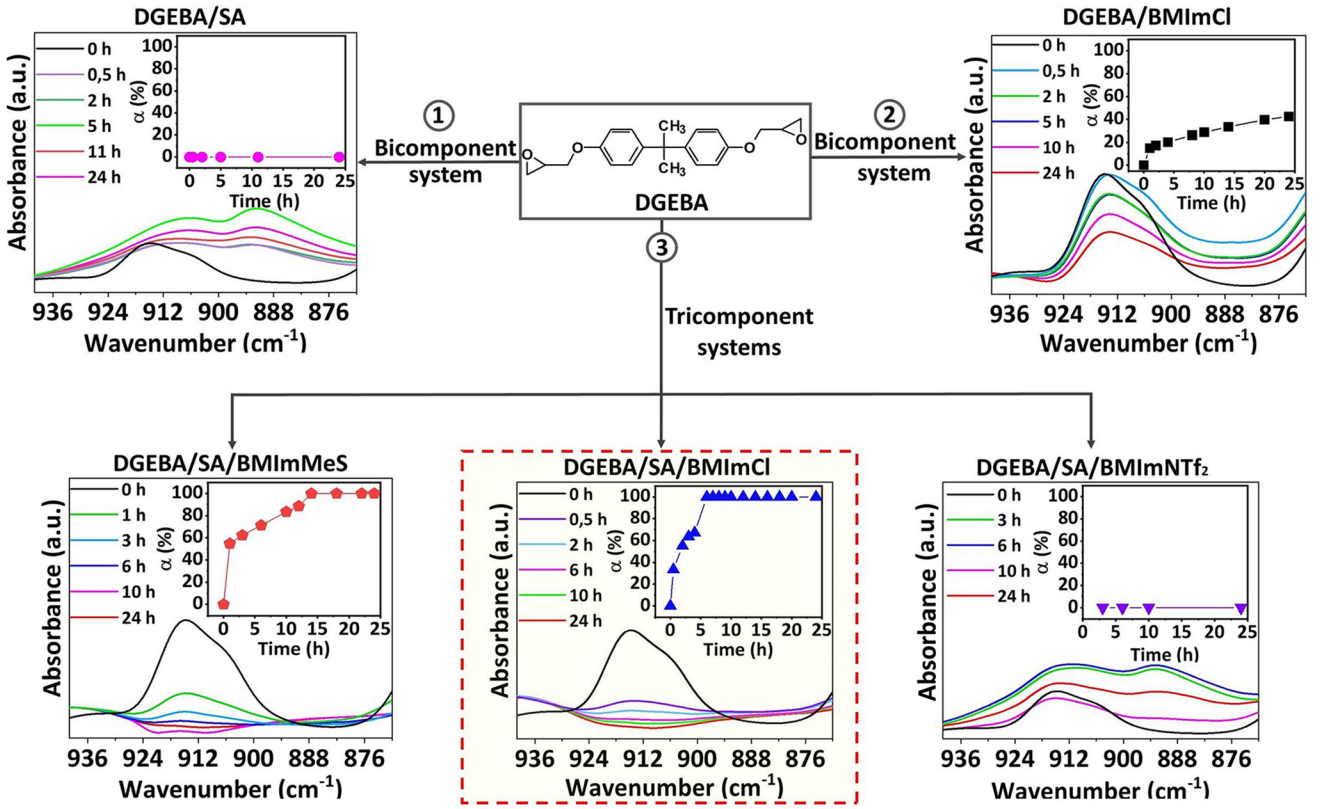

Fig. 2 FTIR spectra of the epoxy band and its conversion (α) *versus* time (inset graphs) for bicomponent DGEBA/SA (routes 1) and DGEBA/BMImCl (route 2) systems, and tricomponent DGEBA/SA/BMImMeS, DGEBA/SA/BMImCl, and DGEBA/SA/BMImNTf$_2$ systems (route 3). The whole FTIR spectra of all systems are available in ESI.†

Hoffmann elimination from the newly formed polymer chain.[26,42] Under the mild conditions investigated, the rate of homopolymerization is very slow, showing an epoxy ring consumption below 50% after 24 h (Fig. 2, route 2).

On the other hand, the tricomponent system (DGEBA/SA/BMImCl) shows a homogeneous transparent mixture and a fast epoxy ring-opening, proven by the complete disappearance of the epoxy band at 915 cm^{-1} within 5 h of reaction (Fig. 2, route 3, DGEBA/SA/BMImCl) and by the appearance of ester stretching vibrational band at 1730 cm^{-1} (Fig. S7†). Thus, herein BMImCl has a triple role as (i) initiator of the dicarboxylic acid/epoxy ring reaction, (ii) solvent for SA and (iii) compatibility agent of DGEBA/SA. Moreover, the ^{1}H NMR spectra confirm the FTIR results showing a gradual disappearance of the epoxy ring signals (signal 1 at 2.68 ppm, 2.82 ppm and signal 2 at 3.29 ppm) in the DGEBA/SA/BMImCl system at 80 °C reaching the complete epoxy ring conversion into esters in *ca.* 5 h (Fig. 4c). This tricomponent reaction platform was also tested with adipic acid showing the fast epoxy ring-opening and ester group formation (Fig. S8†). The similar reaction progress of the tricomponent systems with SA and adipic acid demonstrates the universality of this approach.

Since we previously observed that the IL-anions play a major role in the epoxy ring-opening mechanism,[31] three tricomponent systems DGEBA/SA/IL with different ILs based on their anion basicity and coordination strength, (BMImNTf$_2$, BMImMeS and BMImCl) are compared (Fig. 2, route 3).

The use of BMImNTf$_2$ leads to a non-homogeneous mixture without evidence of epoxy ring-opening (see Fig. 2, route 3, DGEBA/SA/BMImNTf$_2$) and no ester bond formation (Fig. S9†). The NTf$_2^-$ anion is considered a weak base, however, it acts as a poor nucleophile in our tricomponent system, probably due to the anion bulkiness and, consequently, a steric hindrance that disables the epoxide ring-opening.[26,31,43] Differently, DGEBA/SA/BMImMeS produces a homogeneous and transparent mixture with defined epoxy ring-opening and ester formation as indicated by the FTIR spectra (Fig. S10†). This system shows a complete epoxy conversion after *ca.* 13 h of reaction at 80 °C, indicating a slower reaction compared to the DGEBA/SA/BMImCl (100% of epoxy conversion after 5 h) (Fig. 2, route 3, see conversion curves insets for DGEBA/SA/BMImMeS and DGEBA/SA/BMImCl). Although the reactivity of IL anions is strongly dependent on many factors such as the reaction medium and temperature,[24,31,44,45] our results indicate that the anion is directly involved in the mechanism of these tricomponent reactions, where the Cl$^-$ anion shows the best catalytic effect.

For this reason, DGEBA/SA/BMImCl was investigated in greater depth, willing to unveil its mechanism. Accordingly,

the MALDI-TOF mass spectrum of the DGEBA/SA/BMImCl system after 24 h reaction at 80 °C (Fig. 3a) shows the formation of three distributions of molecular ions (sodium adducts), which present the same mass increment of 458 Da corresponding to the DGEBA-SA repeating unit, and two different types of end-groups (COOH and Cl-opened epoxides, Fig. 3b). Furthermore, the MALDI-TOF mass spectrometry evidence the presence of a monomeric DGEBA-derived structure with two terminal Cl-opened epoxy rings (the violet diamond marked structure of m/z = 434, Fig. 3b). The end-group analysis enables us to investigate the initiation mechanism of epoxy ring-opening induced by IL in the presence of SA.

Three IL-based routes of initiation of the epoxy ring-opening are well-described in the literature: carbene formation, imidazolium decomposition and counter-ion route (anion nucleophilic attack).[26] At the reaction conditions of this study, no direct effect of the imidazolium cation, related to its decomposition, is observed. This can be stated based on the ^{1}H NMR spectrum signals 10 and 9 (Fig. 4a, at 9.34 and 3.86 ppm, respectively), which do not show any change in the imidazolium ring related to its deprotonation or dealkylation during the reaction. Moreover, no intermediates containing the imidazolium ring were detected by MALDI-TOF. This hypothesis is also corroborated by many previous studies showing that carbene formation and imidazolium ring dealky-

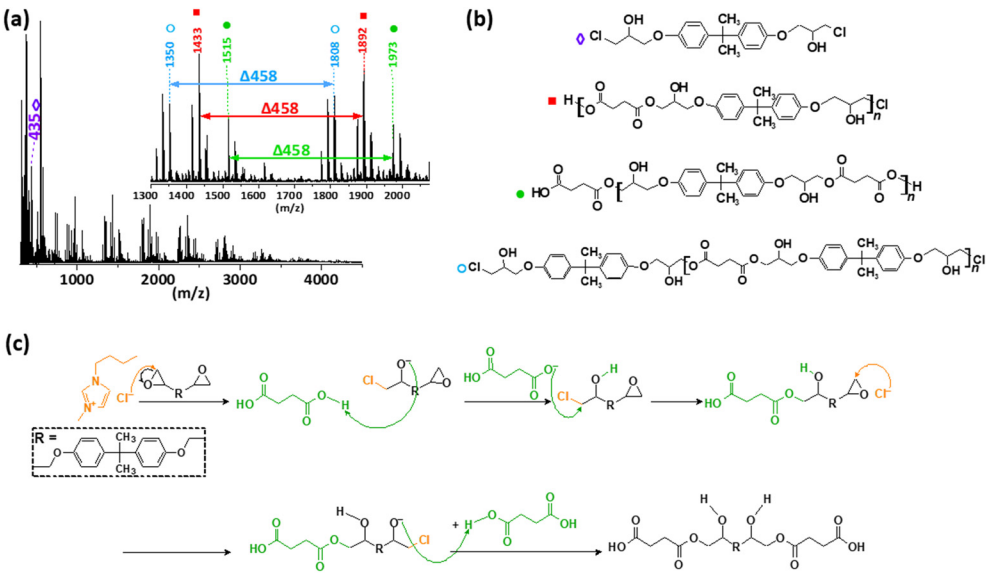

Fig. 3 (a) MALDI-TOF spectra of DGEBA/SA/BMImCl after 24 h, (b) structures detected in MALDI-TOF of DGEBA/SA/BMImCl and (c) the main reaction pathway proposed for DGEBA/SA/BMImCl showing linear SA-DGEBA polymer chain formation *via* BMImCl-initiated acid-epoxy addition.

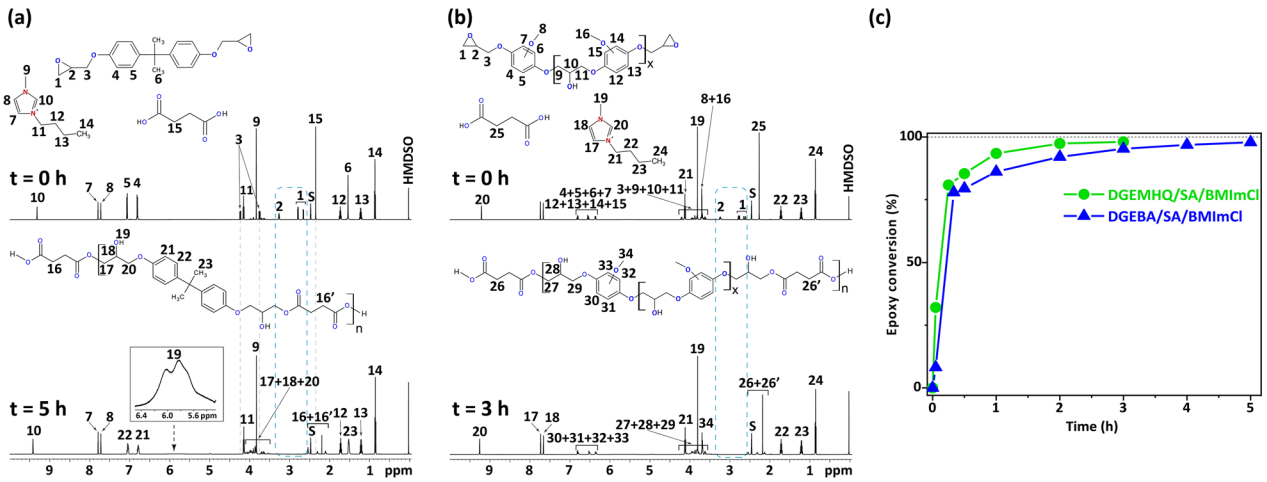

Fig. 4 (a) ^{1}H NMR of DGEBA/SA/BMImCl at t = 0 h and after full epoxy consumption (t = 5 h), (b) ^{1}H NMR of DGEMHQ/SA/BMImCl at t = 0 h and after full epoxy consumption (t = 3 h), and (c) epoxy conversion *versus* time calculated from NMR for both systems.

lation only occur at much higher temperatures and require specific conditions.[26]

Based on the aforementioned, the main reaction in the tricomponent DGEBA/SA/BMImCl system is proposed as the polyaddition of epoxy resin and dicarboxylic acid (Fig. 3c),[46] which is initiated by a nucleophilic attack of the IL-anion.[26,31] Herein, the chloride anion of BMImCl attacks the less hindered carbon of the oxirane ring (Fig. 3c). At the same time, the epoxy ring is activated by the acidic proton from SA. Then, a subsequent nucleophilic attack of SA-anion on the carbon associated with Cl is performed releasing Cl^-, which becomes available for the next epoxy ring-opening initiation, forming a tandem reaction system. The initiator (Cl^-) thus remains chemically bound only during the ring-opening process and then the carboxylic acid is attached to the DGEBA structure backbone, obtaining an alternating linear SA–DGEBA–SA structure (the green circle marked distribution, at m/z = 599 in Fig. 3b). This mechanism proves our concept that SA works as a binding building block.

Since a reliable protocol was established for DGEBA/SA/BMImCl, it was further tested using a bio-based epoxy resin (DGEMHQ). Accordingly, the DGEMHQ/SA/BMImCl system was prepared and reacted at 80 °C. The ring opening in this system is detected by FTIR, as evidenced by the total consumption of the epoxy band (915 cm^{-1}) within 3 h and the formation of ester groups (1730 cm^{-1}, Fig. S11†).[16,47] Also, a broad band at around 3300 cm^{-1} attributed to the OH groups is formed as a result of the oxirane ring-opening during the reaction between SA and DGEMHQ (Fig. S11†).[48]

The ^{1}H NMR also evidences the epoxy ring-opening in DGEMHQ/SA/BMImCl, where signal 1 at 2.68 ppm, 2.82 ppm and signal 2 at 3.29 ppm (Fig. 4b) vanish after 3 h of reaction. The signals from the imidazolium ring remain unchanged during the reaction (signals 19 and 20, at 3.86 ppm and 9.28 ppm, respectively, in Fig. 4b) proving that the initiation mechanism does not involve the IL cation. This is in accordance with the mechanistic study of the DGEBA/SA/BMImCl system showing an epoxy initiation mechanism *via* IL chloride anion (Fig. 3c). It is worth mentioning that in this system the initial monomer DGEMHQ is slightly oligomerized, which is indicated by the presence of the group of ^{1}H NMR signals around 4 ppm (signals 9, 10 and 11 in Fig. 4b).[49] Epoxy conversion calculated from the ^{1}H NMR spectra shows a similar trend for both systems, DGEBA/SA/BMImCl (100% at *ca.* 5 h) and DGEMHQ/SA/BMImCl (100% at *ca.* 3 h) (Fig. 4c).

Ionic liquid recycling

Subsequently, we investigated the recyclability of BMImCl using a very mild and simple approach, consisting of the direct extraction with distilled water. The IL recovery reaches 79% (details are in the Experimental section), which is correlated to the free (non-bonded) IL. The remaining 21% is physically bonded IL plasticizing the epoxy network formed. The FTIR spectrum of the recycled BMImCl (Fig. 5a) shows consistently all the characteristic bands related to the imidazolium ring at 1568 cm^{-1}, C–N stretching vibration at 1169 cm^{-1} and

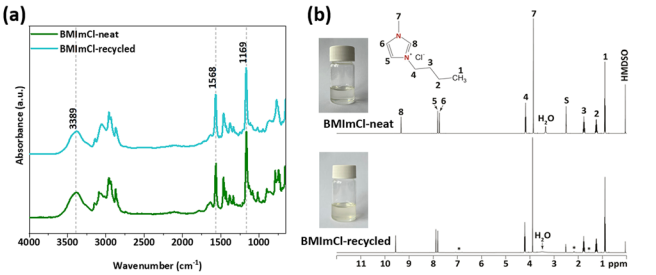

Fig. 5 (a) FTIR and (b) ^{1}H NMR spectra of the neat and recycled BMImCl. Insets show the photos of the neat and recycled BMImCl. The traces of impurities (residuals from the reaction mixture) are denoted by an asterisk (*).

the broad band at 3389 cm^{-1} attributed to quaternary amine salt with chloride.[50] The peak assignment of IL signals in the ^{1}H NMR spectrum of the recycled BMImCl is nearly identical to the neat BMImCl (Fig. 5b) and is also in great consistency with the literature[51,52] revealing that BMImCl remains unaltered during the reaction and recovery processes.

Optimized epoxy networks

As demonstrated above, this platform only works properly as a tricomponent (epoxy resin/dicarboxylic acid/IL) system that, on one hand, demands enough IL (as a solvent/compatibilizer) for proper interaction between epoxy and dicarboxylic acid and, on the other hand, as little IL as possible (as an initiator) to avoid reducing the final molecular weight of the step-growth reaction products.[53] Therefore, our next effort was to understand the influence of the reduced amount of IL in the tricomponent system, to reach an optimized process that is more suitable for scaling up.

The IL content was gradually reduced, reaching an optimum epoxy resin/dicarboxylic acid/IL molar ratio of 1/1/0.2 (8 times less IL than in the initial system). This IL content is the lowest possible for obtaining a homogeneous system and keeping a sufficiently fast reaction. The progress of the epoxy-acid addition for DGEBA/SA/BMImCl at this optimized ratio was followed by FTIR, showing epoxy ring-opening along with ester formation at a slower rate than in system DGEBA/SA/BMImCl (1/1/1.6) (Fig. S12†).

The products of DGEBA/SA/BMImCl and DGEMHQ/SA/BMImCl at the optimized molar ratio (1/1/0.2) tricomponent systems, were submitted to a post-curing process (120 °C, 48 h) yielding solid and optically homogeneous materials (Fig. 6a); *i.e.* ones that can be used in applications such as cast systems and encapsulants for electronics, composites, protective coatings, *etc.*, replacing traditional epoxides.[12] The FTIR spectra of DGEBA/SA/BMImCl and DGEMHQ/SA/BMImCl solid products confirm the complete reaction (Fig. 6b). The DMTA results of both materials (Fig. 6c) display the shape of storage modulus (G') curve typical for thermoset materials with a visible rubbery plateau, slightly increasing with the temperature indicating the formation of covalent networks. The crosslinking mechanism is most probably related to the presence of secondary

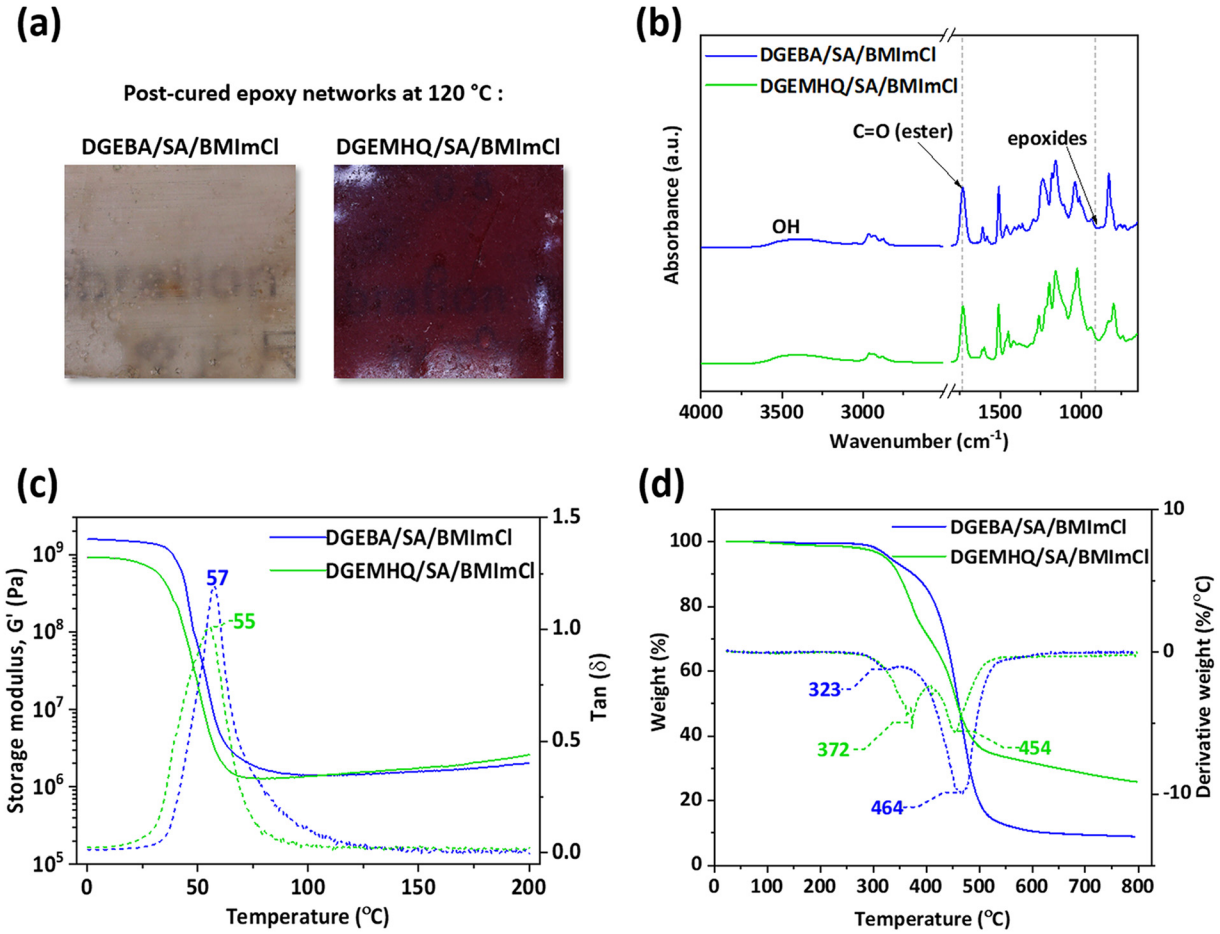

Fig. 6 (a) Photos, (b) FTIR spectra, (c) DMTA results and (d) TGA results of post-cured tricomponent DGEBA/SA/BMImCl and DGEMHQ/SA/BMImCl systems.

hydroxyl groups formed during the acid-epoxy addition reaction (Fig. 3c).

These hydroxyl groups are capable of further reacting (i) with SA *via* condensation forming ester linkages or (ii) with epoxides promoting epoxy ring opening and formation of ether linkages or (iii) with ester bonds *via* transesterification.[44,54,55]

Both systems at the glassy state show the high G' values which are typical for epoxy materials (Fig. 6c).[56] Upon heating, the transition from glassy to a rubbery state is clearly visible from the steep G' drop when the temperature reaches *ca.* 45 °C. The main transition temperature (T_α) is clearly observed and determined as the tan δ curves maximum; both materials exhibit one T_α at 57 °C (DGEBA/SA/BMImCl) and 55 °C (DGEMHQ/SA/BMImCl). Similar T_α and G' values at the rubber state of both materials signify similar rigidity and crosslink density, which also means that, when using our IL-based tricomponent platform, the bio-based epoxide is a competitive sustainable alternative to petrochemical-based epoxides.

The TGA results (Fig. 6d) show that both post-cured epoxides are thermally stable up to *ca.* 250 °C with $T_{d5\%}$ of 331 °C (DGEBA/SA/BMImCl) and 324 °C (DGEMHQ/SA/BMImCl). This agrees with previously reported epoxy/IL systems,[27,44,57] showing that the addition of dicarboxylic acids does not compromise the good thermal stability of the systems. The thermal stability of our samples is also comparable to classical high-performance amine cured-epoxy materials.[48,58] The TGA results further reveal a similar two-stage decomposition of both materials (Fig. 6d), which is typical for crosslinked epoxy materials.[13,44] The first loss is connected with the decomposition of residual IL (BMImCl)[59] and weak bonds (herein ester groups) in epoxides,[13] while the second weight loss comprises thermal degradation and pyrolysis of the remaining material. A char yield (at 790 °C) was much higher for DGEMHQ/SA/BMImCl (25 wt%) compared to DGEBA/SA/BMImCl (9 wt%) due to the high content of aromatic species from DGEMHQ, which are graphitized during TGA in a nitrogen atmosphere. These results are promising for potential use in flame retardancy applications.[60]

Conclusions

Our VOC-free, one-pot tricomponent reaction platform with a recyclable IL-medium based on the epoxy resin (DGEBA or

DGEMHQ), succinic acid and imidazolium IL, and performed in temperatures as low as 80 °C, successfully delivers (in gram scale) competitive sustainable alternatives to classical epoxy systems. After testing different ILs (BMImCl, BMImMeS, and BMImNtf$_2$) in the DGEBA/SA/IL reaction, the IL-anion (Cl^-, MeS^-, or NTf_2^-) strongly affects the progress of the reaction, where Cl^- yielded the best results by reaching 100% of epoxides conversion in only 5 h. The nucleophilic attack of the IL-anion on the epoxy group was identified as the initiation mechanism of this tandem reaction, where the dicarboxylic acid forms an α-hydroxy ester bond with epoxy and acts as a binding building block. Moreover, IL plays a triple role as solvent, compatibilizer and initiator and, due to its high solvation strength, allows functional reactions in molar ratios as low as 10 mol% (*i.e.* epoxy/dicarboxylic acid/IL = 1/1/0.2) while also presenting recyclability rate up to 79% (for epoxy/dicarboxylic acid/IL = 1/1/1.6).

Our model systems (DGEBA/SA/BMImCl and DGEMHQ/SA/BMImCl) yielded soft transparent solids that can be post-cured into sturdy translucent solid materials with T_α and G' values similar to some classical cured epoxy resins (T_α = 55–57 °C, G'_{glass} ~ 1 GPa and $G'_{rubbery}$ ~ 2 MPa), and outstanding thermal stability ($T_{d5\%}$ ~ 330 °C and T_{dmax} above 400 °C).

Altogether, besides the intrinsically increased sustainability of this platform presented by the aforementioned mild reaction conditions, VOC-free character and IL-recyclability, it also allows replacing the classical petroleum-based epoxies with bio-based ones.

Another added advantage is the use of multifunctional carboxylic acid binding building blocks that allow vast system variations by applying these bio-based precursors due to their abundance in nature. We believe it will be a very useful platform for manufacturing the products of the fast-growing bio-based epoxy resin market, estimated to reach USD 220.1 million by the year 2027.[61] Moreover, this reaction platform produces epoxy materials bearing β-hydroxyl esters, which might be adapted as dynamic ester crosslinks for the design of reprocessable epoxy vitrimers.[56] This approach will be further elaborated in our next paper.

Author contributions

Marwa Rebei contributed to the project conceptualization, performed all the experiments and wrote the paper. Andrii Mahun performed and interpreted the NMR data. Zuzana Walterová and Olga Trhlíková performed and interpreted the mass spectrometry data. Ricardo K. Donato and Hynek Beneš conceptualized and supervised the project, and supported the writing and editing of the paper.

Conflicts of interest

There are no conflicts to declare.

Acknowledgements

We gratefully acknowledge financial support from the Czech Science Foundation (project no. 22-05244S).

References

1 F. C. Binks, G. Cavalli, M. Henningsen, B. J. Howlin and I. Hamerton, *Polymer*, 2018, **150**, 318–325.
2 M. Döring and U. Arnold, *Polym. Int.*, 2009, **58**, 976–988.
3 Y. J. Woo and D. S. Kim, *J. Therm. Anal. Calorim.*, 2021, **144**, 119–126.
4 F. Mustata and N. Tudorachi, *J. Therm. Anal. Calorim.*, 2016, **125**, 97–110.
5 E. Duemichen, M. Javdanitehran, M. Erdmann, V. Trappe, H. Sturm, U. Braun and G. Ziegmann, *Thermochim. Acta*, 2015, **616**, 49–60.
6 H. R. Khalafi, M. Ehsani and H. A. Khonakdar, *Polym. Adv. Technol.*, 2021, **32**, 1251–1261.
7 W. R. Ashcroef, in *Chemistry and Technology of Epoxy Resins*, ed. B. Ellis, Chapman and Hali, UK, 1st edn, 1993, ch. 2, pp. 37–70.
8 W. Wang, G. Zhou, B. Yu and M. Peng, *Composites, Part B*, 2020, **197**, 108044.
9 S. Yu, W. Lee, B. Seo and C. S. Lim, *Polymers*, 2018, **10**, 782.
10 C. Ding and A. S. Matharu, *ACS Sustainable Chem. Eng.*, 2014, **2**, 2217–2236.
11 R. K. Donato and A. Mija, *Polymers*, 2020, **12**, 1–64.
12 S. Ma and D. C. Webster, *Macromolecules*, 2015, **48**, 7127–7137.
13 C. Ding, P. S. Shuttleworth, S. Makin, J. H. Clark and A. S. Matharu, *Green Chem.*, 2015, **17**, 4000–4008.
14 A. Jäger, R. K. Donato, M. Perchacz, K. Z. Donato, Z. Starý, R. Konefał, M. Serkis-Rodzeń, M. G. Raucci, A. M. Fuentefria and E. Jäger, *J. Mater. Chem. B*, 2020, **8**, 9980–9996.
15 S. K. Sahoo, V. Khandelwal and G. Manik, *Polym. Adv. Technol.*, 2018, **29**, 2080–2090.
16 A. Li and K. Li, *ACS Sustainable Chem. Eng.*, 2014, **2**, 2090–2096.
17 J. M. Morancho, X. Ramis, X. Fernández-Francos, O. Konuray, J. M. Salla and À. Serra, *J. Therm. Anal. Calorim.*, 2020, **142**, 607–615.
18 J. D. McCoy, W. B. Ancipink, C. M. Clarkson, J. M. Kropka, M. C. Celina, N. H. Giron, L. Hailesilassie and N. Fredj, *Polymer*, 2016, **105**, 243–254.
19 R. T. Zeng, Y. Wu, Y. D. Li, M. Wang and J. B. Zeng, *Polym. Test.*, 2017, **57**, 281–287.
20 F. I. Altuna, C. E. Hoppe and R. J. J. Williams, *RSC Adv.*, 2016, **6**, 88647–88655.
21 F. F. Wong, C. M. Lin, K. L. Chen, Y. H. Shen and J. J. Huang, *Macromol. Res.*, 2010, **18**, 324–330.
22 Y. Yin, M. Liu, W. Wei, C. Zheng, J. Gao, W. Zhang, C. Zheng, P. Deng and Y. Xing, *J. Adhes. Sci. Technol.*, 2018, **32**, 1114–1127.

23 S. A. Prikhod'ko, A. Y. Shabalin, V. V. Bardin, I. V. Eltsov, I. K. Shundrina, V. N. Parmon and N. Y. Adonin, *RSC Adv.*, 2017, **7**, 17497–17504.
24 H. Maka, T. Spychaj and R. Pilawka, *Ind. Eng. Chem. Res.*, 2012, **51**, 5197–5206.
25 H. Mąka, T. Spychaj and K. Kowalczyk, *J. Appl. Polym. Sci.*, 2014, **131**, 40401.
26 F. C. Binks, G. Cavalli, M. Henningsen, B. J. Howlin and I. Hamerton, *Polymer*, 2018, **139**, 163–176.
27 T. K. L. Nguyen, S. Livi, B. G. Soares, H. Benes, J. F. Gérard and J. Duchet-Rumeau, *ACS Sustainable Chem. Eng.*, 2017, **5**, 1153–1164.
28 H. Mąka, T. Spychaj and R. Pilawka, *eXPRESS Polym. Lett.*, 2014, **8**, 723–732.
29 B. G. Soares, S. Livi, J. Duchet-Rumeau and J. F. Gerard, *Macromol. Mater. Eng.*, 2011, **296**, 826–834.
30 N. Halawani, R. K. Donato, H. Benes, J. Brus, L. Kobera, S. Pruvost, J. Duchet-Rumeau, J. F. Gérard and S. Livi, *Polymer*, 2021, **218**, 1–11.
31 M. Perchacz, L. Matějka, R. Konefał, L. Seixas, S. Livi, J. Baudoux, H. Beneš and R. K. Donato, *ACS Sustainable Chem. Eng.*, 2019, **7**, 19050–19061.
32 P. Nockemann, K. Binnemans and K. Driesen, *Chem. Phys. Lett.*, 2005, **415**, 131–136.
33 S. Nikafshar, O. Zabihi, S. Hamidi, Y. Moradi, S. Barzegar, M. Ahmadi and M. Naebe, *RSC Adv.*, 2017, **7**, 8694–8701.
34 M. G. González, J. C. Cabanelas and J. Baselga, in *Infrared Spectroscopy - Materials Science, Engineering and Technology*, ed. T. Theophanides, InTech, Croatia, 2012, ch. 13, pp. 261–284.
35 A. A. Silva, S. Livi, D. B. Netto, B. G. Soares, J. Duchet and J. F. Gérard, *Polymer*, 2013, **54**, 2123–2129.
36 M. Leclère, S. Livi, M. Maréchal, L. Picard and J. Duchet-Rumeau, *RSC Adv.*, 2016, **6**, 56193–56204.
37 N. Poisson, G. Lachenal and H. Sautereau, *Vib. Spectrosc.*, 1996, **12**, 237–247.
38 L. Matějka, S. Pokomý and K. Dušek, *Polym. Bull.*, 1982, **7**, 123–128.
39 W. J. Blank, Z. A. He and M. Picci, *J. Chem. Inf. Model.*, 2003, **53**, 1689–1699.
40 Q. A. Poutrel, J. J. Blaker, C. Soutis, F. Tournilhac and M. Gresil, *Polym. Chem.*, 2020, **11**, 5327–5338.
41 F. C. Binks, G. Cavalli, M. Henningsen, B. J. Howlin and I. Hamerton, *React. Funct. Polym.*, 2018, **133**, 9–20.
42 A. P. A. Carvalho, D. F. Santos and B. G. Soares, *J. Appl. Polym. Sci.*, 2020, **137**, 1–11.
43 B. C. Ranu and S. Banerjee, *J. Org. Chem.*, 2005, **70**(11), 4517–4519.
44 S. Livi, C. Chardin, L. C. Lins, N. Halawani, S. Pruvost, J. Duchet-Rumeau, J. F. Gérard and J. Baudoux, *ACS Sustainable Chem. Eng.*, 2019, **7**, 3602–3613.
45 M. S. Fedoseev, M. S. Gruzdev and L. F. Derzhavinskaya, *Int. J. Polym. Sci.*, 2014, 607341_1–607341_8.
46 L. Matějka, S. Pokornj and K. Dušek, *Makromol. Chem.*, 1985, **186**, 2025–2036.
47 R. Tadros and D. C. Timm, *Macromolecules*, 1995, **28**, 7441–7446.
48 F. Mustata, N. Tudorachi and I. Bicu, *J. Anal. Appl. Pyrolysis*, 2015, **112**, 180–191.
49 F. G. Garcia and B. G. Soares, *Polym. Test.*, 2003, **22**, 51–57.
50 S. A. Dharaskar, M. N. Varma, D. Z. Shende, C. K. Yoo and K. L. Wasewar, *Sci. World J.*, 2013, 395274_1–395274_9.
51 H. Wang, Z. Li, Y. Liu, X. Zhang and S. Zhang, *Green Chem.*, 2009, **11**, 1568–1575.
52 S. K. Singh and A. Singh, *ChemistrySelect*, 2018, **3**, 3570–3574.
53 M. P. Aplan and E. D. Gomez, *Ind. Eng. Chem. Res.*, 2017, **56**, 7888–7901.
54 K. Tangthana-Umrung, Q. A. Poutrel and M. Gresil, *Macromolecules*, 2021, **54**, 8393–8406.
55 E. Fonseca, V. D. da Silva, J. S. Klitzke, H. S. Schrekker and S. C. Amico, *Polym. Test.*, 2020, **87**, 106556.
56 P. G. Falireas, J. M. Thomassin and A. Debuigne, *Eur. Polym. J.*, 2021, **147**, 110296.
57 B. Guenther Soares, S. Livi, J. Duchet-Rumeau and J. F. Gerard, *Polymer*, 2012, **53**, 60–66.
58 K. B. Manning, N. Wyatt, L. Hughes, A. Cook, N. H. Giron, E. Martinez, C. G. Campbell and M. C. Celina, *Macromol. Mater. Eng.*, 2019, **304**, 1–16.
59 A. Efimova, G. Hubrig and P. Schmidt, *Thermochim. Acta*, 2013, **573**, 162–169.
60 M. Zhi, Q. Liu, H. Chen, X. Chen, S. Feng and Y. He, *ACS Omega*, 2019, **4**, 10975–10984.
61 Global Bio-Based Epoxy Resins Market, By Type, By Ingredient, By Form, By Application, By End User, Estimation & Forecast, **https://www.researchandmarkets.com/reports/5574734/global-bio-based-epoxy-market-research-report**, (accessed Feburary 2022).

Supporting Information

VOC-free tricomponent reaction platform for epoxy network formation mediated by a recyclable ionic liquid

Marwa Rebei[a], Andrii Mahun[a], Zuzana Walterová[a], Olga Trhlíková[a], Ricardo K. Donato[a,b,*], Hynek Beneš[a,*]

[a]*Institute of Macromolecular Chemistry, Czech Academy of Sciences, Heyrovského nám. 2, Prague 6, 162 06, Czech Republic*

[b]*National University of Singapore, Center for Advanced 2D Materials, Singapore 117546, Singapore*

*Corresponding authors: Hynek Beneš (benesh@imc.cas.cz), Ricardo K. Donato (donato@nus.edu.sg)

Number of pages: 9

Number of figures: 12

Purification of 1-butyl-3-methylimidazolium chloride

The active carbon (5 w%) was added to the IL in presence of dichloromethane to decrease the viscosity of the mixture. The mixture was stirred for 24 h, then filtered and was left to dry at room temperature. The solvent was removed under vacuum. After, the ionic liquid was put in a freezer overnight for crystallization. The structure and purity of IL was confirmed by ^{1}H NMR (600 MHz - DMSO-d_6 - Fig. S1), δ 9.33 (s, 1H), 7.81 (t, J = 1.76 Hz, 1H), 7.74 (t, J = 1.73 Hz, 1H), 4.18 (t, J = 7.17 Hz, 2H), 3.86 (s, 3H), 1.76 (quint, J = 7.26 Hz, 2H), 1.25 (sext, J = 7.6, 2H), 0.89 (t, J = 7.37 Hz, 3H).

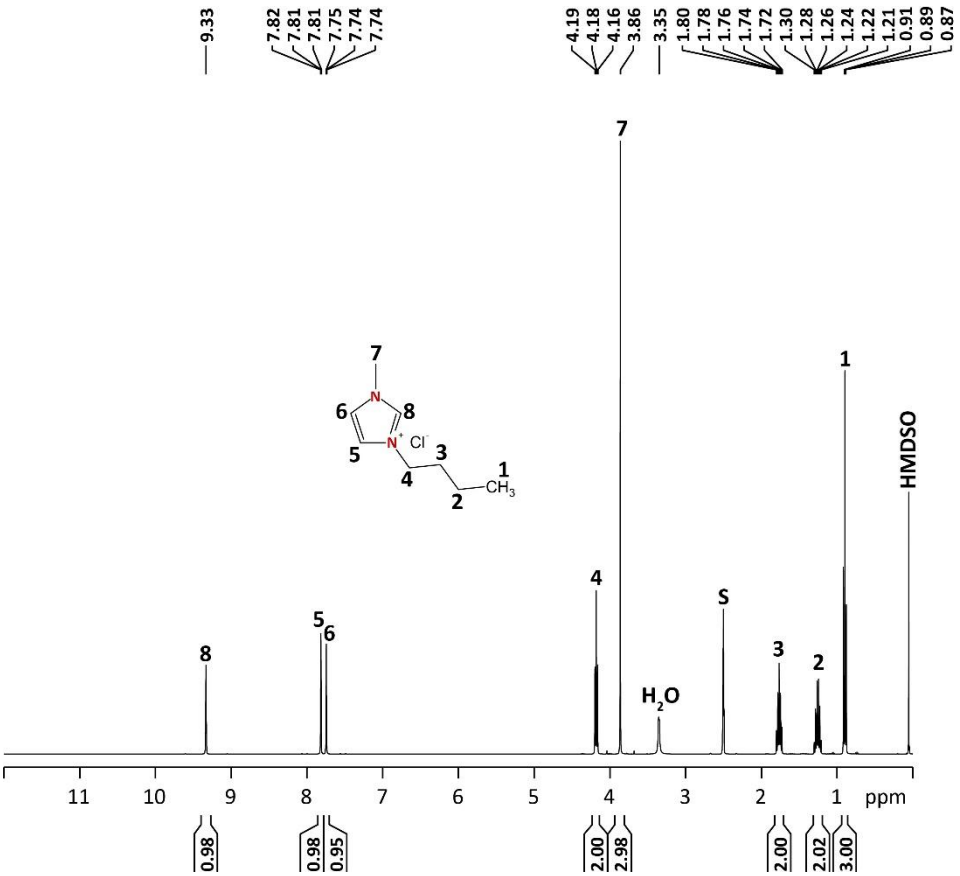

Figure S1: ^{1}H NMR spectra of BMImCl (in DMSO-d_6).

Synthesis of bio-based epoxy resin (DGEMHQ)

The synthesis of bio-based epoxy resin was proceeded as follows: methoxyhydroquinone (1 mol), TEBAC (1 mol) and epichlorohydrin (10 mol), were mixed at room temperature for 1 h and at 80 °C for 30 min. The mixture was then cooled down to room temperature and 266 mL of NaOH solution (5 M) and of TEBAC (0.1 mol) were added to the mixture and it was stirred for 30 min at 25 °C. After, a mixture of ethyl acetate/distilled water was added to the mixture and mixed for 5 min. Then, an extraction was carried out in an aqueous phase with ethyl acetate. The organic phase containing the epoxy resin was rinsed with an aqueous solution of sodium chloride. The excess of ethyl acetate and epichlorohydrin was eliminated by rotary evaporator. The final product was dried overnight under vacuum and measurements as FTIR, ^{1}H and ^{13}C NMR, GC/MS were carried out.

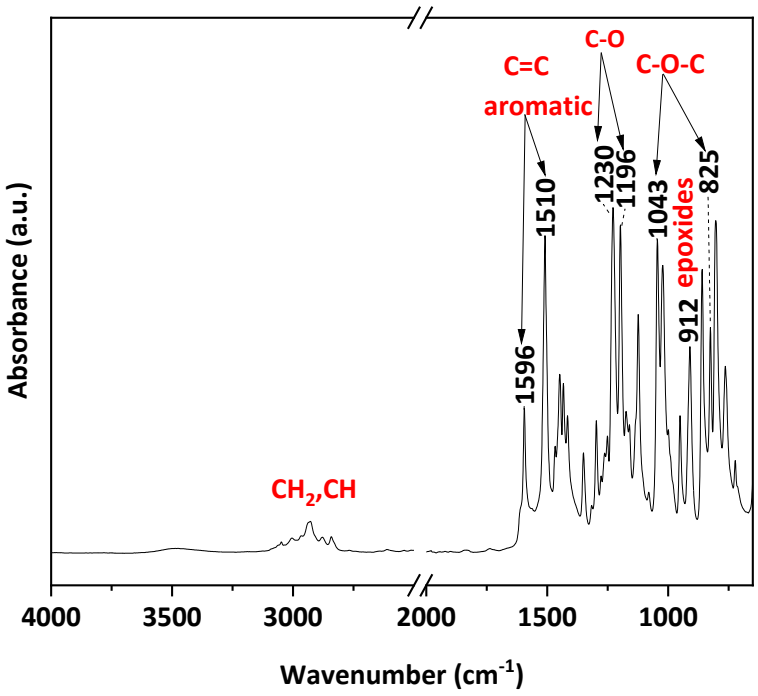

Figure S2. FTIR spectra of bio-based epoxy (DGEMHQ).

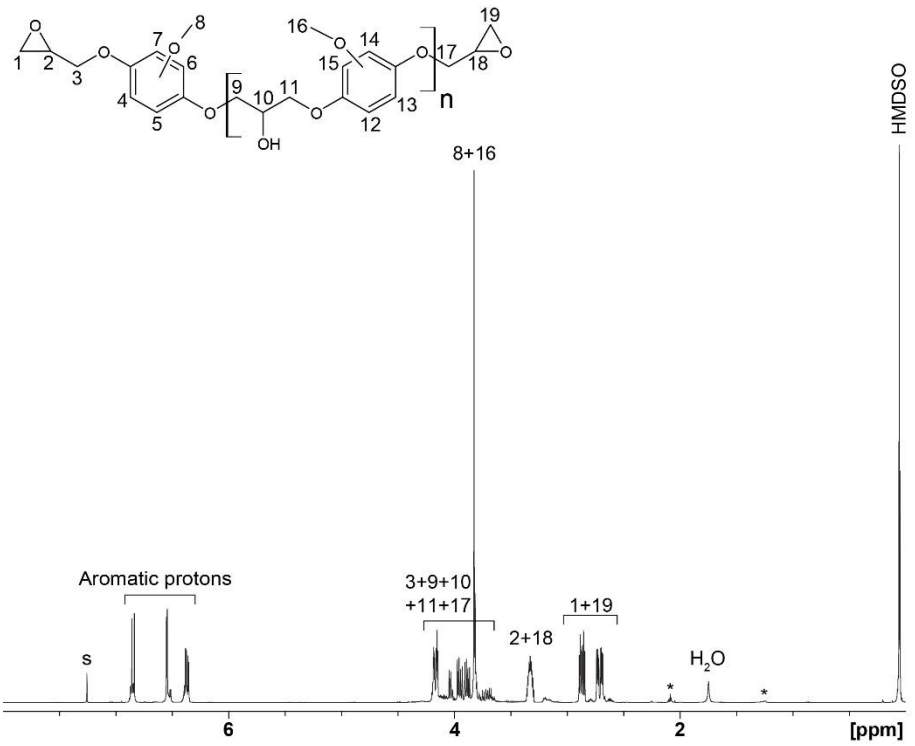

Figure S3. ^{1}H NMR spectra of DGEMHQ. Traces of impurities are denoted by an asterisk (*).

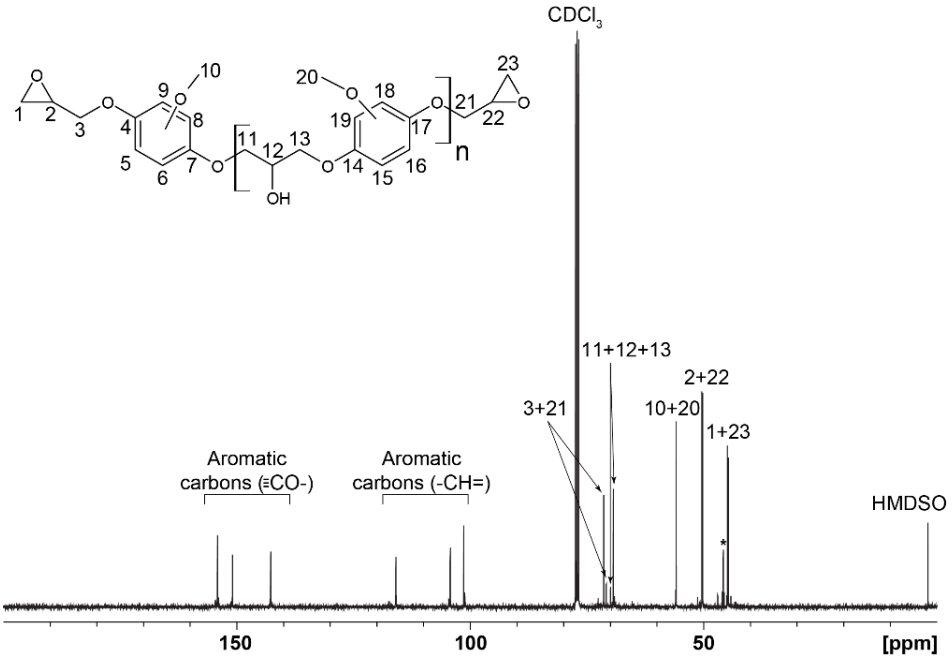

Figure S4. ^{13}C NMR spectra of DGEMHQ. Traces of impurities are denoted by an asterisk (*).

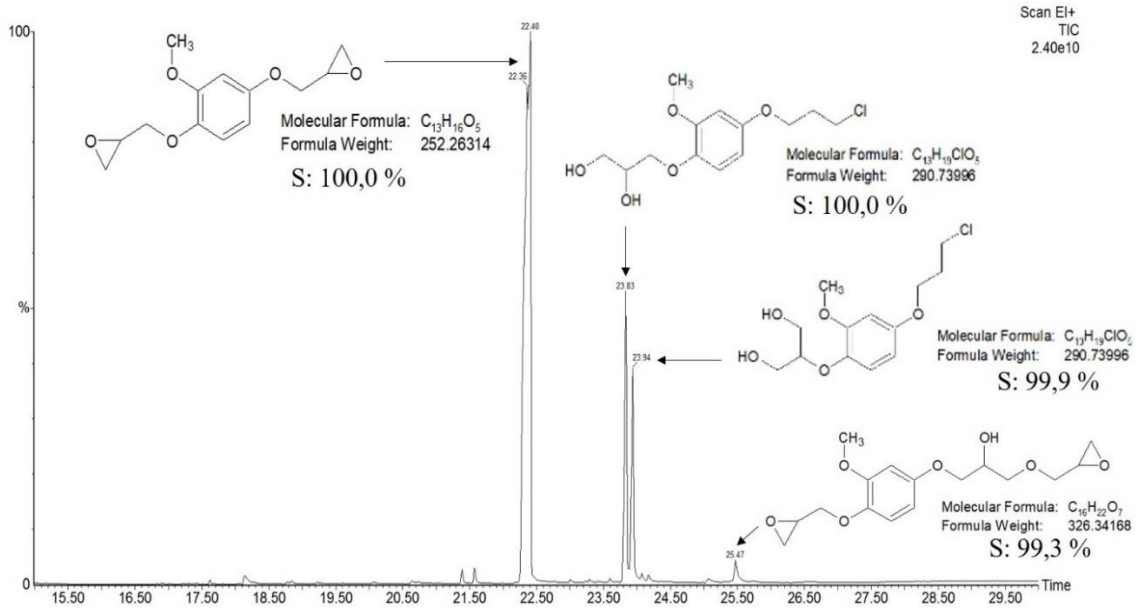

Figure S5. GC/MS spectra of DGEMHQ.

Epoxide ring-opening mechanism investigation

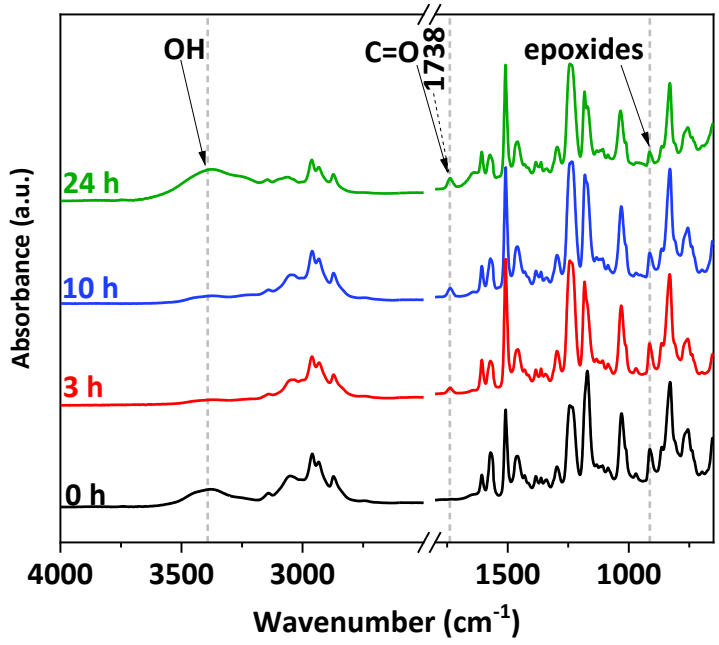

Figure S6. FTIR spectra of system DGEBA/BMImCl (1/1.6) cured at 80 °C.

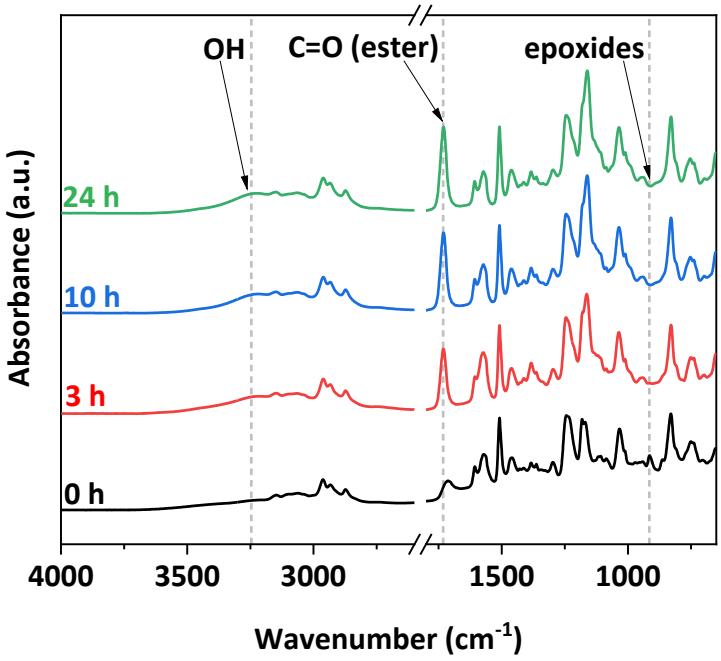

Figure S7. FTIR spectra of system DGEBA/SA/BMImCl (1/1/1.6) cured at 80 °C.

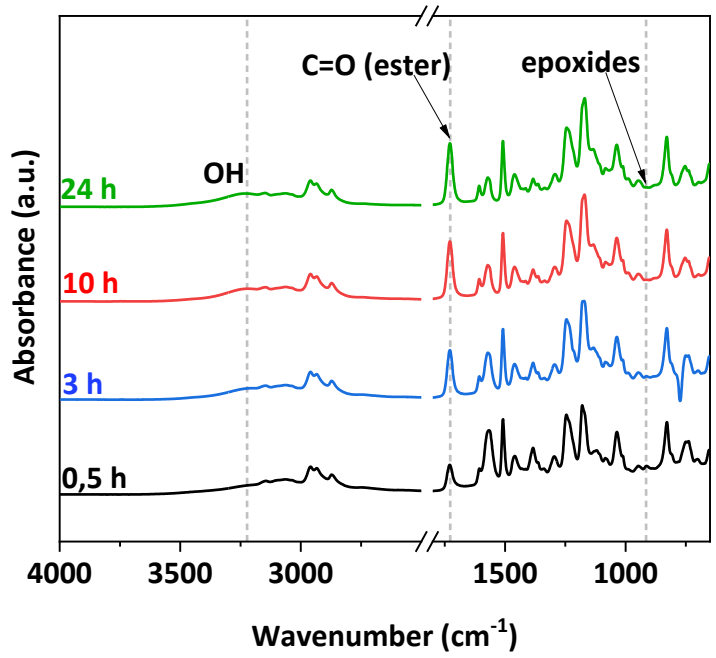

Figure S8. FTIR spectra of system DGEBA/Adipic acid/BMImCl (1/1/1.6) cured at 80 °C.

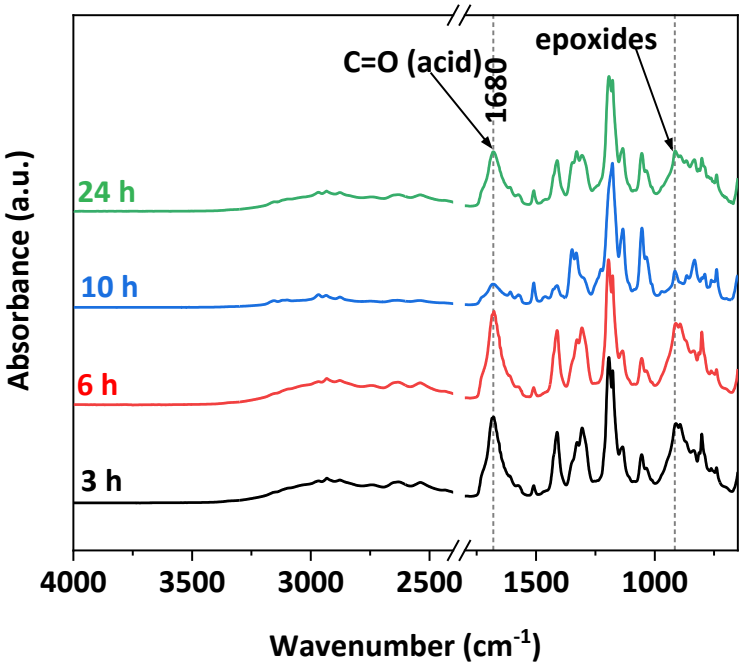

Figure S9. FTIR spectra of system DGEBA/SA/BMImNTf$_2$ (1/1/1.6) cured at 80 °C.

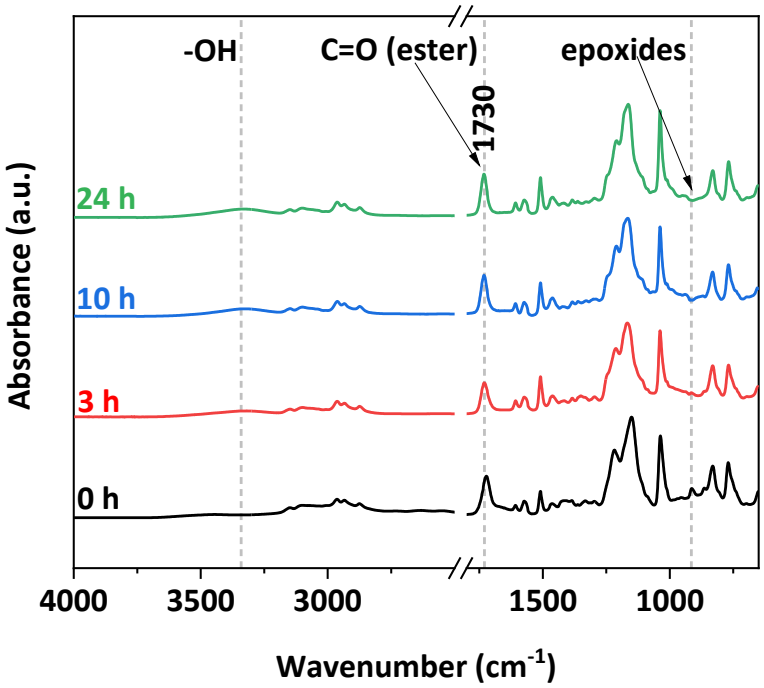

Figure S10. FTIR spectra of system DGEBA/SA/BMImMeS (1/1/1.6) cured at 80 °C.

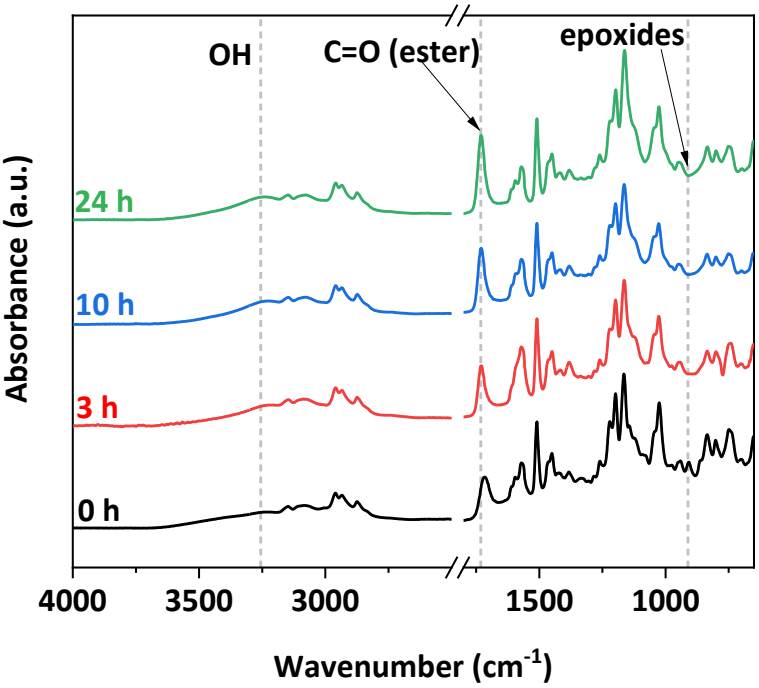

Figure S11. FTIR spectra of system DGEMHQ/SA/BMImCl (1/1/1.6) cured at 80 °C.

Optimized epoxy networks

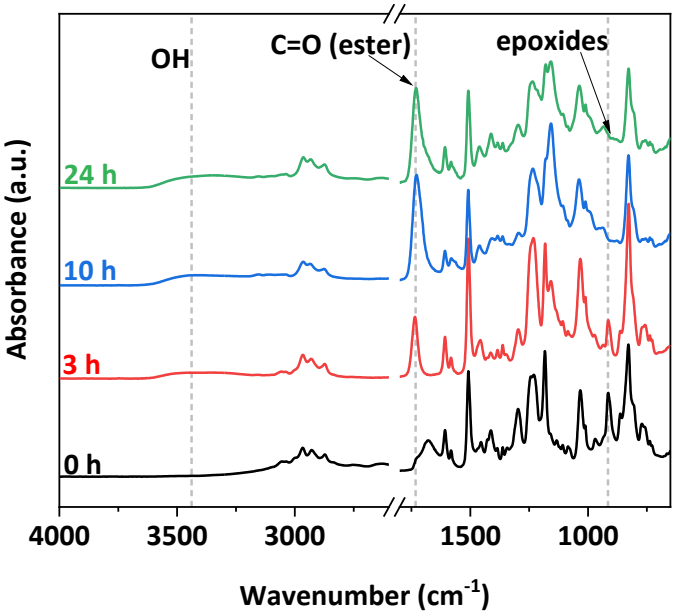

Figure S12. FTIR spectra of system DGEBA/SA/BMImCl (1/1/0.2) cured at 80 °C.

Appendix 2

M. Rebei, O. Kočková, M. Řehák, S. Abbrent, A. Vykydalová, J. Honzíček, P. Ecorchard, H. Beneš. (2024). Accelerating effect of metal ionic liquids for epoxy-anhydride copolymerization. *Eur. Polym. J.*, 212 (2024) 113077.

European Polymer Journal 212 (2024) 113077

Contents lists available at ScienceDirect

European Polymer Journal

journal homepage: www.elsevier.com/locate/europolj

Accelerating effect of metal ionic liquids for epoxy-anhydride copolymerization

Marwa Rebei [a], Olga Kočková [a], Matouš Řehák [c], Sabina Abbrent [a], Anna Vykydalová [b], Jan Honzíček [d], Petra Ecorchard [b], Hynek Beneš [a,*]

[a] Institute of Macromolecular Chemistry, Czech Academy of Sciences, Heyrovského nám. 2, Prague 6 162 06, Czech Republic
[b] Institute of Inorganic Chemistry, Czech Academy of Sciences, Husinec-Řež 1001, 250 68 Řež, Czech Republic
[c] Department of General and Inorganic Chemistry, Faculty of Chemical Technology, University of Pardubice, Studentská 573, 532 10 Pardubice, Czech Republic
[d] Institute of Chemistry and Technology of Macromolecular Materials, Faculty of Chemical Technology, University of Pardubice, Studentská 573, 532 10 Pardubice, Czech Republic

ARTICLE INFO

Keywords:
Ionic liquid
Epoxy resin
Copolymerization
Anhydride
Cross-linking
Kinetics

ABSTRACT

One of the main drawbacks of high-performance epoxy-anhydride thermosets is slow cross-link kinetics requiring high temperature and long curing cycle. Herein, the accelerating effect of imidazolium metal-based ionic liquids (MILs) bearing $(FeCl_4)^-$, $(ZnCl_4)^{2-}$, and $(CoCl_4)^{2-}$ anions on epoxy-anhydride copolymerization was investigated. It was observed that MILs accelerated bisphenol diglycidyl ether (DGEBA) – methylhexahydrophthalic anhydride (MHHPA) cross-linking, better than the reference catalysts (1-methylimidazole and 1-butyl-3-methylimidazolium chloride), especially at low temperatures through their ability to activate a rapid anhydride ring opening and formation of carboxyl groups, which initiates polyesterification. A detailed investigation of the polymerization mechanism revealed the formation of alternating epoxy-anhydride copolymers although several MILs-induced initiation mechanisms were detected. Despite the multiple-initiation consisting of imidazole, counter anion, and polyesterification pathways, the cross-linking kinetics was successfully fitted up to vitrification by the Kamal-Sourour model. Finally, MILs-induced cross-linking leads to homogeneous network build-up enabling to produce thermosetting materials with an increased cross-link density, a glass transition temperature above 150 °C, and excellent thermal stability.

1. Introduction

The alternating copolymerization of epoxides and cyclic anhydrides has always been a promising and bourgeoning area of research [1] due to its capability of providing thermosetting materials exhibiting excellent thermal, mechanical and optical properties which allow production of high-tech engineering materials for electrical and electronic applications and composite matrices for aerospace and transport [2–5]. Unlike other curing agents, anhydride hardeners can provide highly cross-linked epoxy networks exhibiting a high glass transition temperature (T_g), low reaction heat release and reduced shrinkage [2,6]. Nevertheless, the epoxy-anhydride systems suffer from the limitation of being less reactive, requiring high curing temperatures, long curing cycles and associated high energy costs. Therefore, suitable accelerators promoting anhydride ring opening have to be added [5].

The most common accelerators of the epoxy-anhydride reaction are highly reactive tertiary amines [7] and imidazoles [8,9]. In particular, 1-substituted and 1-unsubstituted imidazoles are promising initiators for the anionic alternating copolymerization of epoxides and cyclic anhydrides [10,11]. Short pot life, too high curing temperatures, and low stability are the main drawbacks of imidazole compounds. Therefore, solutions for improving imidazole processability by stabilizing the lone pair of nitrogen atoms are sought. One strategy involves the preparation of metal-imidazole complexes. In particular, zinc and cobalt metals have proven to be efficient anionic initiators for the ring-opening of epoxides, specifically Zn/imidazole complexes $[M(imidazole)_2(anion)_2]$ [12]. Unfortunately, metal-imidazole complexes are mostly crystalline substances with very low solubility in epoxy systems [13]. Thus, the use of a solvent is often required, which limits its applicability due to the release of volatile compounds [14,15]. On the other hand, the use of discrete metal and rare earth metal complexes enables well-controlled polymerization progress, [1] however, their cost and toxicity often limit

* Corresponding author.
E-mail address: benesh@imc.cas.cz (H. Beneš).

https://doi.org/10.1016/j.eurpolymj.2024.113077
Received 19 February 2024; Received in revised form 24 April 2024; Accepted 25 April 2024
Available online 26 April 2024

their widespread use [16].

To overcome the above-mentioned drawbacks, ionic liquids (ILs) have been considered in terms of their use as catalysts to provide a ‘‘greener’’ and solvent-free one-pot reaction medium [17]. ILs are recognized as efficient catalysts/initiators for ring-opening polymerization [18–20]. Their structure combines various cation options (imidazolium, pyridinium, phosphonium, etc.) with a variety of anions (halogens, phosphates, imide, triflate, etc.) [21,22]. Different combinations of cations and anions give rise to the possibility of physical property tuning, resulting in outstanding properties, such as excellent chemical and thermal stability, negligible vapor pressure, and good conductivity [23,24]. Based on this knowledge, ILs are considered promising accelerators for epoxy cross-linking in solvent-free medium [17,25,26].

Recently, a new class of ILs, metal-based ionic liquids (MILs), containing a metal atom in the IL anion, has been explored [27]. Typical MILs are composed of $[MX_4]^{2-}$ anions, where M can consist of various metals, e.g. Zn, Co, Fe, Ni, and Cu, and X is a halide, usually chloride, tetrahedrally coordinated to metal atoms [27]. Bis(1-alkyl-3-methylimidazolium) tetrahalogenomanganate $[C_{2\text{-}4}mim]_2[MnCl_4]$, [28] ethyl methyl imidazolium iron(III)chloride [EMIMCl]$FeCl_3$, [29] $[BMIM]_2[CoCl_4]$ and $[BMIM]_2[ZnCl_4]$ are typical examples of synthesized MILs.[30] By introducing a metal into an imidazolium-based IL structure, its Lewis acid character can be enhanced [29,31,32]. It has been shown that the acid-base character of MILs can affect their catalytic activity [27]. Nevertheless, to date only a few applications of MILs as catalysts / accelerators for polymerization have been reported in the literature; e.g. the use of Ln-containing ILs in electric and magnetic switchable devices [27] or the application of aluminum, palladium, zinc, and iron-based ILs for polystyrene formation [33,34]. A recent study reported the accelerating effect of magnetic phosphonium- and imidazolium-based ILs with $FeCl_4$ anions on epoxy–anhydride curing reaction [35].

Based on our previous study showing the catalytic ability of the chloride anion of imidazolium IL, [36] in this work, we hypothesize an accelerating effect of imidazolium MILs for epoxy–anhydride copolymerization due to the enhanced Lewis acidity of MIL-anions bearing Fe, Zn, and/or Co atoms. Therefore, a series of MILs are synthesized and used as accelerators for epoxy – anhydride cross-linking under solvent-free conditions. A detailed kinetic investigation using differential scanning calorimetry (DSC) and near-infrared (NIR) spectroscopy is performed and kinetic parameters are determined via isothermal modeling. MALDI-TOF mass spectrometry enables us to propose a MILs-induced epoxy – anhydride copolymerization mechanism. Finally, the produced epoxy networks are characterized using dynamic mechanical analysis (DMA) and thermogravimetric analysis (TGA).

2. Experimental

2.1. Materials

Bisphenol A diglycidyl ether epoxy resin DGEBA (D.E.R 332) with an epoxy equivalent weight of 179 g/mol was supplied by DOW Chemicals. Hexahydro-4-methylphthalic anhydride (MHHPA, 96 %) and 1-methylimidazole (1MIM, 99 %) were provided by Sigma Aldrich. 1-butyl-3-methylimidazolium chloride (BMIMCl, 99 %) was supplied by Iolitech. Iron (III) chloride (anhydrous, 98 %) and cobalt (II) chloride (anhydrous, 99 %) were supplied by Acros Organics, while zinc (II) chloride (anhydrous, p.a.) was provided by Lach-Ner.

2.2. Synthesis of epoxy-anhydride networks

In the present study, metal-based ionic liquids (MILs) incorporating Zn (II), Co (II), or Fe (II) were synthesized in accordance with established methodologies outlined in previous reports [37–42]. Comprehensive details of the synthesis procedure and characterization methods are described in the Supporting Information (SI). Subsequently, the epoxy monomer (DGEBA) and anhydride (MHHPA) were mixed in an equimolar ratio with various amounts (from 0.05 to 5.00 mol%) of 1-methylimidazole (1MIM), 1-butyl-3-methylimidazolium chloride (BMIMCl), 1-butyl-3-methylimidazolium tetrachloroferrate ((BMIM)$FeCl_4$), 1-butyl-3-methylimidazolium tetrachlorocobaltate ($(BMIM)_2CoCl_4$), or 1-butyl-3-methylimidazolium tetrachlorozincate ($(BMIM)_2ZnCl_4$). The resulting mixtures were homogenized for 10 min, followed by casting into open aluminum molds. The curing process proceeded at 80 °C for 4 h, 150 °C for 2 h, and finally at 180 °C for 4 h in a vacuum oven to avoid bubbles formation and mitigate undesired oxidation. For a comparative analysis of the overall reactivity and final material properties, reference samples, DGEBA/MHHPA/1MIM using the conventional catalyst 1-methylimidazole [43] along with DGEBA/MHHPA/BMIMCl were employed. The structural representations and acronyms of the catalysts used are elucidated in Fig. 1.

2.3. Model reaction of monofunctional epoxy and anhydride

1,2-Epoxy-3-phenoxypropane (phenyl glycidyl ether, PGE, 99 %, Sigma-Aldrich) and MHHPA were mixed in an equimolar ratio and then 2.70 mol% of 1MIM, BMIMCl, (BMIM)$FeCl_4$, $(BMIM)_2CoCl_4$, or $(BMIM)_2ZnCl_4$ was added and homogenized using a magnetic stirrer. The reaction was carried out at 80 °C. The mixture was regularly sampled and the reaction progress was monitored using FTIR and MALDI-TOF mass spectrometry.

2.4. Monitoring of the epoxy-anhydride cross-linking

Near-infrared (NIR) spectra were acquired using a Nicolet iS50 FTIR spectrometer (Thermo Fisher Scientific) in transmission mode using an HT-32 heating cell and handmade cuvettes made of two glass slides and tape as spacers to determine the thickness of the sample (d = 1 mm). Dynamic runs were performed from 30 to 300 °C at a heating rate of 5 °C/min. The isothermal runs were performed at 60 °C for 2 h. In both types of time-resolved experiments the spectra were collected every 20 s (32 scans per spectrum, data spacing of 1 cm^{-1}). The collected spectra were integrated using a fixed two-point baseline in the regions of 4502–4568, 4803–4867, 5100–5190, 5210–5272, and 6800–7132 cm^{-1} to monitor the epoxy, anhydride, ester, moisture, and hydroxy groups, respectively. The integral intensities obtained were calibrated based on the intensity of the integrated reference band in the region 4592–4652 cm^{-1}. The conversions of epoxy, anhydride, ester, moisture, and hydroxy groups are defined as follows (equations 1–5):

$$\alpha(t)_{Epoxy} = 1 - \frac{A_{4530}(t)}{A_{5430}(t=0)} \Big/ \frac{A_{4622}(t)}{A_{4622}(t=0)} \quad (1)$$

$$\alpha(t)_{Anhydride} = 1 - \frac{A_{4828}(t)}{A_{4828}(t=0)} \Big/ \frac{A_{4622}(t)}{A_{4622}(t=0)} \quad (2)$$

$$\alpha(t)_{Ester} = \frac{A_{5158}(t)}{A_{5158}(max)} \Big/ \frac{A_{4622}(t)}{A_{4622}(t=0)} \quad (3)$$

$$\alpha(t)_{Moisture} = 1 - \frac{A_{5252}(t)}{A_{5252}(t=0)} \Big/ \frac{A_{4622}(t)}{A_{4622}(t=0)} \quad (4)$$

$$\alpha(t)_{Hydroxy} = \frac{A_{6985;7030}(t)}{A_{6985;7030}(max)} \Big/ \frac{A_{4622}(t)}{A_{4622}(t=0)} \quad (5)$$

Dynamic and isothermal differential scanning calorimetry (DSC) measurements of the reactive mixtures were performed using a DSC calorimeter (Q 2000, TA Instruments) calibrated for indium. Samples (5–15 mg) were hermetically sealed in Tzero aluminum pans with a pinhole and measured under a nitrogen flow of 50 mL/min. Dynamic DSC runs were performed from 20 °C to 300 °C at a heating rate of 5 °C/min.

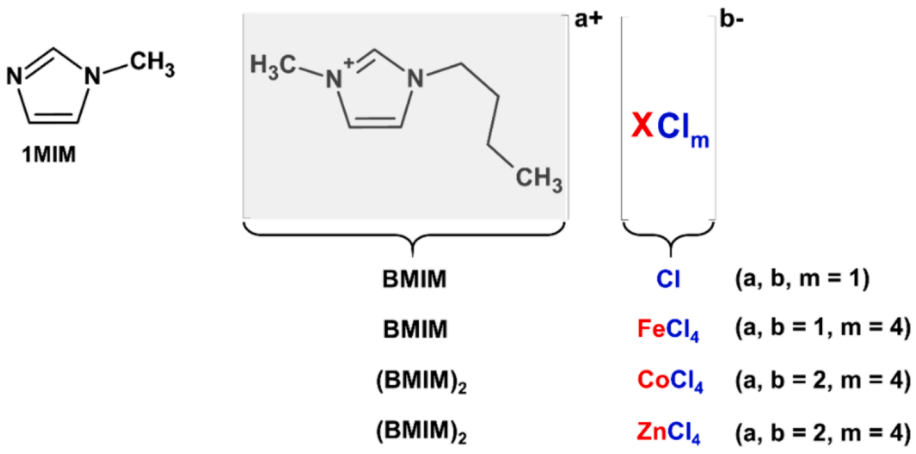

Fig. 1. Structures and acronyms of the used ionic liquids.

The conversion curves (conversion vs. time) were obtained by measuring the reactive mixture in DSC using dynamic and isothermal runs. An additional ramp DSC run at 10 ℃/min was performed to measure the residual reaction heat (ΔH_{res}) after isothermal curing. The conversion of epoxy groups (α) was calculated from the DSC data according to equation (6) [44]:

$$\alpha(t)_{\mathrm{DSC}} = \frac{\int_0^t \frac{dH}{dt}\,dt}{\Delta H_{total}} + \left(1 - \frac{\Delta H_{res} + \Delta H_{iso}}{\Delta H_{total}}\right) \tag{6}$$

where dH/dt is the instantaneous time derivative of the heat during the dynamic or isothermal run, ΔH_{total} is the total enthalpy of the reaction determined from the dynamic DSC runs and ΔH_{iso} is the heat of reaction measured from the isothermal DSC scans.

Then, the epoxy-anhydride cross-linking was modelled using the Kamal-Sourour model [45] according to equation (7):

$$\frac{d\alpha}{dt} = (k_1 + k_2\alpha^m)(1-\alpha)^n \tag{7}$$

where k_1 and k_2 are rate constants for the non-catalytic and the auto-catalytic reactions respectively, and m and n are partial reaction orders. A numerical integration using the 4th order Runge–Kutta method was used to calculate model-predicted α_{sim} values for each tested temperature. These values were then compared to experimentally found α_{exp} (from isothermal DSC) using the ordinary least squares (OLS) error (Microsoft Excel) [46]:

$$OLS = \sum_i [\alpha_{exp} - \alpha_{sim}]_i^2 \tag{8}$$

This OLS criterion was then minimized using the GRG algorithm (Microsoft Excel). By this procedure, the rate constants of non-catalysed (k_1) and auto-catalysed (k_2) reactions were determined for each temperature. The Arrhenius equation was used for the determination of the activation energy of the reactions:

$$k = A\exp\left(-\frac{E_a}{RT}\right) \tag{9}$$

where A is the pre-exponential factor, E_a is the activation energy, and R is the universal gas constant.

2.5. Characterizations

Fourier-transmission infrared spectroscopy (FTIR) measurements of the obtained samples were performed using a Spectrum 100 spectrometer (PerkinElmer) equipped with a mercury–cadmium–telluride (MCT) detector and an universal attenuated total reflectance (ATR) accessory with a diamond prism. The spectra were averaged over 32 scans, with a resolution of 4 cm^{-1}. The disappearance of the peak at 915 cm^{-1} was followed during the reaction, attributed to the C-O stretching of oxirane group [47].

MALDI-TOF mass spectra were acquired using an UltrafleXtreme TOF – TOF mass spectrometer (Bruker Daltonics, Bremen, Germany) equipped with a 2000 Hz smartbeam-II laser (355 nm) in the positive ion reflectron mode. Panoramic pulsed ion extraction and external calibration were used for molecular weight assignment. The dried droplet method was used in which the solutions of the sample (10 mg/mL), matrix DHB (2,5-Dihydroxybenzoic acid; 20 mg/mL), and ionizing agent sodium trifluoroacetate (CF_3COONa; 10 mg/mL) in THF were mixed in the volume ratio 4:20:1. 1 μL of the mixture was deposited on a ground steel target.

Dynamic-mechanical and thermal analysis (DMTA) of the cured epoxy samples was measured on an ARES G2 rheometer (TA Instruments). The temperature dependence of the complex shear modulus (G^*) was determined for rectangular samples (20 × 10 × 2 mm) using oscillatory shear deformation (0.01 – 0.1 % strain) at a frequency of 1 Hz from 25 °C to 220 °C at a temperature ramp rate of 3 °C/min. The main transition temperature (T_α) was determined to be the tan δ peak maximum. The cross-link density (ν_e) was calculated using equation (10):

$$\nu_e = G_R^{'}/RT \tag{10}$$

where $G_R^{'}$ is the storage modulus of the network in the rubbery plateau at $T = T_\alpha + 50$ °C, R is the universal gas constant, and T is the absolute temperature in Kelvin. The average molecular mass between the cross-links (M_c) was calculated by equation (11):

$$M_c = \rho RT/G_R^{'} \tag{11}$$

where ρ is the calculated density, T is the absolute temperature in Kelvin at $T_\alpha + 50$ °C, and G'_R is the storage modulus of the networks in the rubbery plateau at T.

Thermogravimetric analysis (TGA) was carried out using thermogravimetric analyser Pyris 1 TGA (PerkinElmer). A sample of approximately 5 mg was heated from 30 °C to 800 °C at a heating rate of 10 °C/min under nitrogen flow (25 cm^3/min).

3. Results and discussion

3.1. Non-isothermal epoxy-anhydride cross-linking

The synthesized metal-based ionic liquids (MILs) were applied as accelerators for the epoxy-anhydride (DGEBA/MHHPA) reaction and were compared with a metal-free IL (BMIMCl) and a commercially used

catalyst (1MIM) [43,44,48]. First, the cross-linking of DGEBA/MHHPA reactive mixtures with 2.70 mol% of accelerators was studied using non-isothermal (dynamic) DSC at a heating rate of 5 °C/min. Fig. 2(a) plots the DSC runs showing a significant exothermic peak related to the epoxy-anhydride reaction (except for the accelerator-free system, which shows only a small exothermic peak above 230 °C due to non-catalytic curing [49], which leads to a partially cured epoxide with a low final T_g (Table S2, entry 1). Both reference systems (DGEBA/MHHPA/1MIM and DGEBA/MHHPA/BMIMCl) showed similarly one exothermic peak with T_{onset} at approximately 100 °C (Table S2, entries 2 and 3). The MIL-containing systems showed a shift of the main exothermic peak toward lower (DGEBA/MHHPA/(BMIM)$FeCl_4$ and DGEBA/MHHPA/(BMIM)$_2$-$CoCl_4$) or higher (DGEBA/MHHPA/(BMIM)$_2ZnCl_4$) temperatures, while their determined ΔH_{total} values were slightly lowered compared to the conventionally catalyzed systems (Fig. 2(a) and Table S2).

Moreover, the DGEBA/MHHPA/(BMIM)$FeCl_4$ system displayed an additional exotherm, appearing as a new peak at low temperatures between 60 and 75 °C (Fig. 2(a)). This peak was the most intense for the system with (BMIM)$FeCl_4$, while for the systems with (BMIM)$_2ZnCl_4$ and (BMIM)$_2CoCl_4$ it appeared as a small shoulder, which intensity increased with the increasing MIL content (Fig. S4-S6). The presence of two well-defined peaks in the DSC thermograms most likely indicates the occurrence of an additional reaction mechanism [44]. A similar low-T exotherm during the curing of the epoxy-anhydride system containing (BMIM)$FeCl_4$ was recently described by Freitas *et al.*, who suggested the formation of active species through the interaction of the $(FeCl_4)^-$ anion and the carbonyl group of the anhydride [35].

The non-isothermal conversion (α_{DSC}) curves (Fig. 2(b)) show that the addition of MILs accelerates the cross-linking reaction in the low-temperature region (60–70 °C), where there is a sudden increase in conversion (the jump is most noticeable for the system with (BMIM)$FeCl_4$), leading to a divergence from the sigmoid shape of the conversion curve typical of reference (imidazole-accelerated) system.

To deeper explore the origin of the low-T exotherm and to obtain better insight into the curing mechanism of DGEBA/MHHPA/MILs systems, non-isothermal cross-linking (heating rate of 5 °C/min) was monitored using NIR spectroscopy, which enabled us to follow the evolution of the characteristic bands of epoxy (4530 cm^{-1}), anhydride (4828 cm^{-1}), ester (5158 cm^{-1}), hydroxyl (the broad overlapping OH bands of alcohol and carboxylic acid functionalities in the region of 6800–7130 cm^{-1}) groups and moisture (5252 cm^{-1}, Fig. S7 and Table S3) [50–52]. The decreasing intensity of the epoxy and anhydride bands with increasing temperature during cross-linking shows an ongoing curing process in all studied systems (Fig. 3). Consequently, the ester group content gradually increased with increasing reaction temperature. The graphs further show that anhydride consumption was always faster at the beginning of the reaction and synchronized with decreasing moisture content, suggesting that the MHHPA ring opening was initiated by water at the initial stage of the reaction (Fig. 3). The deviation between the epoxy and anhydride conversion curves, observed before the copolymerization is initiated, can be ascribed to a higher level of moisture in the formulation owing to the hygroscopic nature of the MILs. In the case of the MILs-containing systems, this decrease in moisture content was connected to an increase in the hydroxyl band that appeared at 90, 110, and 60 °C for the DGEBA/MHHPA system with (BMIM)$_2CoCl_4$, (BMIM)$_2ZnCl_4$, and (BMIM)$FeCl_4$, respectively (Fig. 3(a-c)). The increased intensity of the OH group bands indicates the formation of carboxylic acids due to the hydrolysis of the anhydride ring. This reaction is followed by a fast decrease in OH, epoxy, and anhydride functional groups, proving the quick onset of the subsequent esterification reaction. This reaction route was the most significant in the case of the DGEBA/MHHPA system with (BMIM)$FeCl_4$.

To reach more information about the low-T process, the DGEBA/MHHPA/(BMIM)$FeCl_4$ formulation was followed under isothermal conditions at 60 °C (Fig. S8(a)), showing initial fast hydrolysis of anhydride, proved by the decrease of anhydride and moisture bands, followed by a temporary increase of the OH band (due to COOH groups formation) and a final fast consumption of carboxylic functions due to their reaction with the epoxy ring and OH groups producing ester linkages, indicated by the sudden decrease of OH and epoxy bands, and the increase of the ester band. Furthermore, the process is almost stopped when the acidic functions are consumed (after ca 6 min at 60 °C, Fig. S8(a)). Then, the decrease of epoxy and anhydride bands becomes moderate and synchronous, implying a slow subsequent alternating copolymerization (Fig. S8(a)).

At the later stage of curing (at T above ca 100 °C), the consumption of epoxy and anhydride groups is further accelerated until their full consumption (at around 200 °C, Fig. 3 and Fig. S8(b)). The conversion of epoxy and anhydride groups is simultaneous, indicating an overall alternating copolymerization behavior [53]. The OH groups start to increase again at the last stage of the cross-linking reaction, probably due to the formation of sterically-hindered OH groups inaccessible for further reaction due to topological limits of the formed highly cross-linked epoxide network.

3.2. Isothermal cross-linking of epoxy – Anhydride with MILs

For better understanding of the accelerating effect induced by MILs and to determine the kinetic parameters of cross-linking reactions, the isothermal DSC runs were performed with a constant catalyst loading of

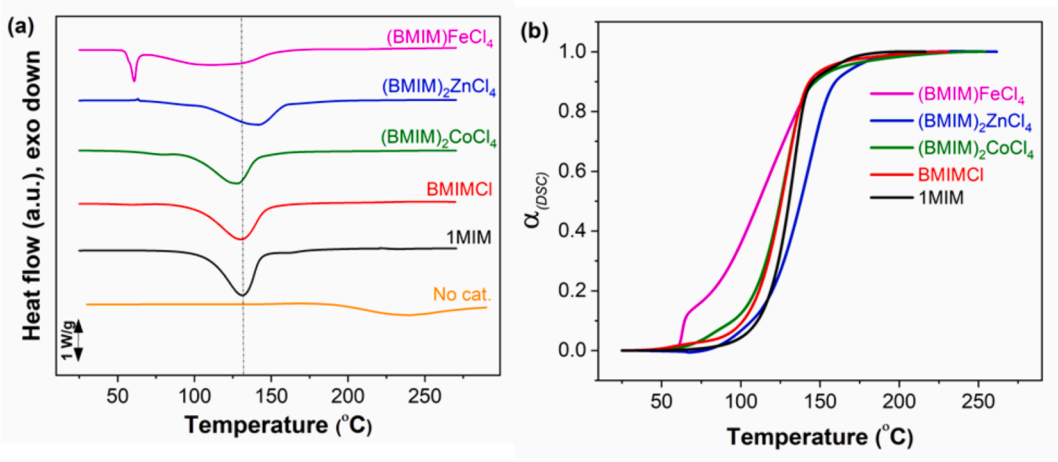

Fig. 2. (a) Non-isothermal (dynamic) DSC curves and (b) conversion (α_{DSC}) curves during non-isothermal cross-linking of DGEBA/MHHPA with 2.70 mol% of catalyst at 5 °C/min.

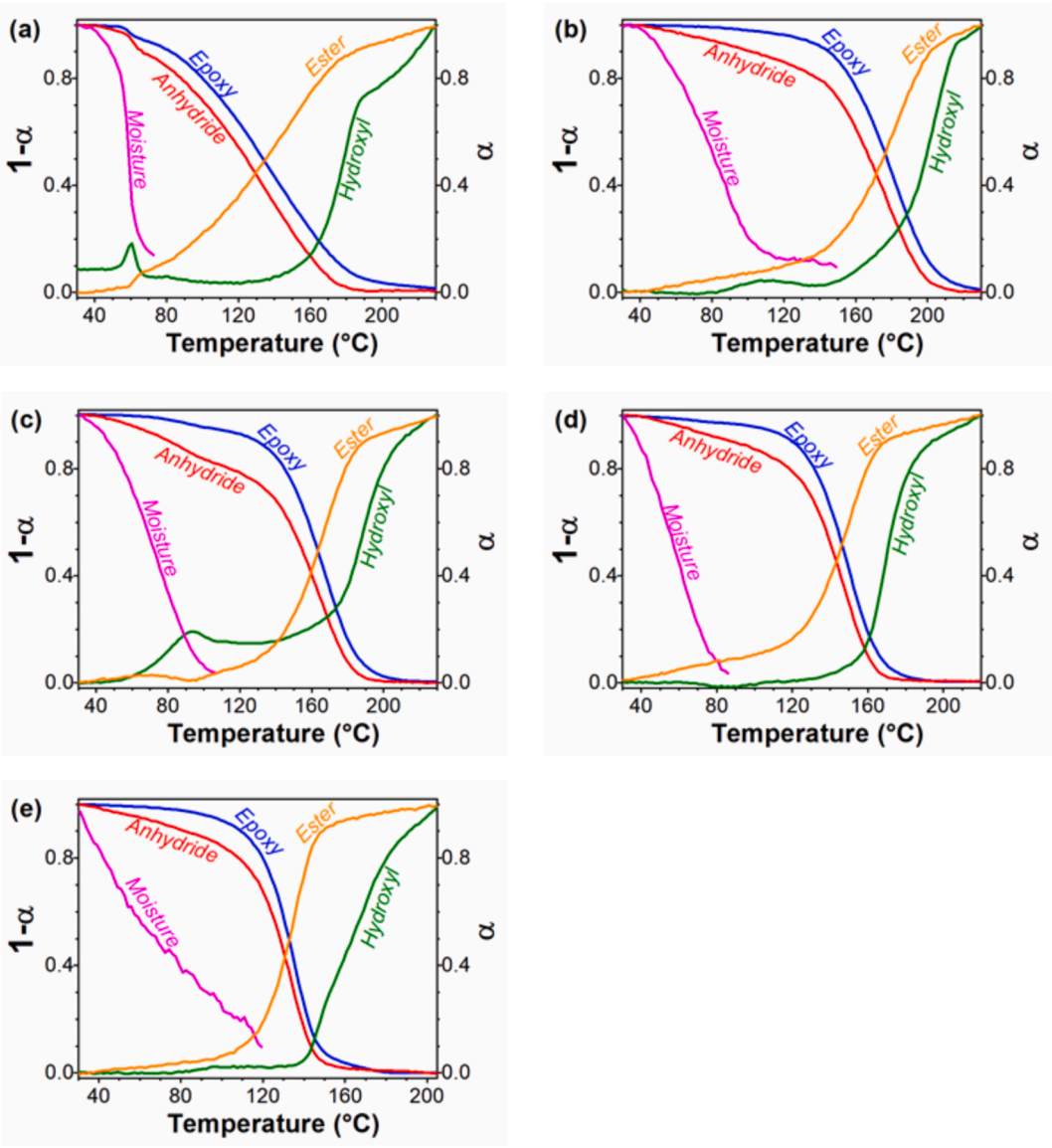

Fig. 3. Development of content of functional groups according to NIR spectroscopy. Non-isothermal (5 °C/min) cross-linking of DGEBA/MHHPA with different accelerators (2.70 mol%): (a) (BMIM)$FeCl_4$, (b) $(BMIM)_2ZnCl_4$, (c) $(BMIM)_2CoCl_4$, (d) BMIMCl, and (e) 1MIM. Left Y-axis for epoxy, anhydride and moisture; Right Y-axis for ester and hydroxyl.

2.70 mol%. Table S4 summarizes the calorimetric isothermal data showing that the application of MILs as accelerators allowed to reach a higher final monomer conversion compared to the reference (1MIM-catalyzed) system. Fig. 4(a-e) compares the isothermal DSC conversion curves of all studied systems, illustrating that the type of accelerator and the curing temperature have a crucial impact on the epoxy-anhydride kinetics.

To better understand the curing kinetics, the experimental results were treated with the autocatalytic Kamal-Sourour model (see equation (7)), which adopts a model-fitting algorithm and is commonly used to describe the autocatalytic behavior of a large number of epoxy curing reactions [48,54–56]. This model proposes that the curing reaction is governed by two, non-catalytic (k_1) and catalytic (k_2) rate constants. The overall reaction order ($m + n$) was initially fixed to 2 based on the literature data [54,57]. The first fitting results for the reference imidazole-catalyzed system showed partial reaction orders of $m = 1$ and $n = 1$ (DGEBA/MHHPA/1MIM, Fig. 4(e)), which were maintained for fitting of all systems. The model simulation correlates well with the experimental data up to conversions of about 0.80 (Fig. 4), describing well the chemically controlled kinetics [58]. At the later stage of curing, the simulation data begin to diverge due to vitrification, as the cross-linking reaction becomes diffusion controlled [54,59,60]. This diffusion–driven reaction cannot be described by this model and new parameters must be considered to describe kinetics beyond vitrification, [46] which is nevertheless out of the scope of this study.

For both reference systems accelerated by either 1MIM or BMIMCl, the simulation curves fitted well the experimental values at all tested temperatures (Fig. 4(d,e)). In contrast, the MILs-induced cross-linking (Fig. 4(a-c)) exhibited good fitting results at higher temperatures and a certain deviation from the model at lower temperatures (100 and 110 °C for (BMIM)$FeCl_4$, and 90 °C for $(BMIM)_2CoCl_4$ and $(BMIM)_2ZnCl_4$). A better fit for the low-T region was obtained when all parameters (k_1, k_2, m and n) of the Kamal-Sourour model were allowed to be adjusted. Then, the fitting results for MIL-containing systems at low temperatures show excellent agreement with the experimental conversion data (blue and magenta lines in Fig. 4(a-c)). However, the reaction orders (m, n) increased significantly, losing their original physical meaning [61]. In general, the reaction orders show only a low variation on the curing

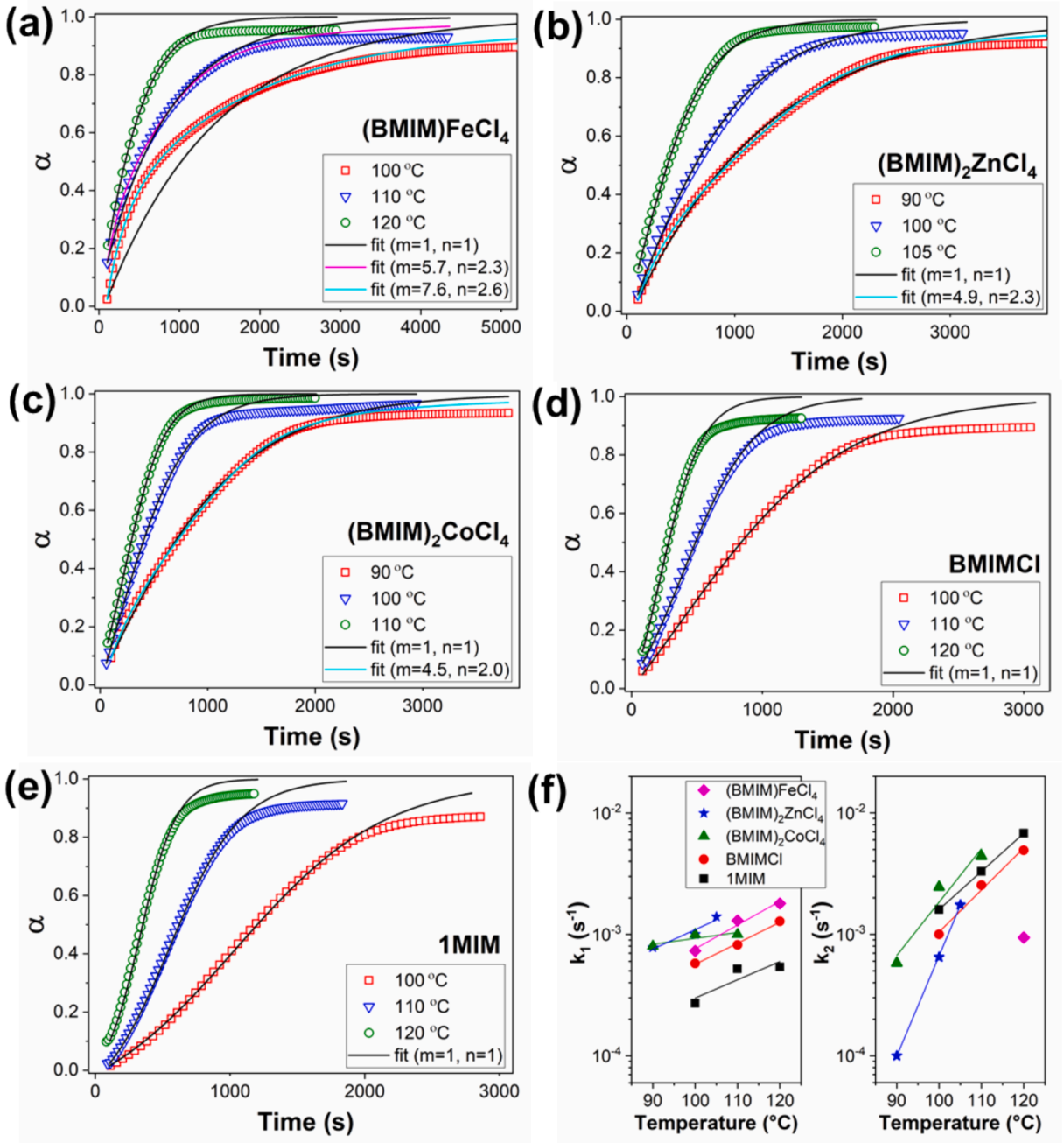

Fig. 4. (a-e) Comparison of experimental (points) and fitted (Kamal-Sourour model fit, lines) values of DSC conversion (α) during isothermal cross-linking of DGEBA/MHHPA with different accelerators (2.70 mol%): (a) (BMIM)$FeCl_4$, (b) $(BMIM)_2ZnCl_4$, (c) $(BMIM)_2CoCl_4$, (d) BMIMCl, and (e) 1MIM. (f) Temperature dependence of k_1 (non-catalytic) and k_2 (catalytic) rate constants of Kamal-Sourour model ($m = 1$, $n = 1$) determined from the fitting of DSC conversion (α) data during isothermal cross-linking of DGEBA/MHHPA with different accelerators (lines are linear fits according to Arrhenius equation (9)).

temperature assuming an unaltered reaction mechanism [62]. Herein, the observed substantial increase in reaction orders, especially in the kinetic exponent m representing the catalytic reaction, suggests an additional cross-linking mechanism proceeding at low temperatures, which is probably related to the formation of new catalytic centers induced by MILs. This observation is in good correlation with the non-isothermal DSC runs (the appearance of the second low-T exotherm, Fig. 2) and NIR results (the fast conversion increase at the low-T region, Fig. 3) described above.

Further insight into the kinetics of the two stages of the cross-linking is gained from the comparison of the rate constants (k_1 and k_2) listed in Table S5 and Fig. 4(f). For both reference DGEBA/MHHPA systems accelerated by 1MIM and BMIMCl, a typical S-shaped conversion curve was observed as a result of the two various curing steps characterized by two different rate constants (a non-catalyzed k_1 and a catalyzed k_2) with two activation barriers (E_{a1} and E_{a2}- calculated from the Arrhenius equation (9) (Fig. S9-S13) [44]. Usually, the non-catalytic route is dominant only at very low temperatures due to its lower activation energy ($E_{a1} < E_{a2}$, Table S5). Herein, for 1MIM- and BMIMCl-accelerated curing, $k_2 > k_1$ in all tested temperature ranges (Fig. 4(f)), which means that the non-catalyzed pathway (k_1) is much slower than the catalyzed route (k_2) and the cross-linking is driven by the catalytic (imidazole) pathway [63]. In contrast, the conversion curves of the MILs-accelerated systems revealed an exponential-like behavior (Fig. 4). Similar behavior for the IL-cured DGEBA was attributed to a change in mechanism due to the presence of chloride anion of IL acting as an initiator/cocatalyst

[55]. Therefore, the exponential kinetics observed for the MILs-induced epoxy-anhydride cross-linking can also be ascribed to the catalytic ability of the MCl_4 anions, especially at low temperatures. Based on the NIR results, this MCl_4-initiated reaction pathway includes formation of carboxylic acids and their subsequent esterification (as evidenced below). The kinetic modelling shows that for MILs-containing systems at low temperatures (90 – 110 °C), the non-catalytic rate constant k_1 is always higher than k_2 (Fig. 4(f)). This indicates that the MILs-accelerated polyesterification pathway involving the formation of new acidic initiation centers and the subsequent rapid monomer conversion causes an increase in the k_1 rate constant. In contrast, at higher temperatures, the catalytic constant k_2 becomes more dominant, and the cross-linking is then driven by the anionic mechanism, similar to the reference systems. The results of the kinetic study show the considerable complexity of the epoxy-anhydride cross-linking accelerated by MILs. This complicates the application of the Kamal-Sourour model, especially at low temperatures, where MIL-induced esterification is the dominant mechanism.

Overall, the activation energies (E_{a1} and E_{a2} values) for the MIL-containing systems are higher than those of the reference systems (Table S5, Fig. S9-S13) and those reported in the literature for epoxy-anhydride systems (60 to 75 kJ/mol) [48,64,65], demonstrating the distinct mechanism of MILs-induced epoxy-anhydride cross-linking.

3.3. Mechanism of epoxy-anhydride cross-linking induced by MILs

The above-mentioned NIR results revealed a complex DGEBA/MHHPA cross-linking mechanism induced by MILs. To find out the origin of the MILs-induced epoxy-anhydride reaction, model reactions between mono-functional epoxy resin, phenyl glycidyl ether (PGE), and MHHPA in the presence of accelerators (MILs, BMIMCl and 1MIM) were conducted. Supposing an alternating copolymerization mechanism, the PGE/MHHPA reaction produces a linear soluble polymer suitable for MALDI-TOF mass spectrometry, allowing the determination of end-groups and repeating units of the growing polymer chains. The PGE/MHHPA reactions were performed at 80 °C to explore the low-*T* curing mechanism. The MALDI-TOF mass spectra of the reaction mixtures after 15 min and the assigned structures are given in Fig. 5 and Fig. S14-18. First, the MALDI-TOF mass spectrum of the imidazole-catalyzed reference system (PGE/MHHPA/1MIM) was analyzed showing only one major distribution with a mass increment of 318 Da, consisting of alternating MHHPA (168 Da) and PGE (150 Da) units, and 82 Da terminal unit assigned to 1-methylimidazolium (Fig. S14). This indicates an initial step involving a nucleophilic attack of 1MIM to the oxirane ring and formation of an alkoxide [53]. In the subsequent propagation step, the alkoxide attacks an anhydride group yielding a carboxylate anion, which is able to open another oxirane ring [66]. This anionic mechanism results in the formation of a strictly alternating copolymer (Scheme S1).

The presence of MILs and BMIMCl as accelerators induced the

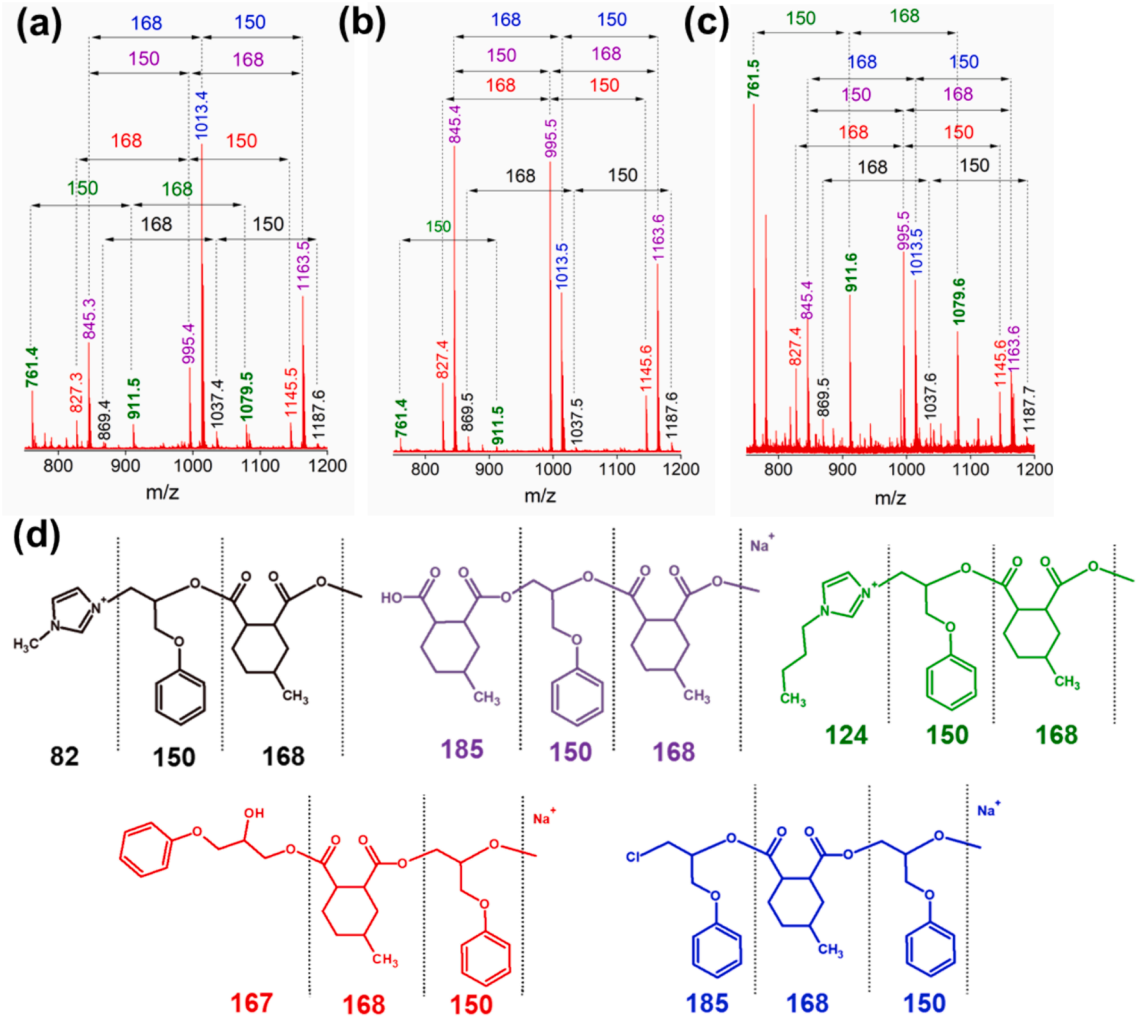

Fig. 5. MALDI-TOF mass spectra (a-c) and assigned structures (d) of PGE/MHHPA reaction mixture after 15 min reaction at 80 °C accelerated by (a) $(BMIM)FeCl_4$, (b) $(BMIM)_2ZnCl_4$, and (c) $(BMIM)_2CoCl_4$. The whole-range MALDI TOF mass spectra are available in SI.

formation of five distributions of molecular ions having different end-groups but the same mass increment of 318 Da, which was composed of alternating PGE (150 Da) and MHHPA (168 Da) units (Fig. 5 and Fig. S15-18), confirming a strictly alternating copolymerization. The different positions of the signals in the mass spectra prove the presence of various end groups and suggest several different initiation mechanisms. It is known that imidazolium ILs can initiate the epoxy ring opening via three main routes: carbene formation, imidazolium decomposition ('imidazole' route) and counter-ion route (anion nucleophilic attack) [36,44,53,67]. Herein, the MALDI-TOF mass spectrometry revealed the dealkylation of butyl (the black-marked structure and signals in Fig. 5) and methyl (the green-marked structure and signals in Fig. 5) chains of the imidazolium ring confirming the initiation mechanism via the 'imidazole' route [67,68]. The formed dealkylated nitrogen atom causes the opening of the epoxy ring, as similarly suggested in Scheme 1(a) to the conventional imidazole catalyst (here 1MIM). Nevertheless, three dominant distributions detected in the MALDI-TOF mass spectra of all MILs-containing systems reveal the formation of structures end-capped with *i*) terminal Cl-opened epoxy ring (the blue-marked structure and signals in Fig. 5), *ii*) OH (the red-marked structure and signals in Fig. 5), and *iii*) COOH (the violet-marked structure and signals in Fig. 5). The presence of Cl and OH end-groups proves the counter-ion nucleophilic initiation route. Herein, the chloride anion of MILs attacks the less hindered carbon of the oxirane ring (in a similar manner as the non-metal BMIMCl [36]) forming an alkoxide anion. This anion can either directly attack another anhydride group to create a carboxylate anion [53] (Scheme 1b) or, due to its willingness to facile hydrolyzation, [69] be first transformed to a hydroxy-alkoxide, which subsequently reacts with another anhydride to form a carboxylate anion (Scheme 1b). In both cases, the reaction further propagates by nucleophilic attack of carboxylate anions to another epoxy ring in an alternate manner [69] obtaining an alternating epoxy-anhydride copolymer (the blue- and red-marked structures and signals in Fig. 5).

At the same time, the formation of carboxyl group end-capped alternating PGE-MHHPA copolymer chains (the violet-marked distribution and signals in Fig. 5 and Fig. S15-18) indicates an additional reaction pathway initiated by carboxyl groups formed during hydrolytic decomposition of anhydride rings. Considering that the formation of carboxyl groups in the low-*T* region is only visible in the case of MILs (see the NIR results above, Fig. 3), it can be assumed that this initiation pathway involves the formation of active species through the interaction between the MCl_4 (especially $FeCl_4$) counter-anion and anhydride ring.

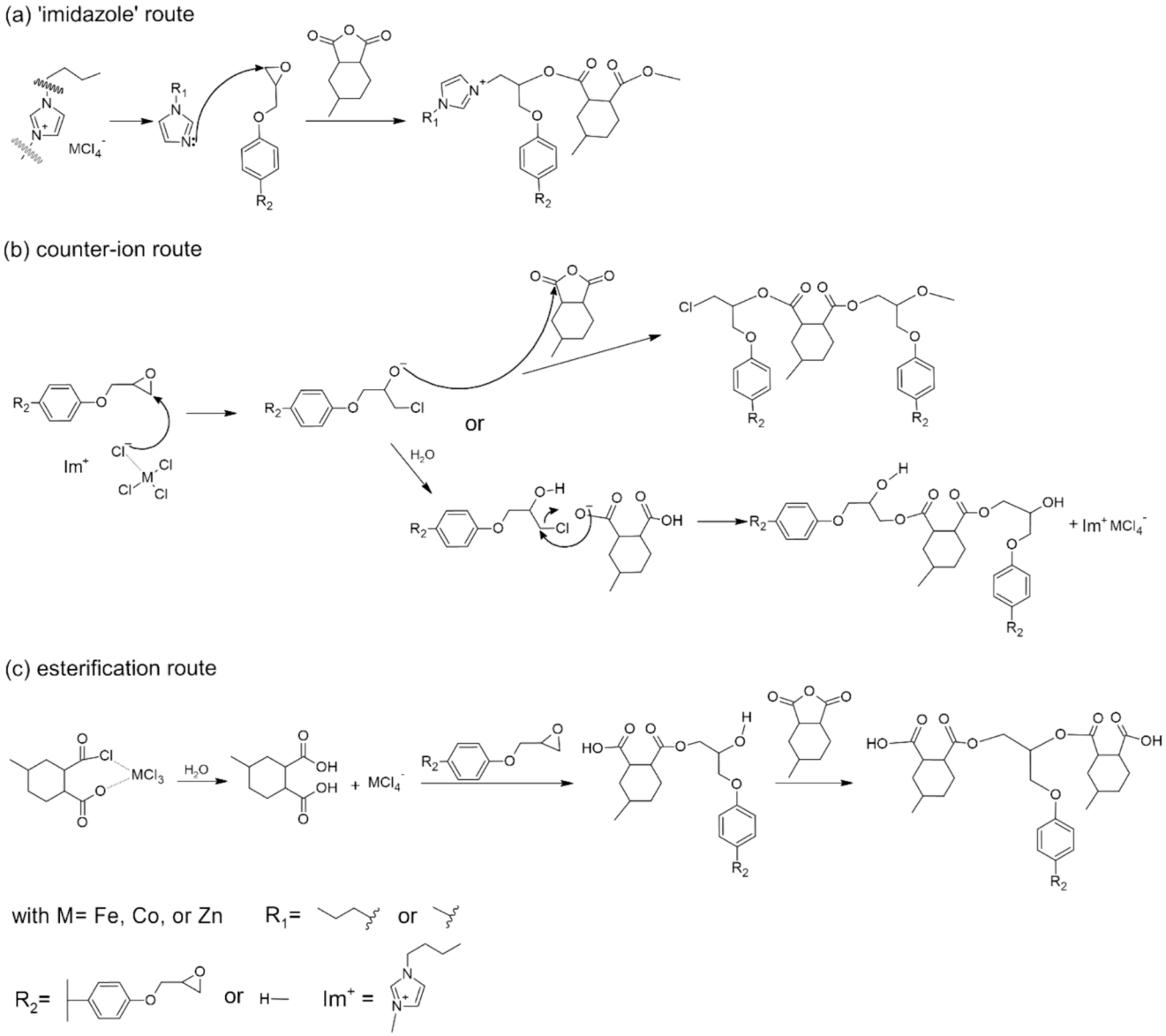

Scheme 1. Proposed mechanisms of epoxy-anhydride reaction initiated by MILs via (a) 'imidazole', (b) counter-ion, and (c) esterification route.

Freitas et *al.* suggested the formation of carboxylate anions with a carbonyl group linked to $FeCl_4$ counter-anion, capable of promoting anionic copolymerization with an oxirane ring [35]. Nevertheless, herein the different reaction mechanism is suggested based on the NIR and MALDI-TOF mass spectrometry results. Due to the Lewis acid character of the MILs [69], an anhydride-MCl_4 counter-anion complex is formed as a first step (Scheme 1c). The generated complex facilitates an attack of trace amounts of water (presumably originating from hygroscopic ILs) which leads to hydrolysis of the cyclic anhydride producing two carboxyl groups. The acidic proton of the carboxylic group activates the epoxy ring and causes its fast opening and formation of a hydroxyester [53]. In general, the carboxylic acid–epoxy esterification is slow and therefore only significant at high temperatures [63]. However, the initiation of the polyesterification pathway is highly accelerated by MILs causing the fast conversion of the anhydride groups to the hydroxyesters at low temperatures and low degrees of conversion. The following propagation step comprises further esterification of the hydroxyesters by reaction with another anhydride group yielding the alternating epoxy-anhydride copolymer with a terminal carboxyl group (Scheme 1c and the violet-marked distribution and signals in Fig. 5 and Fig. S16-18).

Altogether, the MILs-accelerated hydrolysis of the anhydride ring and the subsequent polyesterification substantially affect the overall epoxy-anhydride cross-linking kinetics (as mentioned above). The MILs demonstrate a faster initiation of the epoxy-anhydride reaction and an overall higher reactivity when compared to the conventional non-metallic BMIMCl. This is attributed to the incorporation of the metal chloride anions into the structure of ILs, thereby enhancing its acidity [70]. Numerous studies have proved that chlorometallate ILs exhibit a more pronounced Lewis acid character than conventional ILs [29,31,70,71]. This is controlled by the electrophilicity of the metal and by the mole fraction of the metal chloride used in MIL synthesis [32]. The pronounced Lewis acid property makes the MIL effective catalysts of various reactions, thereby manifesting efficient catalysis in the epoxy-anhydride curing reaction.

3.4. Thermal and mechanical properties of the obtained networks

The first sign of the overall perspective of using MILs as accelerators for the epoxy-anhydride cross-linking can be seen from the achievement of a high T_g of the cross-linked networks after the dynamic DSC runs (Table S2). For deeper comprehension of the properties of the MIL-induced networks, the amount of the accelerators was first optimized using the dynamic DSC runs of reactive systems aiming to reach complete cross-linking reaction (maximal reaction enthalpy, ΔH) and three-dimensional network build-up (maximal T_g, Table S6) [72]. It was found that the amount of 0.2, 1.0 and 1.0 mol% of (BMIM)$FeCl_4$, (BMIM)$_2$-$CoCl_4$, and (BMIM)$_2ZnCl_4$, respectively, was optimal as epoxy-anhydride networks with the highest T_g values were obtained with the content of MILs kept at the lowest possible level. A minimal concentration of accelerator has to be kept to ensure that all reactive moieties can be activated [73] thus avoiding incomplete cross-linking (indicated by the lowered ΔH and T_g values in Table S6). On the other hand, too high contents of accelerators cause a lowering of T_g (Table S6) due to the plasticizing effect [35]. It is worth mentioning that the optimal amount in the case of (BMIM)$FeCl_4$ was found to be 7-fold lower compared to the non-metallic BMIMCl and more than 3-fold lower compared to the conventional 1MIM catalyst which is advantageous from both environmental and economic points of view.

After optimization, all reactive systems were subjected to a complete curing cycle (including the post-curing step at elevated temperature – see experimental part) afterwards the thermomechanical properties of the final epoxy-anhydride networks were evaluated (Fig. 6(a-d) and Table 1).

DMTA shows a one-step change in storage modulus (G') and a single distinct relaxation tan δ peak at 155–160 °C corresponding to the T_g which indicates a homogeneous network structure for all samples with the exception of the DGEBA/MHHPA/BMIMCl and DGEBA/MHHPA/(BMIM)$_2ZnCl_4$ samples. In these cases, a peak shoulder on the tan δ curve in a sub-glass transition region (around 100 °C) appears, indicating a partly heterogeneous network structure [66], probably due to the presence of less cross-linked local domains [74]. However, for all

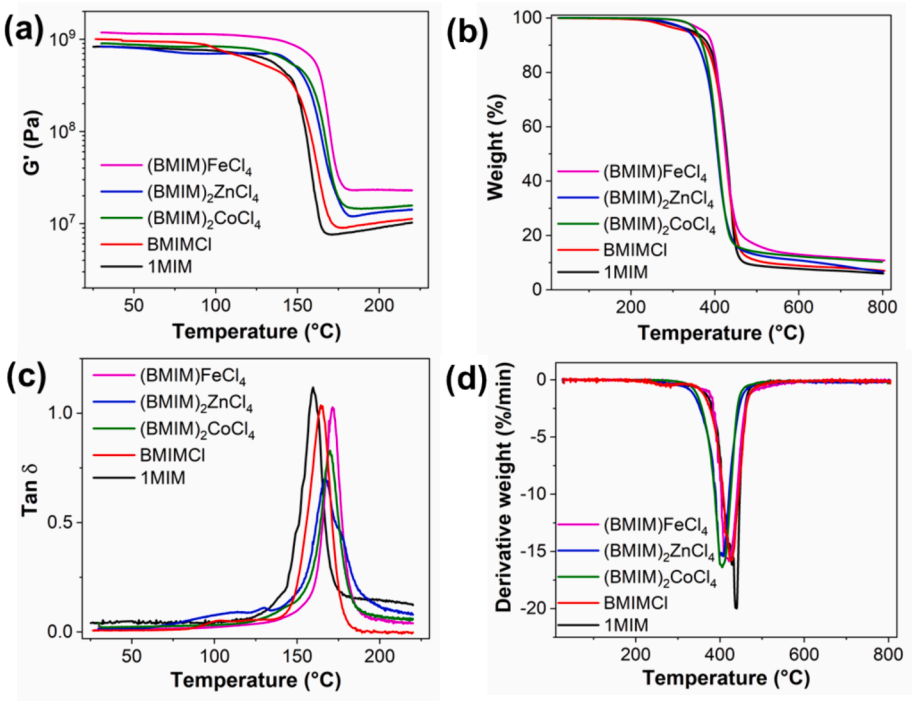

Fig. 6. The DMTA (a,c) and TGA (b,d) results of the epoxy-anhydride networks fabricated using different accelerators: temperature dependence of (a) storage modulus (G') and (c) loss factor (tan δ), and (b) thermogravimetric and (d) derivative weight curves during TGA under N_2 atmosphere.

Table 1
Results of dynamic mechanical and thermal analysis (T_α – maximum of the tan δ peak, M_c – molecular weight between cross-links and ν_e – cross-link density) and thermogravimetric analysis (T_{d5}, T_{d10}, T_{dmax} – temperatures at 5%, 10% and maximum mass loss, and char yield) of the epoxy-anhydride networks prepared using different accelerators.

Accelerator			T_α	M_c	ν_e	T_{dmax}	T_{d5}	T_{d10}	Char
	mol%	wt%	(°C)	(g/mol)	(mmol/cm^3)	(°C)	(°C)	(°C)	(wt.%)
1MIM	2.7	1.3	164	490	2.4	437	349	385	7.0
BMIMCl	2.7	2.8	160	435	2.7	427	333	376	8.1
(BMIM)$FeCl_4$	0.2	0.4	171	207	5.6	419	374	393	11.8
$(BMIM)_2ZnCl_4$	1.0	2.8	167	343	3.4	407	337	359	8.9
$(BMIM)_2CoCl_4$	1.0	2.8	170	308	3.8	406	356	370	11.4

MILs-containing materials, the T_g values were higher than those of the reference DGEBA/MHHPA/1MIM displaying formation of overall dense networks. These findings are in accordance with the determined high G' values at the rubbery region (Fig. 6a). The calculated values of cross-link density (ν_e) and average molecular mass between cross-links (M_c) of the MILs-containing samples (Table 1) indicate the formation of highly cross-linked networks as a result of several cross-link mechanisms during epoxy-anhydride network build-up. The highest ν_e achieved for the (BMIM)$FeCl_4$-containing material correlates well with the largest extent of the low-T esterification cross-link pathway (as suggested in Scheme 1c) for this sample (see the DSC and NIR results above). This suggests that DGEBA/MHHPA networks cured with MILs present not only fast curing but also produce epoxy networks with improved thermo-mechanical properties, which makes these compounds promising agents for newly developed epoxy materials.

The influence of added MILs on the thermal stability of the final networks was evaluated using TGA showing a single decomposition step for all samples (Fig. 6(b,d)). The highest thermal stability (the highest T_{d5} and T_{d10} values, Table 1) and enhanced char-forming ability were observed for the DGEBA/MHHPA samples containing (BMIM)$FeCl_4$ and $(BMIM)_2CoCl_4$, which can be explained by the combination of network homogeneity (see also the DMTA results in Fig. 6(a,c)), high cross-link density (Table 1), and the presence of thermally stable metal anions [75]. In general, the epoxy networks bearing MILs display a higher char yield (8.9–11.8 wt%) than those with 1MIM and BMIMCl (7.0–8.1 wt%, respectively). This char residue improvement is mainly due to the formation of a highly cross-linked structure and the presence of the anionic part of the IL that contains a metal center (Fe, Co, Zn). This could exert a protection of the epoxy matrix from combustion by prohibiting the transfer of volatile compounds and heat through a heat barrier effect [76]. To conclude, the addition of MILs for epoxy-anhydride cross-linking produces DGEBA/MHHPA networks with excellent thermal stability and high char yield.

4. Conclusions

In this work, we have shown that 1-butyl-3-methylimidazolium-based metal ionic liquids (MILs) containing metal-anions such as $(FeCl_4)^-$, $(ZnCl_4)^{2-}$, and $(CoCl_4)^{2-}$ can be used as accelerators for epoxy-anhydride cross-linking reactions, particularly the epoxy-anhydride copolymerization (DGEBA-MHHPA). MILs were found to significantly accelerate the DGEBA-MHHPA cross-linking reaction, especially at low temperatures (60–80 °C) due to their ability to activate a rapid hydrolytic decomposition of the anhydride ring and the subsequent formation of carboxyl groups, which further initiates polyesterification. A detailed investigation of the polymerization mechanism revealed the formation of an alternating epoxy-anhydride copolymer. A complex initiation mechanism induced by MILs was revealed to take place via several pathways, specifically, the so-called imidazole, the counter anion, and the above-mentioned polyesterification routes. A detailed isothermal kinetic study was performed by adopting the autocatalytic Kamal-Sourour model, and the rate constants and activation energies of the investigated systems were adequately determined. The produced epoxy networks are highly cross-linked thermosets (the crosslink density is in the range of 3.4 – 5.6 mmol/cm^3), with high glass transition temperature (approximately 150 °C), and very good thermal resistance.

Our comprehensive investigation demonstrates that MILs are effective accelerators of epoxy – anhydride cross-linking, allowing fast curing at low temperature. Moreover, the thermosetting materials with a high T_g, enhanced cross-linked density and very good thermal resistivity can be obtained. From this point of view, we believe that the study disclosed herein provides valuable insight into the use of MILs as prospective accelerators for high-performance epoxy materials in applications requiring a moderate exotherm profile (typically curing of thick composites) and/or a lower temperature for cure onset (using mold materials sensitive to temperature).

CRediT authorship contribution statement

Marwa Rebei: Writing – original draft, Methodology, Investigation. **Olga Kočková:** Methodology, Data curation. **Matouš Řehák:** Investigation. **Sabina Abbrent:** Writing – review & editing, Formal analysis. **Anna Vykydalová:** Investigation. **Jan Honzíček:** Writing – review & editing, Methodology, Investigation, Funding acquisition, Conceptualization. **Petra Ecorchard:** Writing – review & editing, Methodology, Investigation, Funding acquisition, Conceptualization. **Hynek Beneš:** Writing – review & editing, Supervision, Resources, Project administration, Data curation, Conceptualization.

Declaration of competing interest

The authors declare that they have no known competing financial interests or personal relationships that could have appeared to influence the work reported in this paper.

Data availability

Data will be made available on request.

Acknowledgement

We gratefully acknowledge financial support from the Czech Science Foundation (project no. 22-05244S).

Appendix A. Supplementary material

Supplementary data to this article can be found online at https://doi.org/10.1016/j.eurpolymj.2024.113077.

References

[1] J.M. Longo, M.J. Sanford, G.W. Coates, Ring-opening copolymerization of epoxides and cyclic anhydrides with discrete metal complexes: structure-property relationships, Chem. Rev. 116 (2016) 15167–15197, https://doi.org/10.1021/acs.chemrev.6b00553.

[2] A.I. Barabanova, B.V. Lokshin, E.P. Kharitonova, E.S. Afanasyev, A.A. Askadskii, O. E. Philippova, Curing cycloaliphatic epoxy resin with 4-methylhexahydrophthalic anhydride: catalyzed vs. uncatalyzed reaction, Polymer (guildf). 178 (2019) 121590, https://doi.org/10.1016/j.polymer.2019.121590.

[3] A.I. Barabanova, B.V. Lokshin, E.P. Kharitonova, I.V. Karandi, E.S. Afanasyev, A. A. Askadskii, O.E. Philippova, Cycloaliphatic epoxy resin cured with anhydride in the absence of catalyst, Colloid Polym. Sci. 297 (2019) 409–416, https://doi.org/10.1007/s00396-018-4430-8.

[4] T. Liu, S. Zhang, C. Hao, C. Verdi, W. Liu, H. Liu, J. Zhang, Glycerol induced catalyst-free curing of epoxy and vitrimer preparation, Macromol. Rapid Commun. 40 (2019) 1–6, https://doi.org/10.1002/marc.201800889.

[5] W. Zhao, L. An, S. Wang, Recyclable high-performance epoxy-anhydride resins with DMP-30 as the catalyst of transesterification reactions, Polymers (basel). 13 (2021) 1–18, https://doi.org/10.3390/polym13020296.

[6] J. Parameswaranpillai, N. Hameed, J. Pionteck, E.M. Woo, Handbook of epoxy blends, 2017. doi: 10.1007/978-3-319-40043-3.

[7] S.C. Leguizamon, J. Powers, J. Ahn, S. Dickens, S. Lee, B.H. Jones, Polymerization-induced phase separation in rubber-toughened amine-cured epoxy resins: tuning morphology from the nano- to macro-scale, Macromolecules. 54 (2021) 7796–7807, https://doi.org/10.1021/acs.macromol.1c01208.

[8] P. Reuther, P. Dünnwald, M. Tabatabai, C. Schuh, L. Hartmann, H. Ritter, Thermally controlled acceleration of epoxy resin curing through polymer-bound imidazole derivatives with high latency, ACS Appl. Polym. Mater. 4 (2022) 1150–1158, https://doi.org/10.1021/acsapm.1c01568.

[9] A. Shundo, S. Yamamoto, K. Tanaka, Network formation and physical properties of epoxy resins for future practical applications, JACS Au. 2 (2022) 1522–1542, https://doi.org/10.1021/jacsau.2c00120.

[10] A. Fantoni, T. Koch, S. Baudis, R. Liska, Synthesis and characterization of homogeneous epoxy networks: development of a sustainable material platform using epoxy-alcohol polyaddition, ACS Appl. Polym. Mater. (2022), https://doi.org/10.1021/acsapm.2c01728.

[11] S.K. Ooi, W.D. Cook, G.P. Simon, C.H. Such, DSC studies of the curing mechanisms and kinetics of DGEBA using imidazole curing agents, Polymer (guildf). 41 (2000) 3639–3649, https://doi.org/10.1016/S0032-3861(99)00600-X.

[12] M. Döring, U. Arnold, Polymerization of epoxy resins initiated by metal complexes, Polym. Int. 58 (2009) 976–988, https://doi.org/10.1002/pi.2618.

[13] T. Vidil, F. Tournilhac, S. Musso, A. Robisson, L. Leibler, Control of reactions and network structures of epoxy thermosets, Prog. Polym. Sci. 62 (2016) 126–179, https://doi.org/10.1016/j.progpolymsci.2016.06.003.

[14] Y. Sarazin, J.F. Carpentier, Discrete cationic complexes for ring-opening polymerization catalysis of cyclic esters and epoxides, Chem. Rev. 115 (2015) 3564–3614, https://doi.org/10.1021/acs.chemrev.5b00033.

[15] L.R. Amirova, A.R. Burilov, L.M. Amirova, I. Bauer, W.D. Habicher, Kinetics and mechanistic investigation of epoxy-anhydride compositions cured with quaternary phosphonium salts as accelerators, J. Polym. Sci. Part A Polym. Chem. 54 (2016) 1088–1097, https://doi.org/10.1002/pola.27946.

[16] [a] Samuel Dagorne*[b] and Franck Le Bideau* Dmytro Ryzhakov,[a] Gaël Printz, [b] Béatrice Jacques,[b] Samir Messaoudi,[a] Françoise Dumas, Organo-Catalyzed/Initiated Ring Opening Co-Polymerization of Cyclic Anhydrides and Epoxides: an Emerging Story, Sci. Twent. Century. (2013) 547–563. doi: 10.4324/9781315079097-35.

[17] S. Livi, J. Baudoux, J.F. Gérard, J. Duchet-Rumeau, Ionic liquids: a versatile platform for the design of a multifunctional epoxy networks 2.0 generation, Prog. Polym. Sci. 132 (2022), https://doi.org/10.1016/j.progpolymsci.2022.101581.

[18] F.C. Binks, G. Cavalli, M. Henningsen, B.J. Howlin, I. Hamerton, Examining the kinetics of the thermal polymerisation behaviour of epoxy resins initiated with a series of 1-ethyl-3-methylimidazolium based ionic liquids, Thermochim. Acta. 663 (2018) 19–26, https://doi.org/10.1016/j.tca.2018.02.015.

[19] Y. Yin, M. Liu, W. Wei, C. Zheng, J. Gao, W. Zhang, C. Zheng, P. Deng, Y. Xing, DGEBA/imidazolium ionic liquid systems: the influence of anions on the reactivity and properties of epoxy systems, J. Adhes. Sci. Technol. 32 (2018) 1114–1127, https://doi.org/10.1080/01694243.2017.1402402.

[20] F.C. Binks, G. Cavalli, M. Henningsen, B.J. Howlin, I. Hamerton, Examining the nature of network formation during epoxy polymerisation initiated with ionic liquids, Polymer (guildf). 150 (2018) 318–325, https://doi.org/10.1016/j.polymer.2018.07.046.

[21] T. Welton, Ionic liquids: a brief history, Biophys. Rev. 10 (2018) 691–706, https://doi.org/10.1007/s12551-018-0419-2.

[22] J.P. Hallett, T. Welton, Room-temperature ionic liquids: solvents for synthesis and catalysis. 2, Chem. Rev. 111 (2011) 3508–3576, https://doi.org/10.1021/cr1003248.

[23] P.G. Falireas, J.M. Thomassin, A. Debuigne, Imidazolium-catalyzed dynamic ester cross-links towards reprocessable epoxy vitrimers, Eur. Polym. J. 147 (2021) 110296, https://doi.org/10.1016/j.eurpolymj.2021.110296.

[24] E. Fonseca, V. Demétrio da Silva, J.S. Klitzke, H.S. Schrekker, S.C. Amico, Imidazolium ionic liquids as fracture toughening agents in DGEBA-TETA epoxy resin, Polym. Test. 87 (2020), https://doi.org/10.1016/j.polymertesting.2020.106556.

[25] D. Zielinski, A. Szpecht, P. Hinc, H. Maciejewski, M. Smiglak, Mono N-alkylated DABCO-based ionic liquids and their application as latent curing agents for epoxy resins, ACS Appl. Polym. Mater. 3 (2021) 5481–5493, https://doi.org/10.1021/acsapm.1c00777.

[26] N. Hameed, D.J. Eyckens, B.M. Long, N.V. Salim, J.C. Capricho, L. Servinis, M. De Souza, M.D. Perus, R.J. Varley, L.C. Henderson, Rapid cross-linking of epoxy thermosets induced by solvate ionic liquids, ACS Appl. Polym. Mater. 2 (2020) 2651–2657, https://doi.org/10.1021/acsapm.0c00257.

[27] A.G. Zazybin, K. Rafikova, V. Yu, D. Zolotareva, V.M. Dembitsky, T. Sasaki, Metal-containing ionic liquids: current paradigm and applications, Russ. Chem. Rev. 86 (2017) 1254–1270, https://doi.org/10.1070/rcr4743.

[28] S. Pitula, A.V. Mudring, Synthesis, structure, and physico-optical properties of manganate(II)-based ionic liquids, Chem. - A Eur. J. 16 (2010) 3355–3365, https://doi.org/10.1002/chem.200802660.

[29] I.A. Berezianko, I.V. Vasilenko, S.V. Kostjuk, Acidic imidazole-based ionic liquids in the presence of diisopropyl ether as catalysts for the synthesis of highly reactive polyisobutylene: effect of ionic liquid nature, catalyst aging, and sonication, Polymer (guildf). 145 (2018) 382–390, https://doi.org/10.1016/j.polymer.2018.04.059.

[30] Q. Wang, Y. Geng, X. Lu, S. Zhang, First-row transition metal-containing ionic liquids as highly active catalysts for the glycolysis of poly(ethylene terephthalate) (PET), ACS Sustain. Chem. Eng. 3 (2015) 340–348, https://doi.org/10.1021/sc5007522.

[31] Y. Liu, J. Wang, Lewis acidity and basicity of mixed chlorometallate ionic liquids: Investigations from surface analysis and fukui function, Molecules. 23 (2018), https://doi.org/10.3390/molecules23102516.

[32] J. Estager, J.D. Holbrey, M. Swadźba-Kwaśny, Halometallate ionic liquids-revisited, Chem. Soc. Rev. 43 (2014) 847–886, https://doi.org/10.1039/c3cs60310e.

[33] G.V.S. Dutra, T.S. Teixeira, G.A. Medeiros, P.V. Abdelnur, P.H. Hermes De Araújo, C. Sayer, B.A.D. Neto, F. Machado, On the role of metal-containing imidazolium-based ionic liquid catalysts in the formation of tailored polystyrene, Ind. Eng. Chem. Res. 59 (2020) 21685–21699, https://doi.org/10.1021/acs.iecr.0c04327.

[34] M.A.M. Rahmathullah, A. Jeyarajasingam, B. Merritt, M. VanLandingham, S. H. McKnight, G.R. Palmese, Room temperature ionic liquids as thermally latent initiators for polymerization of epoxy resins, Macromolecules. 42 (2009) 3219–3221, https://doi.org/10.1021/ma802669k.

[35] G. Freitas, R.R. Henriques, L.S. Calheiros, B.G. Soares, Impact of magnetic ionic liquids as catalystson the curing process of epoxy/anhydride system: mechanistic investigation and dynamic-mechanical analysis, J. Appl. Polym. Sci. 139 (2022) 1–12, https://doi.org/10.1002/app.52606.

[36] M. Rebei, A. Mahun, Z. Walterová, O. Trhlíková, R.K. Donato, H. Beneš, VOC-free tricomponent reaction platform for epoxy network formation mediated by a recyclable ionic liquid, Polym. Chem. 13 (2022) 5380–5388, https://doi.org/10.1039/d2py01031c.

[37] M. Rebei, C. Červinka, A. Mahun, P. Ecorchard, J. Honzíček, S. Livi, R.K. Donato, H. Beneš, Fast carbon dioxide–epoxide cycloaddition catalyzed by metal and metal-free ionic liquids for designing non-isocyanate polyurethanes (Accepted manuscript), Mater. Adv. (2024), https://doi.org/10.1039/D3MA00852E.

[38] F. Wang, C. Xu, Z. Li, C. Xia, J. Chen, Mechanism and origins of enantioselectivity for [BMIM]Cl ionic liquids and ZnCl2 co-catalyzed coupling reaction of CO2 with epoxides, J. Mol. Catal. A Chem. 385 (2014) 133–140, https://doi.org/10.1016/j.molcata.2014.01.024.

[39] H.S. Kim, J.J. Kim, H. Kim, H.G. Jang, Imidazolium zinc tetrahalide-catalyzed coupling reaction of CO2 and ethylene oxide or propylene oxide, J. Catal. 220 (2003) 44–46, https://doi.org/10.1016/S0021-9517(03)00238-0.

[40] J. Palgunadi, O.S. Kwon, H. Lee, J.Y. Bae, B.S. Ahn, N.Y. Min, H.S. Kim, Ionic liquid-derived zinc tetrahalide complexes: structure and application to the coupling reactions of alkylene oxides and CO2, Catal. Today. 98 (2004) 511–514, https://doi.org/10.1016/j.cattod.2004.09.005.

[41] S. Hayashi, H.O. Hamaguchi, Discovery of a magnetic ionic liquid [bmim]FeCl4, Chem. Lett. 33 (2004) 1590–1591, https://doi.org/10.1246/cl.2004.1590.

[42] C. Zhong, T. Sasaki, A. Jimbo-Kobayeshi, E. Fujiwara, A. Kobayashi, M. Tada, Y. Iwasawa, Syntheses, structures, and properties of a series of metal ion-containing dialkylimidazolium ionic liquids, Bull. Chem. Soc. Jpn. 80 (2007) 2365–2374, https://doi.org/10.1246/bcsj.80.2365.

[43] R. Dinu, U. Lafont, O. Damiano, A. Mija, High glass transition materials from sustainable epoxy resins with potential applications in the aerospace and space sectors, ACS Appl. Polym. Mater. (2022), https://doi.org/10.1021/acsapm.2c00183.

[44] A. Dzienia, M. Tarnacka, K. Koperwas, P. Maksym, A. Zięba, J. Feder-Kubis, K. Kamiński, M. Paluch, Impact of imidazolium-based ionic liquids on the curing kinetics and physicochemical properties of nascent epoxy resins, Macromolecules. 53 (2020) 6341–6352, https://doi.org/10.1021/acs.macromol.0c00783.

[45] S. Sourour, M.R. Kamal, Differential scanning calorimetry of epoxy cure: isothermal cure kinetics, Thermochim. Acta. 14 (1976) 41–59, https://doi.org/10.1016/0040-6031(76)80056-1.

[46] H. Beneš, J. Dupuy, V. Lutz, F. Lortie, J. Duchet-Rumeau, J.F. Gérard, Synergetic catalytic effect of carbon nanotubes and polyethersulfone on polymerization of glassy epoxy-based systems - Isothermal kinetic modelling, Thermochim. Acta. 590 (2014) 107–115, https://doi.org/10.1016/j.tca.2014.06.023.

[47] M. Perchacz, L. Matějka, R. Konefał, L. Seixas, S. Livi, J. Baudoux, H. Beneš, R. K. Donato, Self-catalyzed coupling between brønsted-acidic imidazolium salts and epoxy-based materials: a theoretical/experimental study, ACS Sustain. Chem. Eng. 7 (2019) 19050–19061, https://doi.org/10.1021/acssuschemeng.9b04810.

[48] C.S. Wang, C. Kwag, Cure kinetics of an epoxy-anhydride-imidazole resin system by isothermal DSC, Polym. Polym. Compos. 14 (2006) 445–454, https://doi.org/10.1177/096739110601400501.

[49] D. Foix, Y. Yu, A. Serra, X. Ramis, J.M. Salla, Study on the chemical modification of epoxy/anhydride thermosets using a hydroxyl terminated hyperbranched polymer, Eur. Polym. J. 45 (2009) 1454–1466, https://doi.org/10.1016/j.eurpolymj.2009.02.003.

[50] S.J. Park, G.H. Kwak, M. Sumita, J.R. Lee, Cure and reaction kinetics of an anhydride-cured epoxy resin catalyzed by N-benzylpyrazinium salts using near-infrared spectroscopy, Polym. Eng. Sci. 40 (2000) 2569–2576, https://doi.org/10.1002/pen.11387.

[51] M. Salzmann, M. Teuchtmann, R. Schledjewski, Determination of the glass transition temperature of an epoxy prepreg by Near Infrared Spectroscopy, Polym. Test. 125 (2023) 108111, https://doi.org/10.1016/j.polymertesting.2023.108111.
[52] Q.F. Liu, D. Li, Y. De Zeng, W.Z. Huang, Determination of gel time of prepreg in copper clad laminate industry by near infrared spectroscopy, J. near Infrared Spectrosc. 29 (2021) 5–10, https://doi.org/10.1177/0967033520963799.
[53] X. Fernàndez-Francos, X. Ramis, À. Serra, From curing kinetics to network structure: A novel approach to the modeling of the network buildup of epoxy-anhydride thermosets, J. Polym. Sci. Part A Polym. Chem. 52 (2014) 61–75, https://doi.org/10.1002/pola.26972.
[54] C.K. Tziamtzi, K. Chrissafis, Optimization of a commercial epoxy curing cycle via DSC data kinetics modelling and TTT plot construction, Polymer (guildf). 230 (2021) 124091, https://doi.org/10.1016/j.polymer.2021.124091.
[55] P. Maksym, M. Tarnacka, A. Dzienia, K. Matuszek, A. Chrobok, K. Kaminski, M. Paluch, Enhanced polymerization rate and conductivity of ionic liquid-based epoxy resin, Macromolecules. 50 (2017) 3262–3272, https://doi.org/10.1021/acs.macromol.6b02749.
[56] M.R.K. and S. SOUROUR, Kinetics and Thermal Characterization of Thermoset Cure, J. Appl. Polym. Sci. 71 (1999) 2401–2408. doi: 10.1002/(sici)1097-4628(19990404)71:14<2401::aid-app12>3.0.co;2-c.
[57] F.I. Altuna, C.C. Riccardi, D.C. Marín Quintero, R.A. Ruseckaite, P.M. Stefani, Effect of an anhydride excess on the curing kinetics and dynamic mechanical properties of synthetic and biogenic epoxy resins, Int. J. Polym. Sci. (2019 (2019).), https://doi.org/10.1155/2019/5029153.
[58] M. Javdanitehran, D.C. Berg, E. Duemichen, G. Ziegmann, An iterative approach for isothermal curing kinetics modelling of an epoxy resin system, Thermochim. Acta. 623 (2016) 72–79, https://doi.org/10.1016/j.tca.2015.11.014.
[59] A.N. Mauri, N. Galego, C.C. Riccardi, R.J.J. Williams, Kinetic model for gelation in the diepoxide-cyclic anhydride copolymerization initiated by tertiary amines, Macromolecules. 30 (1997) 1616–1620, https://doi.org/10.1021/ma9614048.
[60] E. Franieck, M. Fleischmann, O. Hölck, L. Kutuzova, A. Kandelbauer, Cure kinetics modeling of a high glass transition temperature epoxy molding compound (Emc) based on inline dielectric analysis, Polymers (basel). 13 (2021), https://doi.org/10.3390/polym13111734.
[61] S. Vyazovkin, Kinetics of Cross-Linking Polymerization (Curing). Thermal Analysis of Polymeric Materials: Methods and Developments, 1st ed., 2022. doi: doi: 10.1002/9783527828692.ch7.
[62] R. Ren, X. Xiong, X. Ma, S. Liu, J. Wang, P. Chen, Y. Zeng, Isothermal curing kinetics and mechanism of DGEBA epoxy resin with phthalide-containing aromatic diamine, Thermochim. Acta. 623 (2016) 15–21, https://doi.org/10.1016/j.tca.2015.11.011.
[63] X. Ferńandez-Francos, A. Rybak, R. Sekula, X. Ramis, A. Serra, Modification of epoxy-anhydride thermosets using a hyperbranched poly(ester-amide): I. Kinetic study, Polym. Int. 61 (2012) 1710–1725, https://doi.org/10.1002/pi.4259.
[64] H.A. Flores, L.A. Fasce, C.C. Riccardi, On the cure kinetics modeling of epoxy-anhydride systems used in glass reinforced pipe production, Thermochim. Acta. 573 (2013) 1–9, https://doi.org/10.1016/j.tca.2013.09.004.
[65] B.J. Rohde, M.L. Robertson, R. Krishnamoorti, Concurrent curing kinetics of an anhydride-cured epoxy resin and polydicyclopentadiene, Polymer (guildf). 69 (2015) 204–214, https://doi.org/10.1016/j.polymer.2015.04.066.
[66] M. Giebler, C. Sperling, S. Kaiser, I. Duretek, S. Schlögl, Epoxy-anhydride vitrimers from aminoglycidyl resins with high glass transition temperature and efficient stress relaxation, Polymers (basel). 12 (2020) 1–14, https://doi.org/10.3390/POLYM12051148.
[67] F.C. Binks, G. Cavalli, M. Henningsen, B.J. Howlin, I. Hamerton, Investigating the mechanism through which ionic liquids initiate the polymerisation of epoxy resins, Polymer (guildf). 139 (2018) 163–176, https://doi.org/10.1016/j.polymer.2018.01.087.
[68] A.P.A. Carvalho, D.F. Santos, B.G. Soares, Epoxy/imidazolium-based ionic liquid systems: the effect of the hardener on the curing behavior, thermal stability, and microwave absorbing properties, J. Appl. Polym. Sci. 137 (2020), https://doi.org/10.1002/app.48326.
[69] F. de la Cruz-Martínez, M.M. de S. Buchaca, A. Del Campo-Balguerías, J. Fernández-Baeza, L.F. Sánchez-Barba, A. Garcés, C. Alonso-Moreno, J.A. Castro-Osma, A. Lara-Sánchez, Ring-opening copolymerization of cyclohexene oxide and cyclic anhydrides catalyzed by bimetallic scorpionate zinc catalysts, Polymers (Basel). 13 (2021). doi: 10.3390/polym13101651.
[70] W. Wu, Y. Lu, H. Ding, C. Peng, H. Liu, The acidity/basicity of metal-containing ionic liquids: Insights from surface analysis and the Fukui function, Phys. Chem. Chem. Phys. 17 (2015) 1339–1346, https://doi.org/10.1039/c4cp04603j.
[71] A.W. Taylor, S. Men, C.J. Clarke, P. Licence, Acidity and basicity of halometallate-based ionic liquids from X-ray photoelectron spectroscopy, RSC Adv. 3 (2013) 9436–9445, https://doi.org/10.1039/c3ra40260f.
[72] M. Fache, R. Auvergne, B. Boutevin, S. Caillol, New vanillin-derived diepoxy monomers for the synthesis of biobased thermosets, Eur. Polym. J. 67 (2015) 527–538, https://doi.org/10.1016/j.eurpolymj.2014.10.011.
[73] G. Couture, L. Granado, F. Fanget, B. Boutevin, S. Caillol, Limonene-based epoxy: Anhydride thermoset reaction study, Molecules. 23 (2018), https://doi.org/10.3390/molecules23112739.
[74] R.J. Varley, B. Dao, T. Nguyen, S. Lee, T. Nishino, Effect of aromatic substitution on the cure reaction and network properties of anhydride cured triphenyl ether tetraglycidyl epoxy resins, Polym. Adv. Technol. 30 (2019) 1525–1537, https://doi.org/10.1002/pat.4584.
[75] C. Zheng, M. Liu, Y. Yin, Y. Zhang, W. Wei, P. Deng, C. Zheng, Kinetics and thermal properties of epoxy resins containing the ionic liquid [C6mim]FeCl4, RSC Adv. 6 (2016) 11407–11411, https://doi.org/10.1039/c5ra26150c.
[76] M. Zhi, Q. Liu, H. Chen, X. Chen, S. Feng, Y. He, Thermal stability and flame retardancy properties of epoxy resin modified with functionalized graphene oxide containing phosphorus and silicon elements, ACS Omega. 4 (2019) 10975–10984, https://doi.org/10.1021/acsomega.9b00852.

Supporting information
Accelerating effect of metal ionic liquids for epoxy-anhydride copolymerization

Marwa Rebei[†], Olga Kočková[†], Matouš Řehák[§], Sabina Abbrent[†], Anna Vykydalová[ϕ], Jan Honzíček[Δ], Petra Ecorchard[ϕ], Hynek Beneš[†,]*

[†]*Institute of Macromolecular Chemistry, Czech Academy of Sciences, Heyrovského nám. 2, Prague 6, 162 06, Czech Republic*

[ϕ]*Institute of Inorganic Chemistry, Czech Academy of Sciences, Husinec-Řež 1001, 250 68 Řež, Czech Republic*

[§]*Department of General and Inorganic Chemistry, Faculty of Chemical Technology, University of Pardubice, Studentská 573, 532 10, Pardubice, Czech Republic*

[Δ]*Institute of Chemistry and Technology of Macromolecular Materials, Faculty of Chemical Technology, University of Pardubice, Studentská 573, 532 10, Pardubice, Czech Republic*

*Corresponding author: Hynek Beneš (benesh@imc.cas.cz)

Number of pages: 22

Number of figures: 18

Number of tables: 6

Number of schemes: 1

Synthesis of metal-based ionic liquids (MILs)

The metal-based ionic liquids (MILs) were synthesized by reacting BMIMCl (10 g, 57.3 mmol) with a metal chloride, $FeCl_3$ (9.3 g, 57.3 mmol), $CoCl_2$ (3.8 g, 29.3 mmol), or $ZnCl_2$ (3.9 g, 28.6 mmol) at 100 °C, 150 °C, or 80 °C, respectively, for 2-6 h. The liquids were then filtered over a pad of celite and heated to approximately 100 °C to remove unreacted metal chloride. The obtained MILs were stored in an argon atmosphere using conventional Schlenk-line techniques [1]. The MILs yielded 81 – 99 % of the product and were characterized by FTIR spectra shown in Figure S1. The ^{1}H and ^{13}C NMR spectra were measured only for $(BMIM)_2ZnCl_4$, and compared to BMIMCl (Figures S2 and S3). TGA determined thermal stabilities of MILs, and all thermograms are presented in Figure S4. Elemental analysis of the metal content of each IL is presented in Table S1.

Analysis of the metal-based ionic liquids (MILs)

The structural and thermal stability analysis of the synthesized imidazolium-based ILs bearing anionic transition metals, namely $(BMIM)FeCl_4$, $(BMIM)_2CoCl_4$, and $(BMIM)_2ZnCl_4$, were investigated using various analytical techniques, including FTIR, ^{1}H and ^{13}C NMR, AAS and TGA. The FTIR spectra exhibited indicative bands of the imidazolium ring, with characteristic peaks observed at 1630 and 1570 cm^{-1} corresponding to the stretching vibration of C=C and C=N groups, respectively (Figure S1). Additionally, the bands in the range 2800 to 3000 cm^{-1} were attributed to the C-H stretching modes of the butyl chain of the imidazolium ring [2,3]. In the BMIMCl spectra, the peak observed at 853 cm^{-1} attributed to the hydrogen bonding between N-H of the imidazolium ring and the Cl anion was shifted to 843 cm^{-1} in $(BMIM)_2CoCl_4$, and $(BMIM)_2ZnCl_4$, and to 828 cm^{-1} in $(BMIM)FeCl_4$. This is explained by the increased strength of the hydrogen bond resulting from the larger anion species present in the MIL ($ZnCl_4^{2-}$, $CoCl_4^{2-}$, and $FeCl_4^{-}$) [3,4]. The ^{1}H and ^{13}C NMR spectra of $(BMIM)_2ZnCl_4$

further confirmed the formation of an imidazolium ring compared to BMIMCl (Figure S2-S3). This is proven by the presence of signals for δ(^{1}H) at 9.314 (s, N-C*H*-N) for BMIMCl and 9.166 (s, N-C*H*-N) for BMIMZnCl$_4$. The δ(^{13}C) were found at 136.642 (1C, N-*C*H-N) for BMIMCl and 136.530 (1C, N-*C*H-N) for (BMIM)$_2$ZnCl$_4$.

The metal content in the IL was determined by AAS analysis (see Table S1). The cobalt, zinc and iron contents correspond to theoretical values. The water content of the synthesized MILs was further verified using FTIR and TGA/MS analyses. Both spectra exhibited evidence of a minimal amount of adsorbed water in the samples (Figure 2 and Table S1). The thermograms of the MILs showed a decomposition of the adsorbed water from 0.5 to 1 wt% in the temperature range between 120 and 150 °C (Figure 2 (a-c)). Additionally, the synthesized MILs showed overall high thermal stability. The MIL bearing FeCl$_4$ anion started to decompose at T ~ 195 °C, while (BMIM)$_2$CoCl$_4$ and (BMIM)$_2$ZnCl$_4$ at approximately 250 °C. This indicates that (BMIM)$_2$CoCl$_4$ and (BMIM)$_2$ZnCl$_4$ have slightly higher thermal stability than (BMIM)FeCl$_4$.

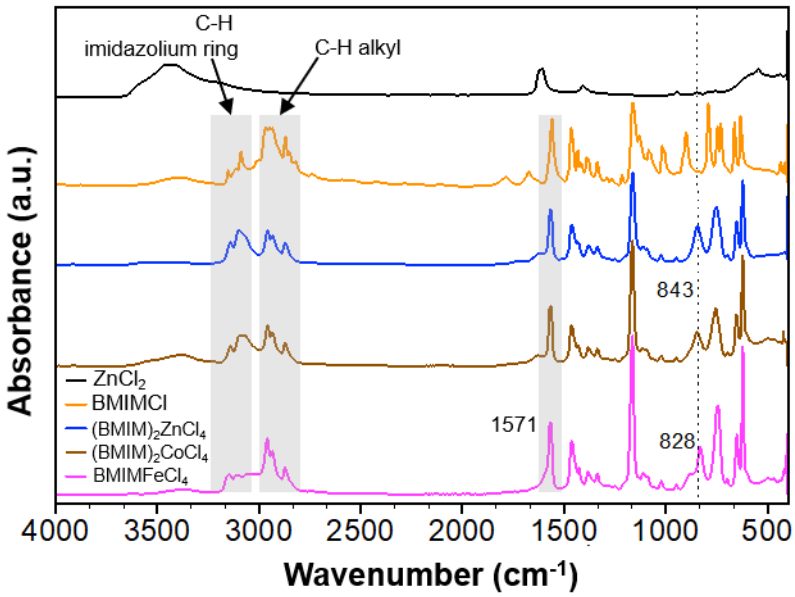

Figure S1. FTIR spectra of BMIMCl, (BMIM)FeCl$_4$ (BMIM)$_2$CoCl$_4$ (BMIM)$_2$ZnCl$_4$.

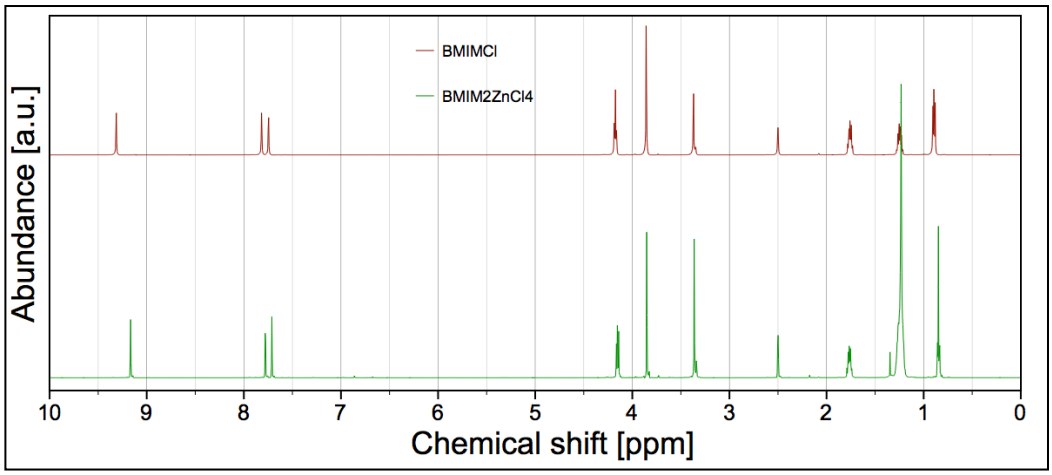

Figure S2. ^{1}H NMR (DMSO-D6) spectra of BMIMCl and $(BMIM)_2ZnCl_4$.
BMIMCl: δ 0.893 (t, H_3C-) 1.247 (m, -CH_2-CH_3) 1.758 (p, -CH_2-CH_2-CH_3) 3.371 (s, H_2O) 3.856 (s, H_3C-N) 4.174 (t, -CH_2-CH_2- CH_2-CH_3) 7.746 (s, H_2C=CH_2-N-R) 7.817 (s, H_2C=CH_2-N-CH_3) 9.314 (s, N-C*H*-N). $BMIMZnCl_4$: δ 0.848 (t, H_3C-) 1.232 (m, -CH_2-CH_3) 1.776 (p, -CH_2-CH_2-CH_3) 3.363 (s, H_2O) 3.851 (s, H_3C-N) 4.152 (t, -CH_2-CH_2- CH_2-CH_3) 7.711 (s, H_2C=CH_2-N-R) 7.779 (s, H_2C=CH_2-N-CH_3) 9.166 (s, N-C*H*-N).

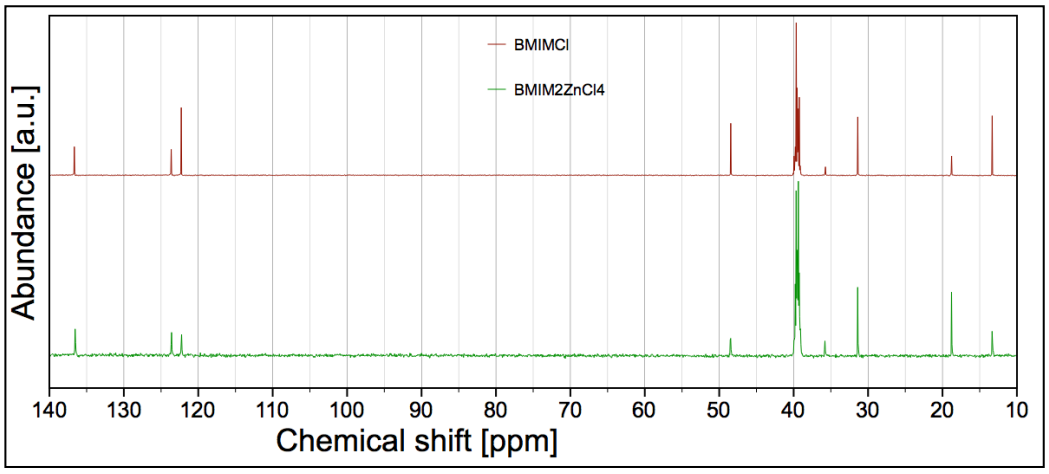

Figure S3. ^{13}C NMR (DMSO-D6) spectra of BMIMCl and $(BMIM)_2ZnCl_4$.
BMIMCl: δ 13.321 (1C, -*C*H_3) 18.793 (1C, -*C*H_2-CH_3) 31.391 (1C, -*C*H_2- CH_2-CH_3) 35.748 (1C, H_3*C*-N) 48.446 (1C, *C*H_2-CH_2- CH_2-CH_3) 122.287 (1C, H_2C=*C*H_2-N-R) 123.621 (1C, H_2C=*C*H_2-N-CH_3) 136.642 (1C, N-*C*H-N). $BMIMZnCl_4$: δ 13.321 (1C, -*C*H_3) 18.793 (1C, -*C*H_2-CH_3) 31.401 (1C, -*C*H_2- CH_2-CH_3) 35.827 (1C, H_3*C*-N) 48.501 (1C, *C*H_2-CH_2- CH_2-CH_3) 122.269 (1C, H_2C=*C*H_2-N-R) 123.615 (1C, H_2C=*C*H_2-N-CH_3) 136.530 (1C, N-*C*H-N).

Table S1. The AAS results showing the metal content of MILs. The TGA/MS results (in nitrogen atmosphere) showing the water content and the onset decomposition temperature ($T_{d,\ onset}$).

	$(BMIM)_2CoCl_4$	$(BMIM)_2ZnCl_4$	$BMIMFeCl_4$
Theoretical metal content, %	12.30	11.03	16.58
Experimental metal content, %	12.74	11.04	16.75
Water content (wt%)	1	1	0.5
$T_{d,\ onset}$ (°C)	243	257	195

Table S2. The dynamic DSC results of the reactive mixture at a heating rate of 5 °C/min using 2.70 mol% of accelerating agent: onset temperature (T_{onset}), maximal peak temperature (T_{max}) and total reaction heat (ΔH_{total}). The glass transition temperature (T_g) of the cured system was determined using the second heating run up to 300 °C at 10 °C/min.

Entry	Formulation	*Cat., phr**	T_{onset}, °C	T_{max}, °C	ΔH_{total}, J/g	T_g, °C
1	No cat.	-	192	237	192±12	110
2	DGEBA/MHHPA/1MIM	1.008	106	130	357±21	134
3	DGEBA/MHHPA/BMIMCl	2.143	101	131	334±16	128
4	DGEBA/MHHPA/ $(BMIM)FeCl_4$	4.024	57	61	343±19	96
5	DGEBA/MHHPA/ $(BMIM)_2CoCl_4$	5.882	97	128	327±14	147
6	DGEBA/MHHPA/ $(BMIM)_2ZnCl_4$	5.962	99	142	331±20	148

*mass related to hundred mass of **DGEBA+MHHPA**

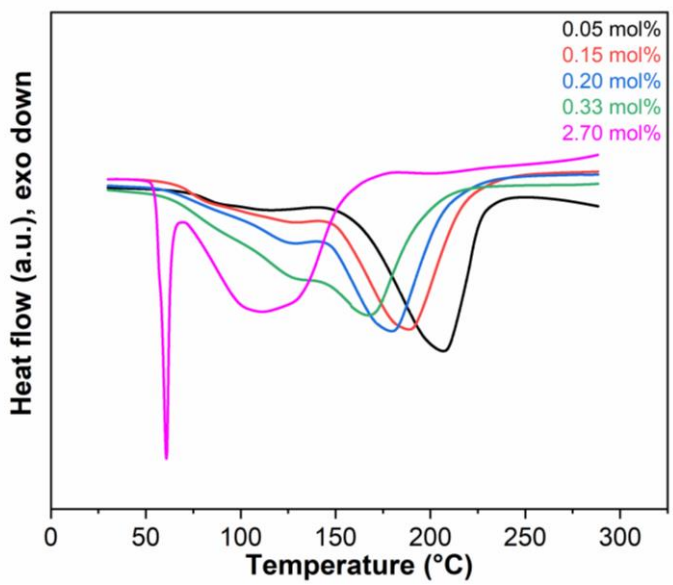

Figure S4. Dynamic DSC results (exo down) of reaction DGEBA/MHHPA/(BMIM)$FeCl_4$ using various mol% of the MIL.

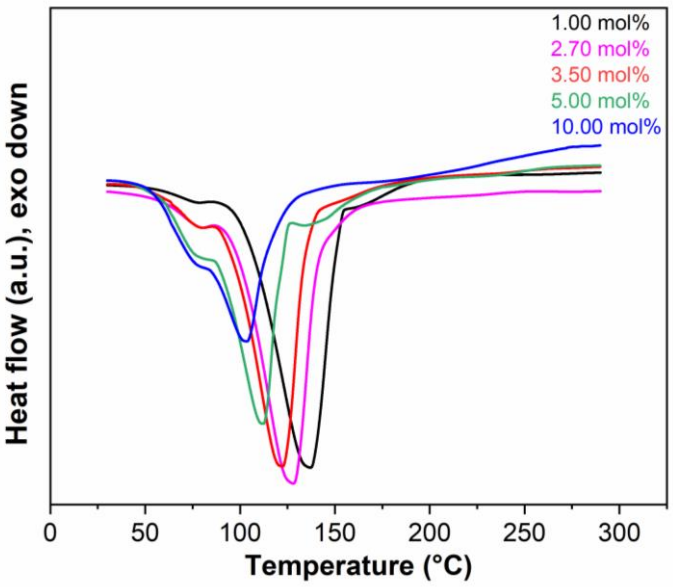

Figure S5. Dynamic DSC results (exo down) of reaction DGEBA/MHHPA/$(BMIM)_2CoCl_4$ using various mol% of the MIL.

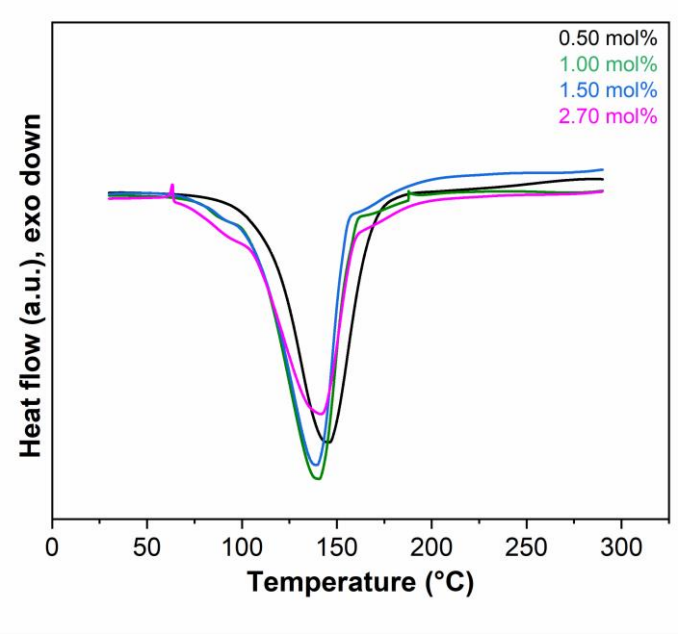

Figure S6. Dynamic DSC results (exo down) of reaction DGEBA/MHHPA/$(BMIM)_2ZnCl_4$ using various mol% of the MIL.

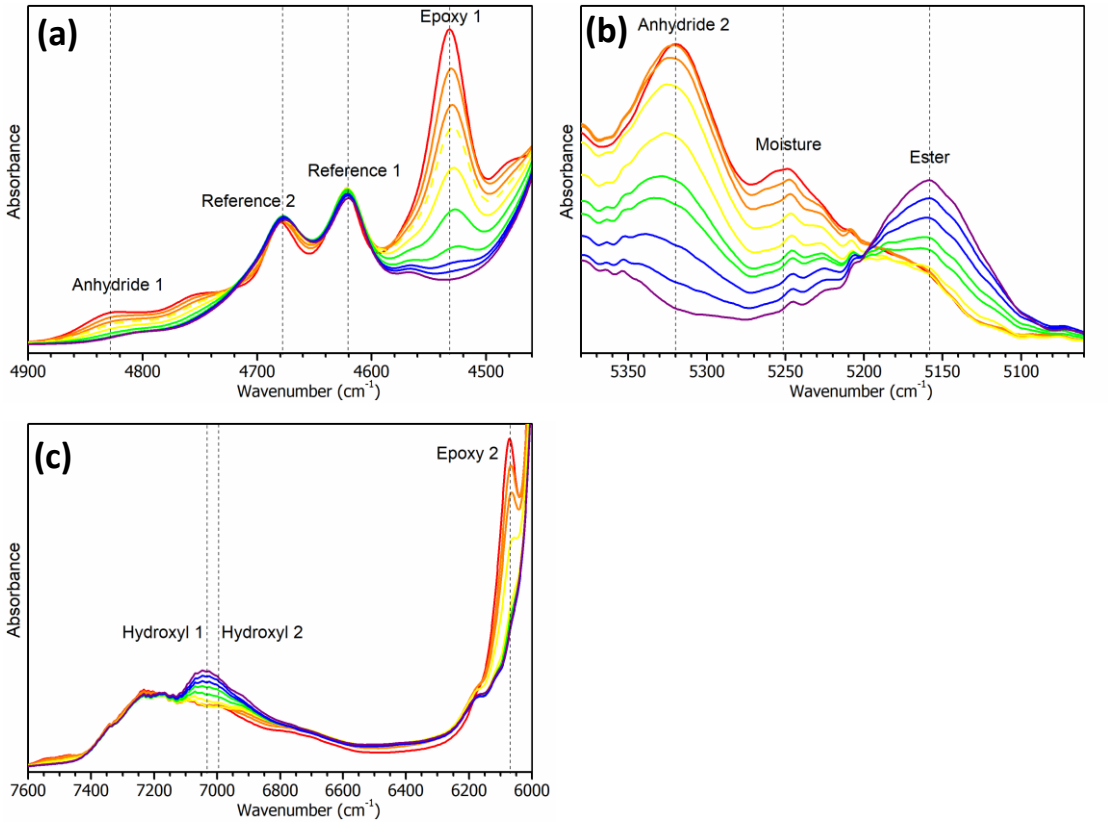

Figure S7. NIR spectra during non-isothermal cross-linking of DGEBA/MHHPA/1MIM showing the evolution of characteristic bands of (a) epoxy, (b) anhydride, moisture and ester, and (c) the hydroxyl bands. Bands from red to purple decrease/increase with the increase in temperature. The moisture band interferes with the ester band in the later stage of the curing process; therefore, it was monitored only in the early phase of the curing process.

Table S3. Assignment of selected bands in NIR spectra.

Wavenumber (cm^{-1})	Assignment	Denotation	Note
7030	O–H stretching, alcohol, first overtone	Hydroxyl 1	Followed together
6985	O–H stretching, carboxylic acid, first overtone	Hydroxyl 2	
6069	C–H stretching of an epoxide methylene group, first overtone	Epoxy 2	
5320	C=O stretching of anhydride, second overtone	Anhydride 2	
5252	Combination band of O–H stretching with H–O–H bending due to moisture	Moisture	Followed
5158	C=O stretching of ester, the second overtone	Ester	Followed
4828	Combination band of C=O stretching of anhydride (first overtone) with C–O stretching	Anhydride 1	Followed
4678	Combination band of aromatic C=C stretching with aromatic C–H stretching	Reference 2	
4622	Combination band of aromatic C=C stretching with aromatic C–H stretching	Reference 1	Reference for followed bands
4530	Combination band of epoxide C–H stretching and C–H bending	Epoxy 1	Followed

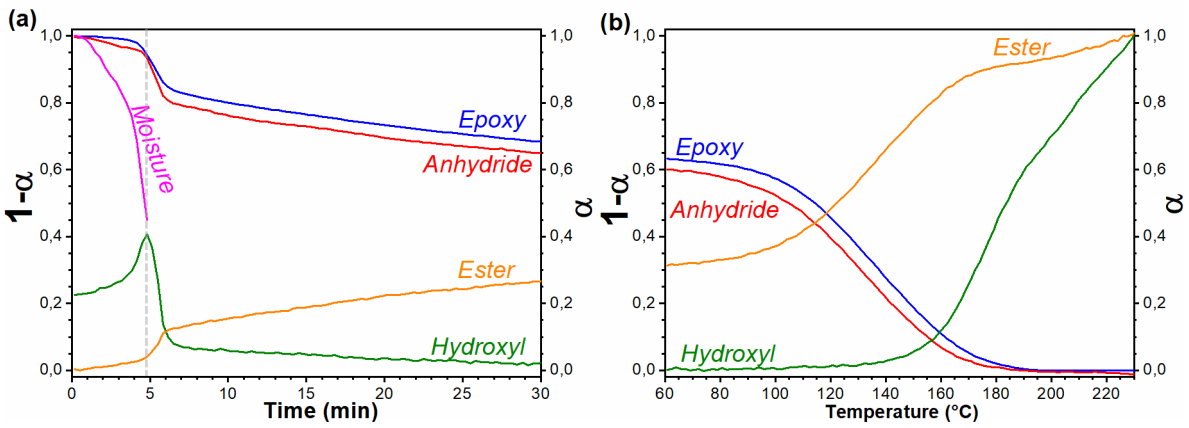

Figure S8. (a) Isothermal NIR of DGEBA/MHHPA/2.70mol% $BMIMFeCl_4$, at 60 °C for 30 min. (b) After 40 min of curing at 60 °C, the reactive mixture was non-isothermally cured at a heating rate of 5 °C/min up to 240 °C, showing an accelerated consumption of epoxy and anhydride groups above ca 100 °C until the full consumption was reached at around 200 °C. At a later stage of curing (>130 °C), the OH groups started to increase again, which indicated the formation of sterically-hindered OH groups due to topological limits of the highly cross-link network. The left axis is for Epoxy, Anhydride and Moisture; the Right axis is for Ester and Hydroxyl.

Table S4. Summary of isothermal DSC data for DGEBA-MHHPA cross-linking using different accelerating agents. The total reaction heat (ΔH_{total}) was determined from the dynamic DSC runs; ΔH_{iso} is the reaction heat during isothermal DSC runs, ΔH_{res} is the residual reaction heat after isothermal curing; ΔH_{loss} is the loss of reaction heat during isothermal DSC runs due to time-lag for reaching and equilibrating target temperature; $\alpha_{initial}$ is the initial conversion of the first point that is recorded during isothermal DSC runs and α_{final} is the final reach conversion during isothermal DSC runs.

Accelerating agent	T (°C)	ΔH_{total} (J/g)	ΔH_{iso} (J/g)	ΔH_{res} (J/g)	ΔH_{loss}[a] (J/g)	$\alpha_{initial}$[b] (%)	α_{final} (%)
1MIM	100	354	306	43	5	1.5	88
	110	354	316	30	8	2.3	92
	120	354	301	18	35	9.9	95
BMIMCl	100	375	315	37	23	6.0	90
	110	375	315	28	32	8.6	93
	120	375	301	25	49	12.8	93
$(BMIM)_2CoCl_4$	90	327	275	21	31	9.3	94
	100	327	292	11	24	7.5	97
	105	327	273	7	47	14.6	98
	110	327	275	5	47	14.5	98
$(BMIM)_2ZnCl_4$	90	321	282	26	13	4.1	92
	100	321	289	13	19	5.8	96
	105	321	266	8	47	14.7	98
$BMIMFeCl_4$	100	342	300	34	8	2.4	90
	110	342	267	24	51	14.9	93
	120	342	255	16	71	20.8	96

[a] $\Delta H_{loss} = \Delta H_{total} - \Delta H_{iso} - \Delta H_{res}$

[b] $\alpha_{initial} = 100 \cdot \Delta H_{loss} / \Delta H_{total}$

Table S5. Kinetic parameters using the Kamal-Sourour model based on isothermal DSC runs of DGEBA-MHHPA systems using different accelerating agents.

Accelerating agent	T (°C)	k_1 (s^{-1})	k_2 (s^{-1})	E_{a1} (kJ/mol)	E_{a2} (kJ/mol)
1MIM	100	$2.7 \cdot 10^{-4}$	$1.6 \cdot 10^{-3}$		
	110	$5.2 \cdot 10^{-4}$	$3.3 \cdot 10^{-3}$	43	88
	120	$5.4 \cdot 10^{-4}$	$6.8 \cdot 10^{-3}$		
BMIMCl	100	$5.8 \cdot 10^{-4}$	$1.0 \cdot 10^{-3}$		
	110	$8.2 \cdot 10^{-4}$	$2.5 \cdot 10^{-3}$	49	97
	120	$1.3 \cdot 10^{-3}$	$4.9 \cdot 10^{-3}$		
$(BMIM)_2CoCl_4$	90	$8.0 \cdot 10^{-4}$	$5.8 \cdot 10^{-4}$		
	100	$1.2 \cdot 10^{-3}$	$1.9 \cdot 10^{-3}$	13	118
	105	$7.8 \cdot 10^{-4}$	$3.8 \cdot 10^{-3}$		
	110	$9.7 \cdot 10^{-4}$	$4.4 \cdot 10^{-3}$		
$(BMIM)_2ZnCl_4$	90	$7.8 \cdot 10^{-4}$	$1.0 \cdot 10^{-4}$		
	100	$1.0 \cdot 10^{-3}$	$6.5 \cdot 10^{-4}$	42	217
	105	$1.4 \cdot 10^{-3}$	$1.7 \cdot 10^{-3}$		
$(BMIM)FeCl_4$	100	$7.3 \cdot 10^{-4}$	0		
	110	$1.3 \cdot 10^{-3}$	0	55	n.d.
	120	$1.8 \cdot 10^{-3}$	$9.4 \cdot 10^{-3}$		

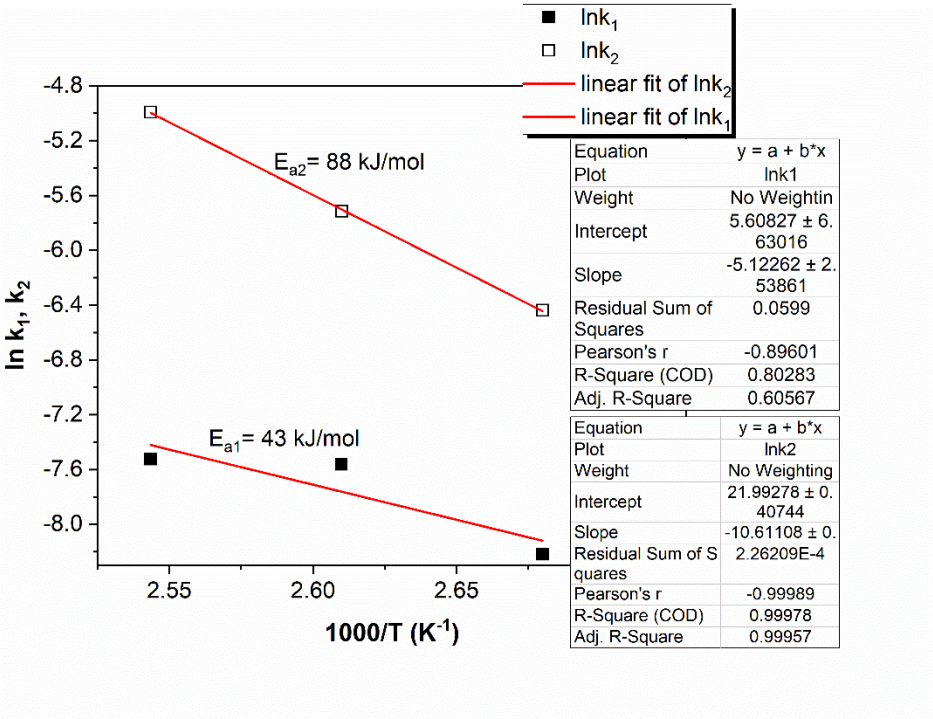

Figure S9. Arrhenius plot of rate constants k_1 and k_2 obtained by the Kamal-Sourour model for the DGEBA/MHHPA/1MIM.

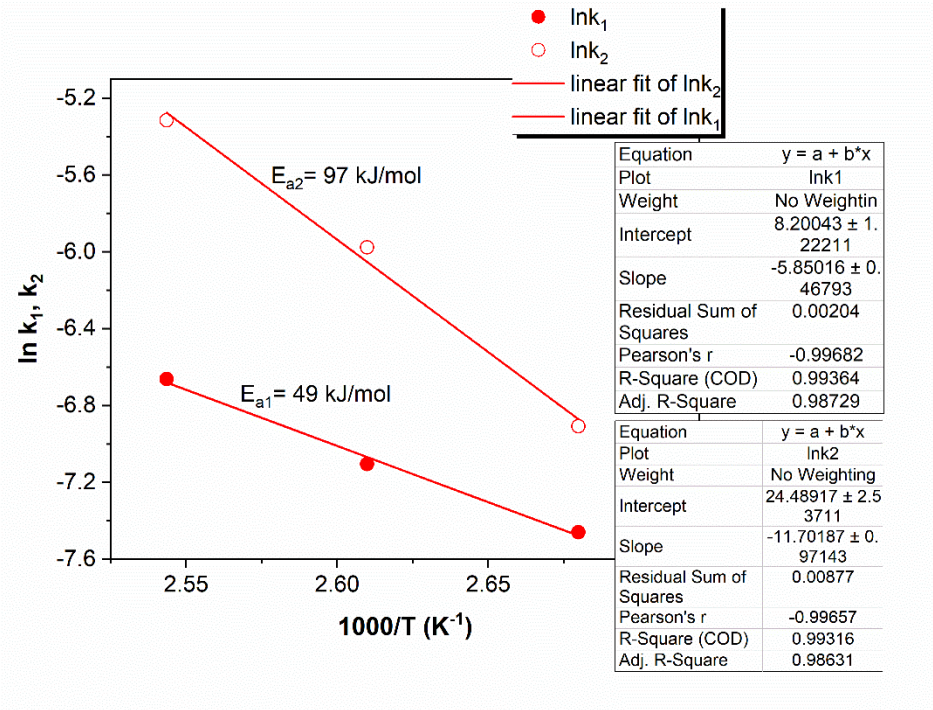

Figure S10. Arrhenius plot of rate constants k_1 and k_2 obtained by the Kamal-Sourour model for the DGEBA/MHHPA/BMIMCl.

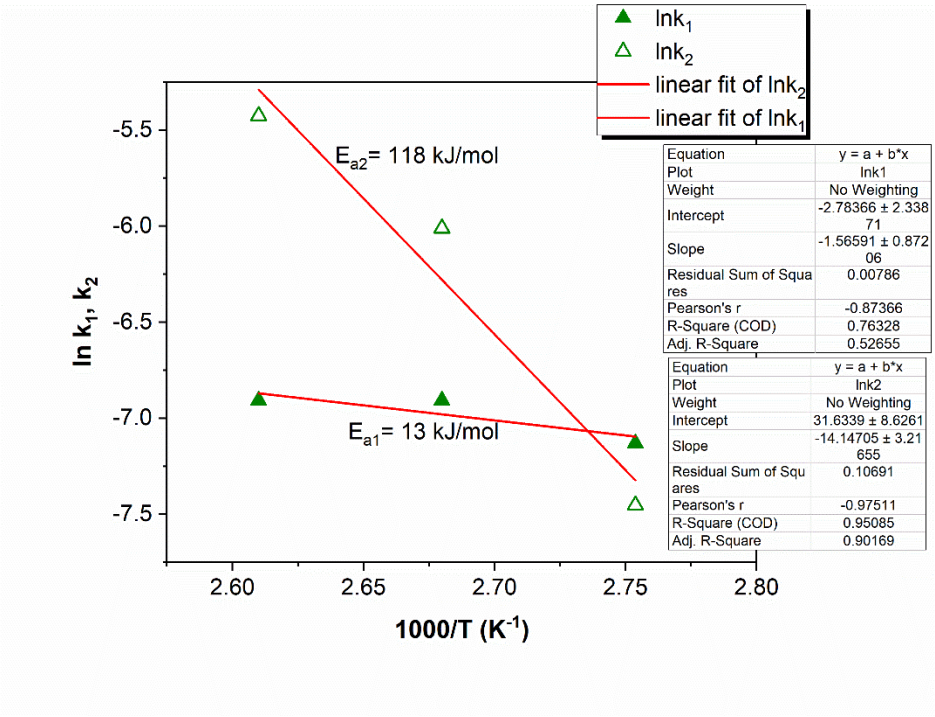

Figure S11. Arrhenius plot of rate constants k_1 and k_2 obtained by the Kamal-Sourour model for the DGEBA/MHHPA/$(BMIM)_2CoCl_4$.

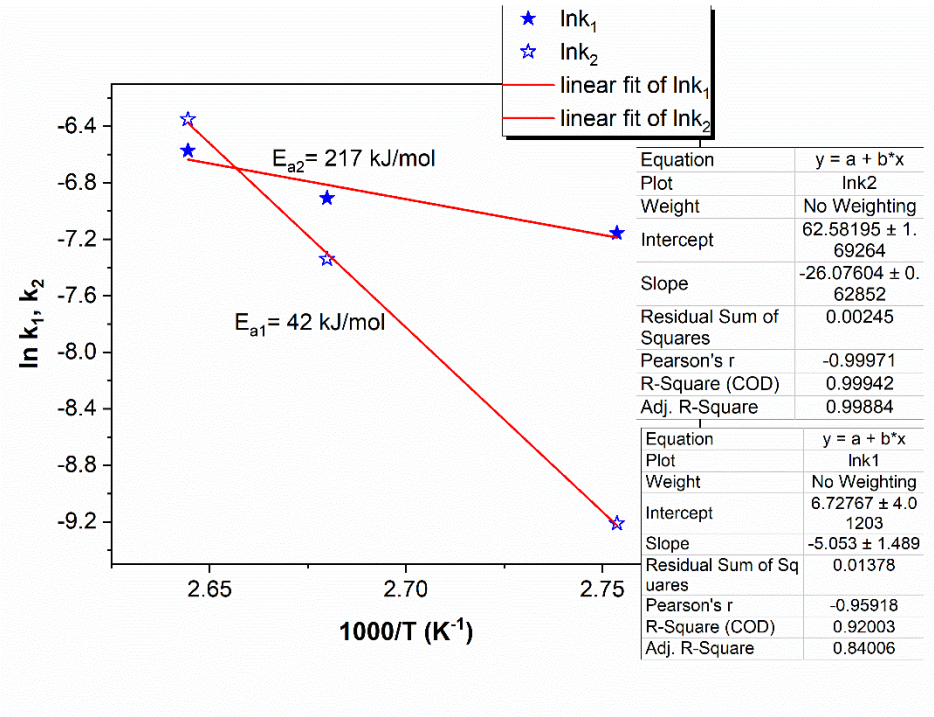

Figure S12. Arrhenius plot of rate constants k_1 and k_2 obtained by the Kamal-Sourour model for the DGEBA/MHHPA/$(BMIM)_2ZnCl_4$.

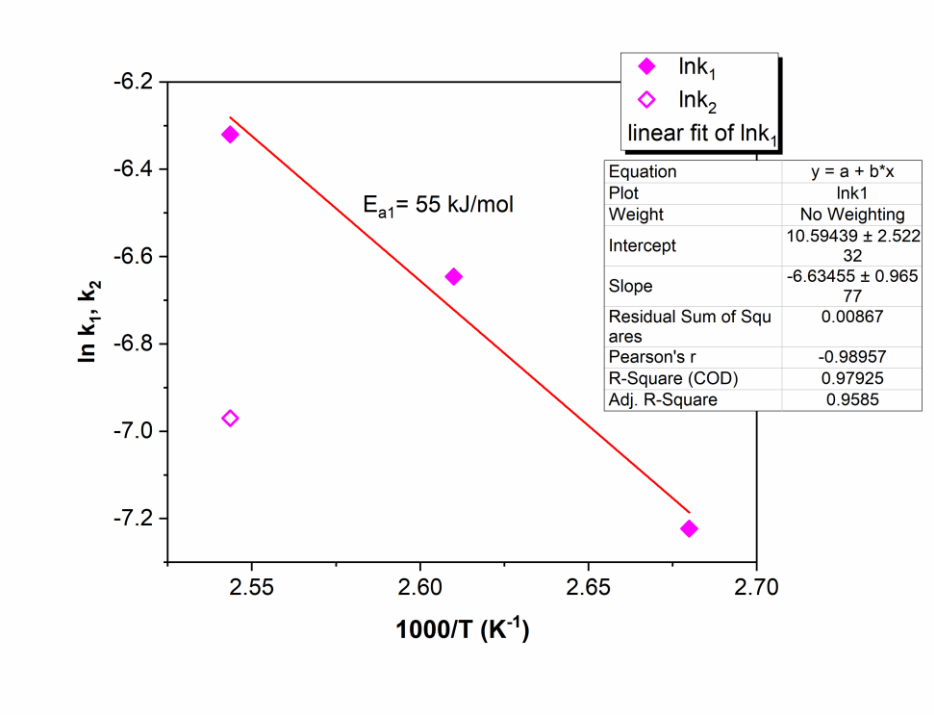

Figure S13. Arrhenius plot of rate constants k_2 obtained by the Kamal-Sourour model for the DGEBA/MHHPA/(BMIM)$FeCl_4$.

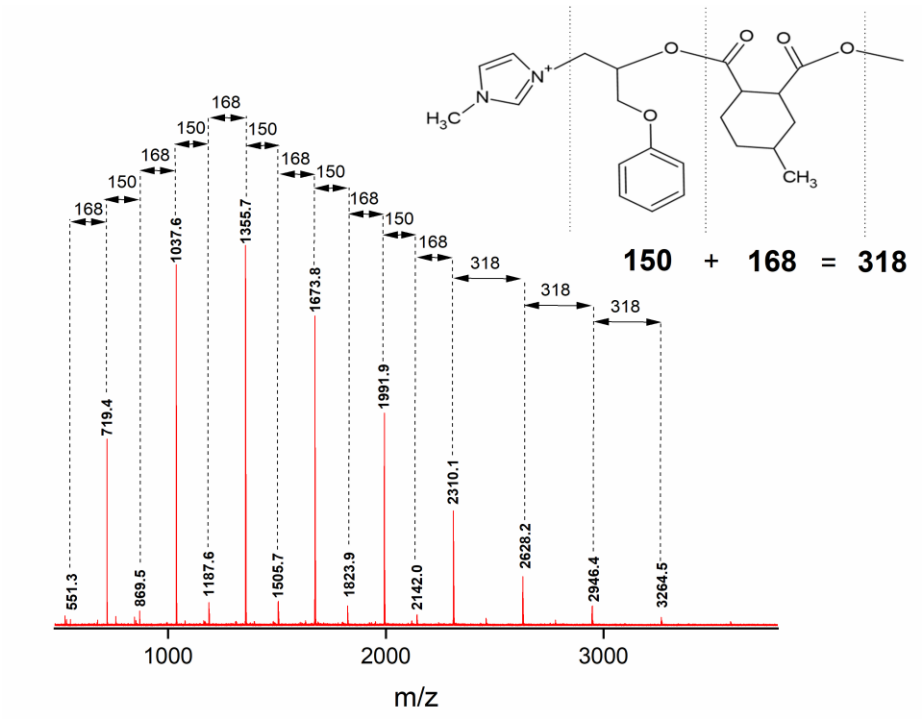

Figure S14. MALDI-TOF mass spectrum of PGE/MHHPA/1MIM after 15 min of reaction at 80 °C.

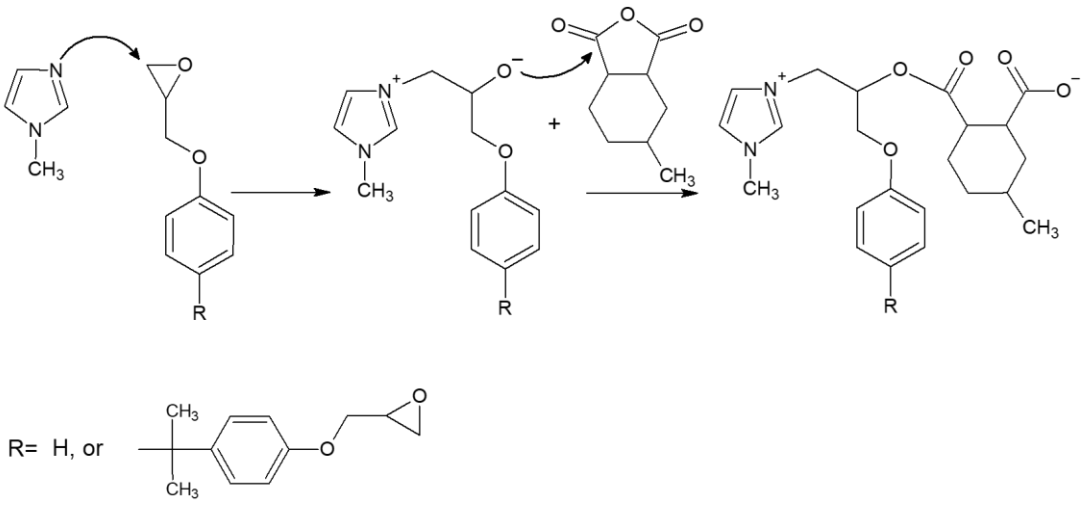

Scheme S1. Initiation and propagation in 1MIM-accelerated epoxy (PGE or DGEBA) – anhydride (MHHPA) anionic copolymerization.

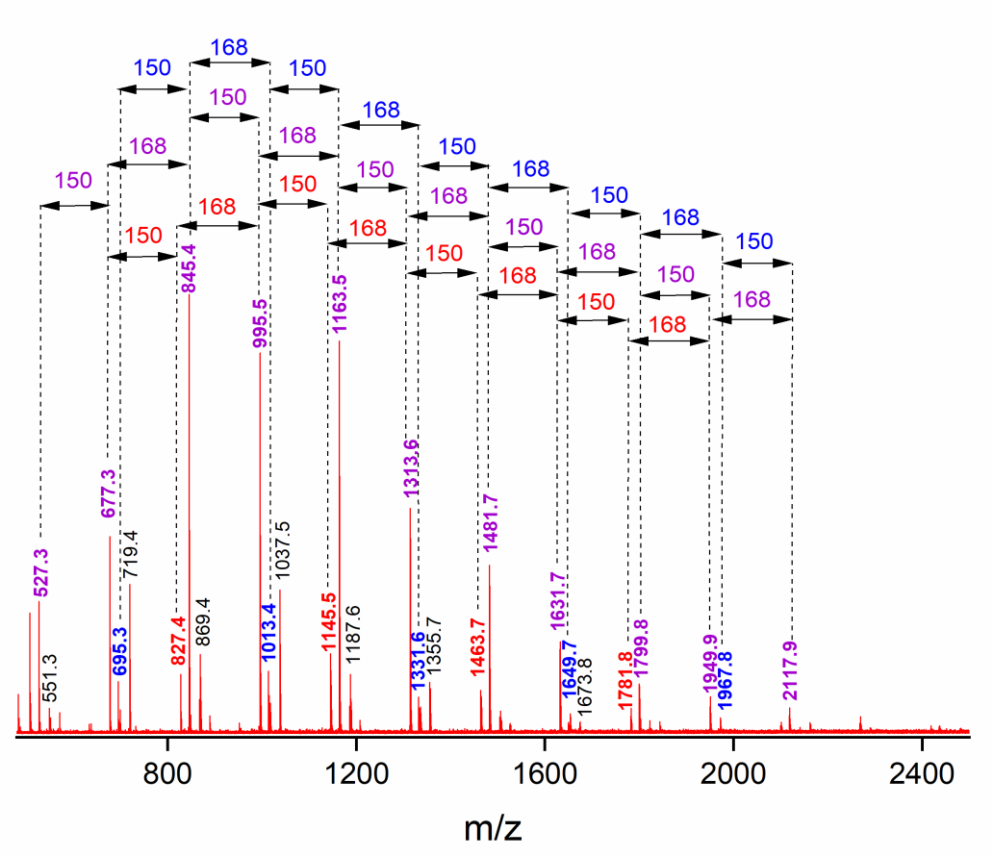

Figure S15. MALDI-TOF mass spectrum of PGE/MHHPA/BMIMCl after 15 min of reaction at 80 °C.

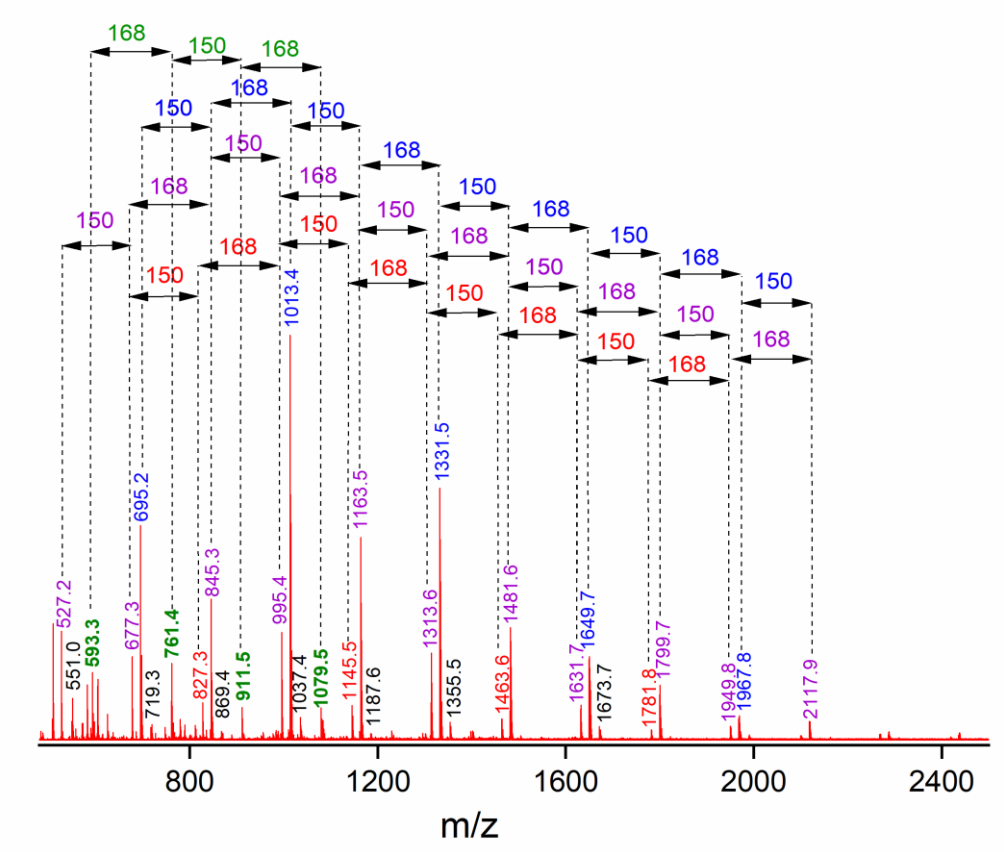

Figure S16. MALDI-TOF mass spectrum of PGE/MHHPA/(BMIM)$FeCl_4$ after 15 min of reaction at 80 °C.

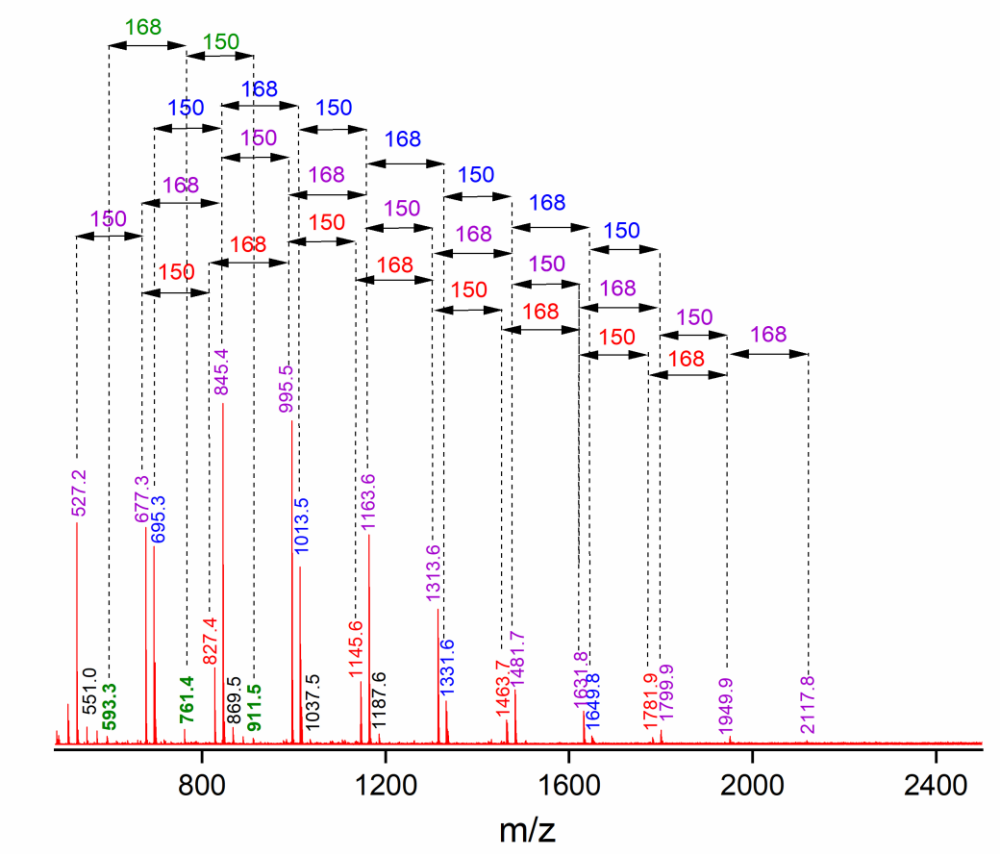

Figure S17. MALDI-TOF mass spectrum of PGE/MHHPA/$(BMIM)_2ZnCl_4$ after 15 min of reaction at 80 °C.

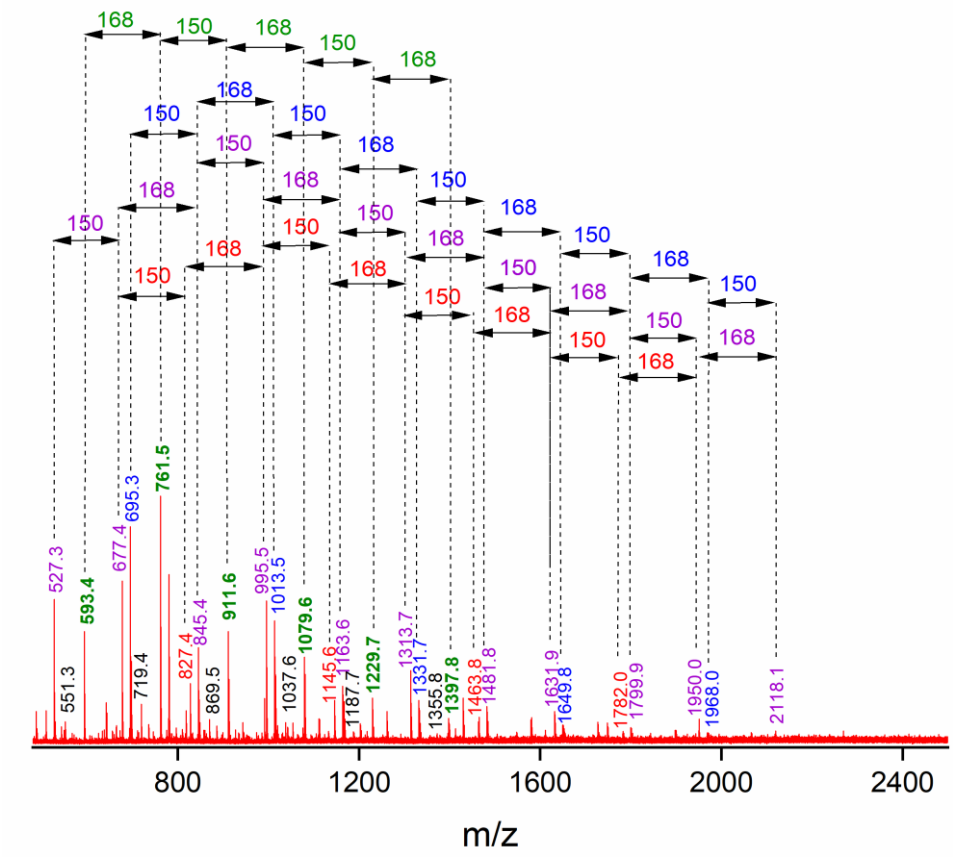

Figure S18. MALDI-TOF mass spectrum of PGE/MHHPA/$(BMIM)_2CoCl_4$ after 15 min of reaction at 80 °C.

Table S6. Dynamic DSC results of the reactive mixture at a heating rate of 5 °C/min.

	DGEBA/MHHPA= 1/1		Dynamic DSC data			
Entries	Catalyst content	Catalyst used	T_{onset}[a], °C	T_{max}[b], °C	ΔH[c], J/g	T_g[d], °C
1	-	No cat.	192	237	192	110
2	2.7 mol%	1MIM	106	130	357	134
3	2.7 mol%	BMIMCl	101	131	334	128
4	0.05 mol%	$(BMIM)FeCl_4$	159	207	267	132
5	0.15 mol%	$(BMIM)FeCl_4$	140	189	342	147
6	0.20 mol%	$(BMIM)FeCl_4$	132	180	338	148
7	0.33 mol%	$(BMIM)FeCl_4$	101	167	337	148
8	0.67 mol%	$(BMIM)FeCl_4$	57	85	331	128
9	2.70 mol%	$(BMIM)FeCl_4$	57	61	343	96
10	0.05 mol%	$(BMIM)_2CoCl_4$	110	137	300	133
11	1.00 mol%	$(BMIM)_2CoCl_4$	102	137	348	145
12	1.50 mol%	$(BMIM)_2CoCl_4$	111	142	326	142
13	2.70 mol%	$(BMIM)_2CoCl_4$	97	128	327	147
14	3.50 mol%	$(BMIM)_2CoCl_4$	92	122	337	130
15	5.00 mol%	$(BMIM)_2CoCl_4$	82	112	325	111
16	10.00 mol%	$(BMIM)_2CoCl_4$	70	103	216	104
17	0.50 mol%	$(BMIM)_2ZnCl_4$	113	146	325	129
18	1.00 mol%	$(BMIM)_2ZnCl_4$	105	140	347	145
19	1.50 mol%	$(BMIM)_2ZnCl_4$	104	140	347	144
20	2.70 mol%	$(BMIM)_2ZnCl_4$	99	142	331	148

[a] Onset temperature of the curing exotherm at 5 °C/min
[b] Temperature at the maximum curing exotherm
[c] Enthalpy of the reaction
[d] Glass transition temperature determined at the midpoint of the transition curve after curing

References

[1] A.M. Borys, An Illustrated Guide to Schlenk Line Techniques, Organometallics. 42 (2023) 182–196. https://doi.org/10.1021/acs.organomet.2c00535.

[2] S. Cha, M. Ao, W. Sung, B. Moon, B. Ahlström, P. Johansson, Y. Ouchi, D. Kim, Structures of ionic liquid-water mixtures investigated by IR and NMR spectroscopy, Phys. Chem. Chem. Phys. 16 (2014) 9591–9601. https://doi.org/10.1039/c4cp00589a.

[3] S. Najafi-Shoa, M. Barikani, M. Ehsani, M. Ghaffari, Cobalt-based ionic liquid grafted on graphene as a heterogeneous catalyst for poly (ethylene terephthalate) glycolysis, Polym. Degrad. Stab. 192 (2021) 109691. https://doi.org/10.1016/j.polymdegradstab.2021.109691.

[4] T.J. Ren, J. Zhang, Y.H. Hu, J.P. Li, M.S. Liu, D.S. Zhao, Extractive desulfurization of fuel oil with metal-based ionic liquids, Chinese Chem. Lett. 26 (2015) 1169–1173. https://doi.org/10.1016/j.cclet.2015.05.023.

Appendix 3

M. Rebei, C. Červinka, A. Mahun, P. Ecorchard, J. Honzíček, S. Livi, R. K. Donato, H. Beneš, Fast carbon dioxide–epoxide cycloaddition catalyzed by metal and metal-free ionic liquids for designing non-isocyanate polyurethanes, *Mater. Adv.*, (2024), Advance Article.

Materials Advances

ROYAL SOCIETY OF CHEMISTRY

PAPER

View Article Online
View Journal

Cite this: DOI: 10.1039/d3ma00852e

Fast carbon dioxide–epoxide cycloaddition catalyzed by metal and metal-free ionic liquids for designing non-isocyanate polyurethanes†

Marwa Rebei,[ab] Ctirad Červinka,[c] Andrii Mahun,[ab] Petra Ecorchard,[d] Jan Honzíček,[e] Sébastien Livi,[f] Ricardo K. Donato[g] and Hynek Beneš *[a]

Received 13th October 2023,
Accepted 28th March 2024

DOI: 10.1039/d3ma00852e

rsc.li/materials-advances

The recycling of industrially produced greenhouse gases, such as CO_2, into high-value-added chemicals is one of the most relevant strategies for reaching climate targets. Herein, we present a two-step strategy for how to efficiently convert renewable carbon dioxide (CO_2) into β-hydroxyurethanes using imidazolium ionic liquids (ILs) bearing metal ($[ZnCl_4]^{2-}$ and $[CoCl_4]^{2-}$) or Cl^- IL-anions as all-in-one catalysts. The first step involves the rapid (1 h) conversion of phenyl glycidyl ether using ILs and supercritical carbon dioxide (7.7 MPa, 80 °C) to cyclic carbonates in high yield (98%). The DFT calculations suggested a comprehensive mechanistic pathway for the IL-catalyzed CO_2-epoxy reaction showing a rate-determining step of the initial epoxide ring opening and the direct participation of IL-anions. Moreover, the applied ILs are also able to catalyze the subsequent reaction of the formed cyclic carbonates with butylamine resulting in fast formation of β-hydroxyurethanes. Thus, the present concept seems to be a promising strategy for designing non-isocyanate polyurethanes (NIPUs).

Introduction

Nowadays, advanced polymeric materials are at the forefront of tackling global challenges, such as environmental issues, while pursuing research on high-performance materials. Thus, the development of new synthetic methods is critical for designing innovative polymer materials and proposing sustainable solutions to meet the requirements of the circular economy, which are durability, reusability, and recyclability. Therefore, scientists must propose functional materials using a design approach to develop molecular brick platforms that allow integration of the required functions at the molecular scale in the initial synthesis steps, for example, the use of industrially produced greenhouse gases, such as CO_2. Their conversion into high-value-added chemicals has become one of the most relevant strategies to reduce global warming and thus limit climate change (the CO_2 concentration in the atmosphere reached levels above 412 ppm in 2020).[1–4]

CO_2 is an inexpensive, non-flammable, and abundant carbon resource, rendering its use in polymer synthesis economically viable on an industrial scale.[1,5–7] In this context, the chemical fixation of CO_2 by cycloaddition of the epoxide ring represents an environmentally benign route to produce polyfunctional cyclic carbonate-based monomers.[8–11] Naturally, the synthesis of cyclic carbonates *via* CO_2 cycloaddition requires catalysts, *e.g.* aluminium porphyrin derivatives[12] or metal-containing catalysts such as zinc and cobalt complexes, usually active at high reaction temperatures and requiring the use of a solvent.[13–15] One of the promising applications of cyclic carbonates is the preparation of so-called non-isocyanate polyurethanes (NIPUs), which are synthesized by ring-opening polymerization of polyfunctional cyclic carbonate monomers with polyamines. NIPUs represent a promising alternative to replace conventional polyurethanes (PUs).[12,16] Nevertheless, the fabrication of NIPUs from cyclic carbonates[17–19] usually requires the addition of suitable catalysts and solvents,[20,21] long reaction time[22] and high temperature,[23] which decreases

[a] Institute of Macromolecular Chemistry of the Czech Academy of Sciences, Heyrovského nám.2, Prague 6, 162 00, Czech Republic. E-mail: benesh@imc.cas.cz
[b] Department of Physical and Macromolecular Chemistry, Faculty of Science, Charles University, Hlavova 8, 12843 Prague, Czech Republic
[c] Department of Physical Chemistry, University of Chemistry and Technology Prague Technická 5, CZ-166 28, Prague 6, Czech Republic
[d] Institute of Inorganic Chemistry of the Czech Academy of Sciences, Husinec-Řež 1001, 250 68 Řež, Czech Republic
[e] Institute of Chemistry and Technology of Macromolecular Materials, Faculty of Chemical Technology, University of Pardubice, Studentská 573, 532 10, Pardubice, Czech Republic
[f] Université de Lyon, CNRS, Université Claude Bernard Lyon 1, INSA Lyon, Université Jean Monnet, UMR 5223, Ingénierie des Matériaux Polymères, F-69621 Cédex, France
[g] National University of Singapore, Center for Advanced 2D Materials, Singapore 117546, Singapore

† Electronic supplementary information (ESI) available. See DOI: https://doi.org/10.1039/d3ma00852e

the reaction sustainability features and environmental aspects. Therefore, the development of new materials enabling efficient CO_2 absorption, capture and NIPU synthesis presents a challenging task to overcome the above-mentioned drawbacks.

Recently, imidazolium, phosphonium, and ammonium-based ionic liquids (ILs) were found to be suitable catalysts for the CO_2 addition to epoxides due to their high thermal stability, tunable structure and simple synthetic routes.[18–20,24–26] Furthermore, ILs offer value by stabilizing metal atoms within their structure, without deactivating the metal's catalytic functionality and synergizing it with its own properties. The result is a functionalized-metal-containing IL (MIL) with high catalytic activity, where the metal atom can be incorporated by the anion while the cation is, *e.g.*, a catalytically active imidazolium ring.[27] These MILs have demonstrated their efficacy as catalysts/initiators for ring-opening polymerization (ROP) reactions of lactones[28–30] and epoxides.[31] Furthermore, the utilization of metal–organic frameworks (MOFs) incorporating ILs has emerged as a promising strategy for the preparation of recyclable porous catalysts employed in the CO_2 cycloaddition to epoxide.[32] However, this approach targets the synthesis of catalysts with desirable properties such as high surface area and porosity, which facilitates the CO_2 adsorption into epoxide compounds efficiently while allowing the fast and facile regeneration of the catalyst; however, such catalysts require high temperatures, long reaction times (12–24 h), and the use of an organic solvent, resulting in less environmentally friendly processes.[33–35]

Based on previous findings showing the remarkable catalytic activity of imidazolium ILs for epoxy ring opening,[36] herein we further investigate the potential of imidazolium ILs in CO_2 cycloaddition. Moreover, we explore the catalytic potential of discrete MILs for the copolymerization of CO_2 and epoxides.[37–39] Herein, we hypothesize that the MIL introduced in the initial step for the synthesis of cyclic carbonates can also catalyse the subsequent reaction between the cyclic carbonates and amines leading to hydroxyurethanes.

In this study, three distinct ILs, a metal-free IL (1-butyl-2-methylimidazolium chloride, BMIMCl) and two imidazolium MILs bearing $[ZnCl_4]^{2-}$ and $[CoCl_4]^{2-}$ anions, were tested as all-in-one catalysts for both the formation of cyclic carbonates and their subsequent aminolysis (ring opening) producing β-hydroxyurethanes. First, the conversion of epoxy groups of monofunctional phenyl glycidyl ether (PGE) to cyclic carbonates catalyzed by ILs was studied using FTIR and NMR spectroscopy. Based on the obtained experimental data and DFT calculations, a comprehensive mechanism of the IL-catalyzed CO_2-epoxy reaction was suggested. The subsequent reaction of the synthesized cyclic carbonates with butylamine without additional catalysis was then studied to verify the future potential of this approach for the rapid solvent-free preparation of NIPU materials.

Experimental

Materials and synthesis

PGE was purchased from Sigma-Aldrich (99%, 150 g mol^{-1}), 1-butyl-3-methylimidazolium chloride (BMIMCl, 99%, 174.67 g mol^{-1}) was purchased from Iolitech and purified before use as described in our previous paper.[36] *n*-Butylamine was purchased from Fluka Chemicals (73.14 g mol^{-1}). The structures of epoxy monomers, amines, and all ILs used are shown in Fig. 1.

Synthesis of bis(1-butyl-3-methylimidazolium) tetrachlorozincate(II), $(BMIM)_2ZnCl_4$

$(BMIM)_2ZnCl_4$ was synthesized by treating BMIMCl (10 g, 57.3 mmol) with $ZnCl_2$ (3.9 g, 28.6 mmol). The reaction mixture was heated to 80 °C for 6 h. The obtained $(BMIM)_2ZnCl_4$ appears as a yellow viscous liquid. Yield: 13.75 g (28.3 mmol, 99%). The ^{13}C and ^{1}H NMR spectra are given in the ESI† (Fig. S1 and S2).

Synthesis of bis(1-butyl-3-methylimidazolium) tetrachlorocobaltate(II), $(BMIM)_2CoCl_4$

$(BMIM)_2CoCl_4$ was synthesized by treating BMIMCl (10 g, 57.3 mmol) with $CoCl_2$ (3.8 g, 29.3 mmol). The reaction mixture was heated to 150 °C for 2 h. The unreacted $CoCl_2$ was removed by filtration over a short Celite pad heated to ~100 °C. The obtained $(BMIM)_2CoCl_4$ appears as a blue viscous liquid. Yield: 13.3 g (27.8 mmol, 97%). The synthesized $(BMIM)_2CoCl_4$ was not characterized using NMR spectroscopy due to its magnetic properties.

Synthesis of cyclic carbonates

The CO_2 addition reactions were performed under supercritical CO_2 (sCO_2) using a stainless-steel high-pressure reactor equipped with a pressure control regulator under solvent-free conditions. PGE (**1a**) was reacted with ILs, *i.e*, BMIMCl, $(BMIM)_2ZnCl_4$, or $(BMIM)_2CoCl_4$, added at various concentrations (1, 5, or 10 mol%) to an open aluminium pan, as shown in Scheme 1(a). The mixture was manually mixed to obtain a

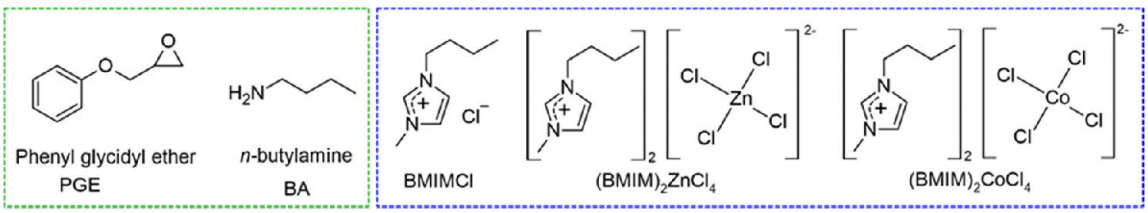

Fig. 1 Structures and acronyms of epoxy monomers, amines and ionic liquids used.

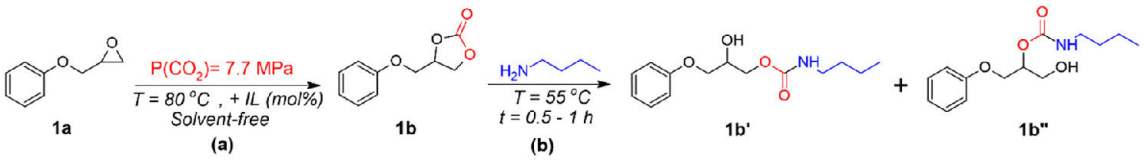

Scheme 1 Simplified schemes of (a) cycloaddition reaction for PGE using ILs, and (b) synthesis of β-hydroxyurethanes from cyclic carbonate.

transparent homogeneous liquid, which was introduced inside the CO_2 reactor. Then, air and moisture were eliminated by purging the reactor with low-CO_2 pressure at RT for 5 min. The reactor containing the reaction mixture was connected to the sCO_2 gas cylinder for the entire reaction time (1 h) at a pressure of 7.7 MPa and a temperature of 80 °C. Afterward, sCO_2 was slowly released, and the reactor was cooled down at room temperature.

The reactions were performed at different times, temperatures, and pressures to reach the final optimal reaction conditions (catalyst loading = 10 mol%, T = 80 °C, and $P(sCO_2)$ = 7.7 MPa) and were subject to FTIR and NMR characterizations.

Synthesis of β-hydroxyurethanes

The cyclic carbonates (**1b**) obtained from the PGE/CO_2/IL reaction were mixed in a stoichiometric amount of *n*-butylamine (BA) without the addition of any solvent or co-catalyst, as shown in Scheme 1(b). The reaction mixture was stirred under mild conditions (T = 55 °C) for 0.5 to 1 h. The reaction progress was followed by FTIR spectroscopy, by following the disappearance of the peak at approximately 1780 cm^{-1} related to the carbonate C—O, of the cyclic carbonate.[31] The disappearance of such a peak proves the ring-opening of the cyclic carbonate and the proceeding of the reaction with functional groups (primary amines). The obtained products were measured in ^{1}H NMR to confirm the structure and provide the β-hydroxyurethane yields.

Characterization

Metal-based ionic liquids characterization techniques

FTIR measurements were performed using a Nicolet iS50 or Nicolet Nexus 670 FTIR spectrometer (Thermo Fisher Scientific). Mid-FTIR was acquired using a built-in diamond ATR (attenuated total reflection) crystal in the region of 4000–400 cm^{-1} (data spacing = 0.5 cm^{-1}). FTIR spectroscopy is considered an easy tool that provides fast proof of the formed characteristic functions, such as the imidazolium ring and alkyl chains. ^{1}H and ^{13}C NMR spectra were recorded using a JEOL 600 MHz (14.1 T) spectrometer, to confirm the structure and characteristic bands of the formed MIL. TGA was performed using a thermogravimetric analyzer Pyris 1 TGA (PerkinElmer) under nitrogen flow (25 cm^3 min^{-1}). A sample of *ca.* 5 mg was heated from 30 to 800 °C at a heating rate of 10 °C min^{-1}. TGA was carried out to study the thermal stability of the MIL. Elemental analysis (AAS) was used to determine the metal content (Co and Zn) in each MIL. The amount of the sample adjusted according to the expected content of the measured element (2–10 mg) was weighed into pre-weighed Eppendorf tubes under dry air in a glove box. The weighed samples were then quantitatively transferred into the water of MilliQ purity in a ratio of 1 : 50. The content of Co and Zn was measured by atomic absorption spectrometry (AAS) using an atomic absorption spectrometer (PerkinElmer, model 3110) with a hollow cathode lamp emitting the spectrum specific for Co and Zn as the light source. An external calibration was used.

Cyclic carbonates' characterization techniques

FTIR measurements of the samples were performed using a Spectrum 100 spectrometer (PerkinElmer) equipped with a mercury–cadmium–telluride (MCT) detector and a universal ATR (attenuated total reflectance) accessory with a diamond prism. The spectra were averaged over 4 scans at a resolution of 4 cm^{-1}. The disappearance of the peak at ~915 cm^{-1} is followed during the reaction as it is attributed to the C–O stretching of the oxirane group.[36,40] Also, the formation of the cyclic carbonates is followed by the intensity increase of the band at ~1790 cm^{-1}.[17] The conversions of epoxy functions were calculated from the integral intensity of the absorption band at 915 cm^{-1} (A) and the reference band at 1600 cm^{-1} (A_{ref}) according to eqn (1):

$$\alpha_{FTIR} = \left(1 - \frac{A}{A_0} \Big/ \frac{A_{ref}}{A_{0;ref}}\right) \times 100 \quad (1)$$

Parameters A_0 and $A_{0;ref}$ are the intensities of the absorption bands for neat epoxy resin at given wavenumbers.

^{1}H NMR spectra were recorded using a Bruker NEO 400 spectrometer operating at 400.1 MHz. NMR spectroscopy was utilized to investigate the structure of organic compounds, determine the components and products of reactions, calculate the reaction yields and provide the molar ratio of isomeric products. All the investigated samples were dissolved in DMSO-d_6 at 295 K. ^{1}H NMR spectra were acquired by applying a 90° pulse (width = 18 μs) with a 10 s recycle delay and 32 scans. The chemical shifts were relative to TMS using hexamethyldisiloxane (HMDSO, 0.05 ppm from TMS in ^{1}H spectra) as an internal standard. In general, the conversion of the initial reagent (*i.e.* epoxides or cyclic carbonates) can be calculated using the following equation (eqn (2)):

$$\alpha_{NMR} = \left(1 - \frac{I_t}{I_0}\right) \times 100 \quad (2)$$

where I_0 and I_t are intensities of the signal from the epoxy ring or cyclic carbonate substituents in the initial mixture at zero

time of the reaction and at a certain time (t) of the reaction, respectively. Melting points of the cyclic carbonates were measured using DSC Q2000 (TA instruments) on samples (10.0 ± 0.5 mg) in hermetically sealed aluminium pans. Experiments were carried out at a heating rate of 10 °C min^{-1}, from 0 to 100 °C (heating/cooling/heating), under nitrogen flow (80 cm^3 min^{-1}).

Computational models

The initial modelling setup assumed a three-molecular gas-phase (isolated) cluster composed of a PGE molecule, a carbon dioxide molecule, and a chloride anion. To investigate the impact of the solvent on the reaction barriers, up to two BMIM cations and an additional chloride anion were optionally included in the simulated clusters for comparison.

Generation of initial structures

First, to obtain a reasonable initial estimate of the geometry of molecular clusters of reactants, intermediate molecules, and products, all participating in individual reaction steps, a simulation annealing on the level of classical molecular dynamics (MD) was performed. This consists of simulating the motion of clusters of several target molecules upon a gradual slow cooling. It starts at an elevated temperature of 227 °C allowing the simulated clusters to escape any spurious potential energy wells. The temperature of the simulated clusters near absolute zero, −273.15 °C, was then reached after simulating its trajectory covering a 2 μs period. Such a procedure typically yields cluster conformations that correspond to the global minimum of their potential energy,[41] which is important to preselect the most beneficial intermolecular contacts and intramolecular conformations of the relevant flexible molecules out of the large space of all theoretical conformations and mutual arrangements of molecules in such clusters. Performing this initial step using the cheap classical MD simulations saves computational resources in the latter stage.

All simulated annealing runs were performed in Lammps software,[42] using an all-atom non-polarizable OPLS force field and a 1 fs time integration step. For BMIMCl, the established CL&P model was used,[43] whereas a flexible force field model was used for carbon dioxide.[44] For PGE, being the primary reactant, and for 1-chloro-3-phenoxypropan-2-olate and 1-chloro-3-phenoxypropan-2-yl carbonate, both expected to occur in the reaction mechanism, the LigParGen utility[45] was used to generate all the required harmonic bonding parameters, OPLS torsion parameters and Lennard-Jones parameters for dispersion interactions according to the OPLS force field library.[46] Atomic charges in the given molecular entities were adopted from the CM1A model, scaling the atomic charges by the default 1.0 factor.[47]

DFT calculations

Geometries of the simulation-annealed clusters were further optimized using density functional theory in Gaussian 16[48] at the B3LYP-D3(BJ)/6-311+G(d,p) level of theory[49,50] to verify the dynamical stability of all optimized configurations of reactants, intermediates and products. Tentative relaxed scans of the potential energy upon variation of the reaction coordinates were attempted to glimpse the possible geometries of the relevant transition states. Finally, geometries of the transition states, corresponding to saddle points on the potential energy surface, and thus determining the reaction energy barriers, were optimized using the Synchronous Transit-Guided Quasi-Newton[51] method as implemented in Gaussian 16. Frequencies of the fundamental vibrational modes were calculated for the clusters of relevant species within the harmonic approximation to assess the thermal and entropic effects on the activation energies. These were plugged together with molecular masses and moments of inertia (based on the optimized geometries) to the rigid-rotor harmonic-oscillator model,[52] yielding enthalpies and Gibbs free energies of all target molecules at ambient conditions. This DFT-based procedure consistently yields relatively accurate energies, allowing us to qualitatively rank the relative stability and thermochemical relationships among the present molecules.

Solvation models

Since the proposed reactions take place in a highly polar medium, a combination of implicit and explicit solvation models was considered to address the solvation effects. The polarizable continuum model using the integral equation formalism[53] was used for modelling the solvent implicitly. Solvent parameters had to be newly defined according to an analysis of the experimental bulk properties of BMIMCl. Namely, its relative permittivity was estimated to be 8.500, resulting from an interpolation of literature data within a homologous series of similar ionic liquids;[54,55] its refractivity was estimated at 1.532, resulting from extrapolations of data measured for binary mixtures, and an effective radius 4.001 Å of the ion pair was estimated from its liquid phase density.[56] As a step towards the explicit solvation, all calculations were performed for comparison also in the explicit presence of either only a single chloride anion, or a single BMIMCl ion pair, or two BMIMCl ion pairs for comparison.

Results and discussion

Synthesis of cyclic carbonates

PGE was reacted with supercritical CO_2 and two types of ILs: (i) the metal-free ILs (BMIMCl) or (ii) the MILs denoted $(BMIM)_2ZnCl_4$ and $(BMIM)_2CoCl_4$ under solvent-free and co-catalyst-free conditions to receive cyclic carbonates. The synthesized MILs were characterized by various techniques, such as FTIR, TGA, NMR, and a detailed discussion of their confirmed structures and thermal stabilities is given in the ESI† (Fig. S1–S3). First, PGE/CO_2/BMIMCl mixtures with IL concentrations of 1, 5 and 10 mol% were reacted in supercritical CO_2 conditions (1 h at 80 °C, 7.7 MPa). The reaction yielded solid materials with

Table 1 CO_2 cycloaddition to PGE catalyzed by ILs: yields and conditions[a]

Entry	IL	IL loading [mol%]	α_{FTIR}[b] (%)	α_{NMR}[c] (%)	TOF[d]	T_m (°C)[e]
1	BMIMCl	5	—	97	9.7	87
2	BMIMCl	10	94	98	9.8	75
3	$(BMIM)_2CoCl_4$	10	99	99	9.9	88
4	$(BMIM)_2ZnCl_4$	10	93	98	9.8	76

[a] Reaction conditions: catalyst loading [mol%] with respect to PGE,7.7 MPa of CO_2, 80 °C, 1 h. [b] The cyclic carbonates yield calculated *via* FTIR spectra (eqn (1)). [c] The cyclic carbonates yield was calculated from the ^{1}H NMR spectra (eqn (2)). [d] TOF related to IL: yield/[(IL loading in mol%) × time]. [e] Melting temperature of cyclic carbonates determined as the onset of melting endotherm from the DSC runs.

melting temperatures (T_m) between 75 and 88 °C, confirmed by DSC (Table 1).

The FTIR spectroscopy allowed fast monitoring of the reaction progress as it constitutes an easy tool to follow the formation of specific functional groups, such as the carbonate bond C—O of cyclic carbonates (structure **1b**, in Scheme 1). Thus, the FTIR spectra of the product with 10 mol% of BMIMCl showed the disappearance of the characteristic peak at 915 cm^{-1} confirming the opening of the oxirane ring.[56–58] This proves at first glance the catalytic ability of imidazolium-based ILs to initiate the ring-opening of epoxy monomers, which is in line with our previous findings using BMIMCl.[36] The use of a lower concentration of ILs (1 and 5 mol%) revealed only a partial opening of epoxy groups (Fig. S4, ESI†). Nevertheless, the formation of cyclic carbonates was observed in all the formed products with all IL concentrations. This is evidenced by the appearance of a new distinct peak at 1787 cm^{-1}, attributed to the carbonate group C—O of cyclic carbonate.[59–62] In summary, it seems that an IL composition of 10 mol% is ideal for obtaining a full epoxy consumption within 1 h in favor of cyclic carbonate formation. Therefore, this concentration was adopted to investigate the proposed systems further. Accordingly, the yield of cyclic carbonates calculated from ^{1}H NMR (eqn (2)) was determined to be 98% and 97% for 10 and 5 mol% of BMIMCl, respectively, while the use of only 1 mol% BMIMCl was not sufficient to achieve the desired cyclic carbonate function. Other studies also reported

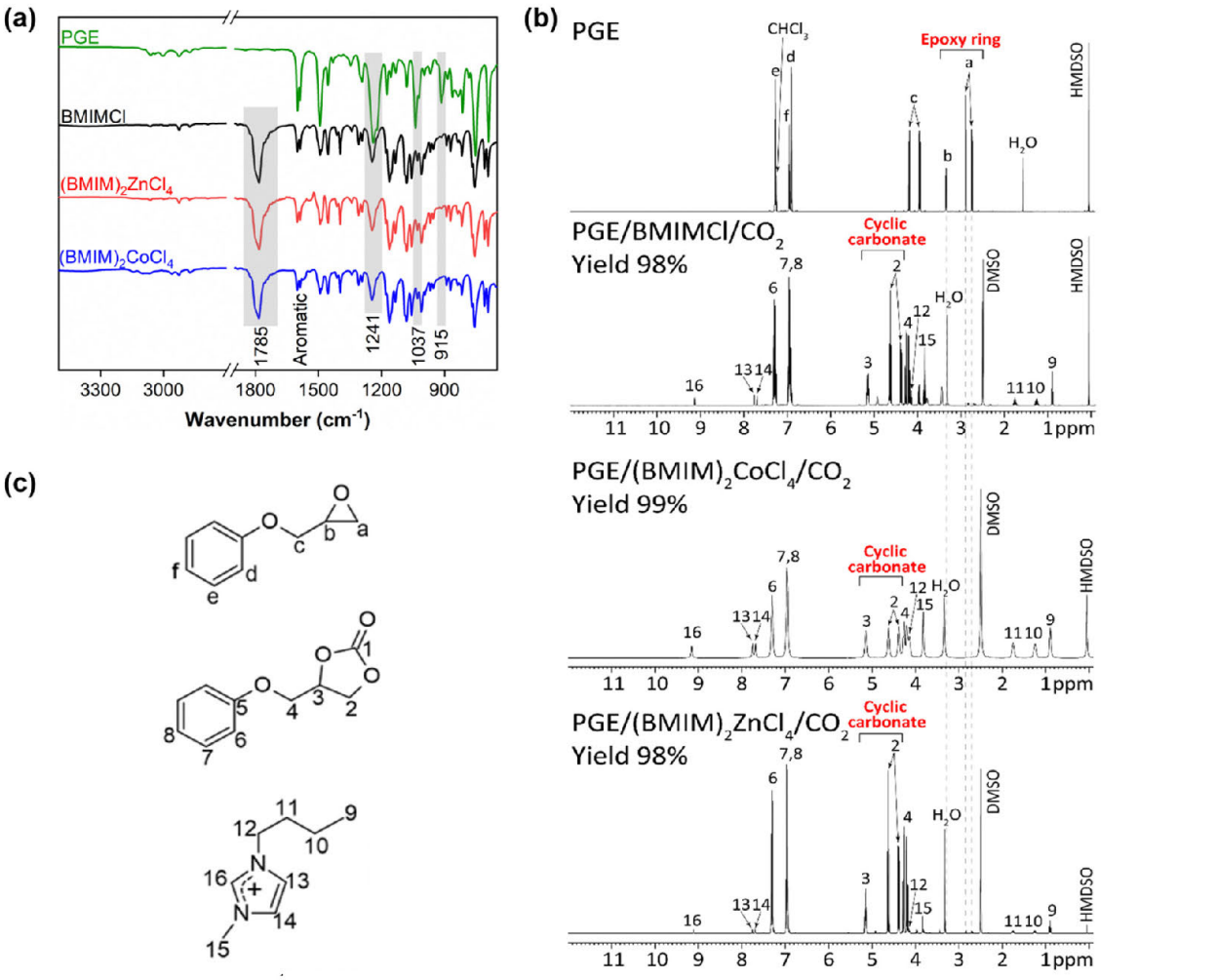

Fig. 2 (a) FTIR and (b) ^{1}H NMR spectra of PGE/CO_2/IL reaction products after 1 h and at 10 mol% of BMIMCl, $(BMIM)_2CoCl_4$, and $(BMIM)_2ZnCl_4$ (c) structures of reactants and products detected in ^{1}H NMR spectra.

similar high cyclic carbonate yields using binary DBU catalytic systems or imidazolium-based ILs.[59,62–65] However, a high temperature ($T \geq 100$ °C)[66–68] and a long reaction time are generally needed.[26,67,69] Meanwhile, our approach does not depend on the conditions mentioned above, yet, we speculate that the high efficiency of the IL obtained could be due to the use of CO_2 pressure. Moreover, in this study, DFT calculations are performed, allowing us to suggest the CO_2 cycloaddition mechanism catalysed by ILs.

To compare the catalytic activity of synthesized MILs with the metal-free BMIMCl, the reactions of PGE/CO_2 mixtures with 10 mol% of $(BMIM)_2ZnCl_4$ and $(BMIM)_2CoCl_4$ were performed by applying the previous conditions (80 °C, 1 h, 7.7 MPa). FTIR and ^{1}H NMR spectroscopy were used to investigate the interactions between the MILs and PGE/CO_2 mixtures (Fig. 2).

The FTIR spectra of reaction products showed a full disappearance of the C–O epoxy band at 915 cm^{-1} suggesting the epoxy ring-opening.[56,57] Additionally, the formation of the C—O band at 1785 cm^{-1} corresponding to the carbonyl of cyclic carbonate was observed (Fig. 2a). Other FTIR bands confirmed the presence of the aromatic backbone of PGE (the bands in the region of 1600 and 1400 cm^{-1})[70] and the C–O ether group of the cyclic carbonate structure (the stretching vibration bands at 1274 and 1037 cm^{-1}).[26]

The full consumption of epoxy rings was also confirmed using the ^{1}H NMR spectroscopy by the disappearance of the respective NMR signals, marked as "*a*" and "*b*" (Fig. 2b and c) at 2.74 ppm, 2.89 ppm and 3.34 ppm. The appearance of new signals "2" and "3" at 4.38 ppm, 4.62 ppm and 5.15 ppm revealed the formation of cyclic carbonates (Fig. 2b and c).[71] Remarkably, the yields of cyclic carbonates obtained from PGE/CO_2 with all ILs were between 98–99% as calculated by ^{1}H NMR, which was further confirmed by FTIR spectroscopy showing similar high yields of the respective cyclic carbonates (93–99%) (Table 1, entries 2–4). A similar result was reported previously by Chen *et al.*, where $(BMIM)_2ZnBr_4$ was used as a catalyst for CO_2 cycloaddition to propylene oxide by obtaining a cyclic carbonate yield of 92.6% after 5 h at room temperature; however, only a yield of 50.5% was obtained when using $(HMIM)_2ZnCl_4$.[72] These results proved the catalytic ability of MILs for the CO_2 cycloaddition. The high catalytic activity of MILs can be explained by their enhanced Lewis acid character due to the presence of an anionic metallic moiety.[73]

Considering the use of PGE as a monomer, the type of the IL's anion (Cl^-, $CoCl_4^{2-}$, $ZnCl_4^{2-}$) exerted little effect on the CO_2 conversion to cyclic carbonates. Conversely, when comparing our results with other studies where metal complexes or organometallic catalysts are used for the CO_2 cycloaddition, such as Zn- and Co-based, we found that our MILs deliver similar if not higher yields of cyclic carbonates, but in a short time frame and under milder reaction conditions.[39,59,74] Moreover, in most of these studies, a combination of a metallic compound, such as dichlorometals or MOFs, and an organic salt in a solvent medium was applied to give cyclic carbonates.[75,76] For example, A. Sibaouih *et al.* used $CoCl_2$ in combination with onium salts and dichloromethane to produce cyclic carbonates from CO_2/propylene oxide reaction at 120 °C.[75] In another study, Yuan *et al.* synthesized and used a Co-based MOF complex for CO_2/epoxy reaction yielding 12.6% of cyclic carbonates when used alone, but 99% after 4 h of reaction, when used with tetrabutylammonium bromide (TBABr).[76]

Computational investigation of the mechanism

To reach a better insight into the mechanism of CO_2 cycloaddition to PGE *via* ILs, a density functional theory (DFT) study was performed on the model reaction PGE/BMIMCl/CO_2. Important points along the proposed reaction path within the potential energy surface, such as any stable intermediate species and transition states, imposing energy barriers for individual reaction steps, were investigated using DFT, microsolvation, and polarizable continuum models (PCM). The analysis of the vibration frequencies calculated for the reacting molecular clusters serves to distinguish unstable entities, exhibiting imaginary vibrational frequencies, corresponding thus to transition states, or stable intermediates, exhibiting only real frequencies.

The computational analysis revealed two transition states that occurred along the fixation of a CO_2 molecule from the initial epoxide to the final cyclic carbonate, along with a stable chlorinated carbonate intermediate (Fig. 3 and Fig. S5, ESI†). The first transition state corresponds to a concurrent opening of the epoxide ring, a nucleophilic attack of the chloride anion on the terminal carbocation, and another attack of the epoxide oxygen on carbon dioxide (TS1 in Fig. 3a). Notably, the chlorinated alcoholate, initially expected to represent another stable intermediate structure along the reaction path, could not be optimized to a minimum on the potential energy surface in the presence of CO_2. All optimization attempts and energy scans of the chlorinated alcoholate immediately converged to the chlorinated carbonate, representing a local minimum on the potential energy surface. Vibrational analysis of the optimized geometry of the alcoholate moiety interacting with CO_2 revealed a single imaginary normal mode, the eigenvectors of which correspond to a scissoring mode of the C–C–O epoxide moiety, approached by the chloride in the nearby presence of CO_2. This confirms the transition state character of the alcoholate moiety in the presence of CO_2. The chlorinated carbonate exhibited only real positive vibrational frequencies, indicating its dynamic stability. Following the torsional mode of its carbonate moiety, an oxygen atom can approach the terminal carbon atom bearing a chlorine substituent. This process can lead to another transition state with a planar arrangement of the terminal CH_2 moiety that is surrounded from up and down, by the chloride and carbonate moieties, respectively. As depicted in Fig. S5 (ESI†), this structure exhibits a single imaginary mode that corresponds to the oscillations of the CH_2 moiety between the respective chlorine and oxygen atoms. This transition state then decays to a cyclic carbonate upon the release of a chloride anion.

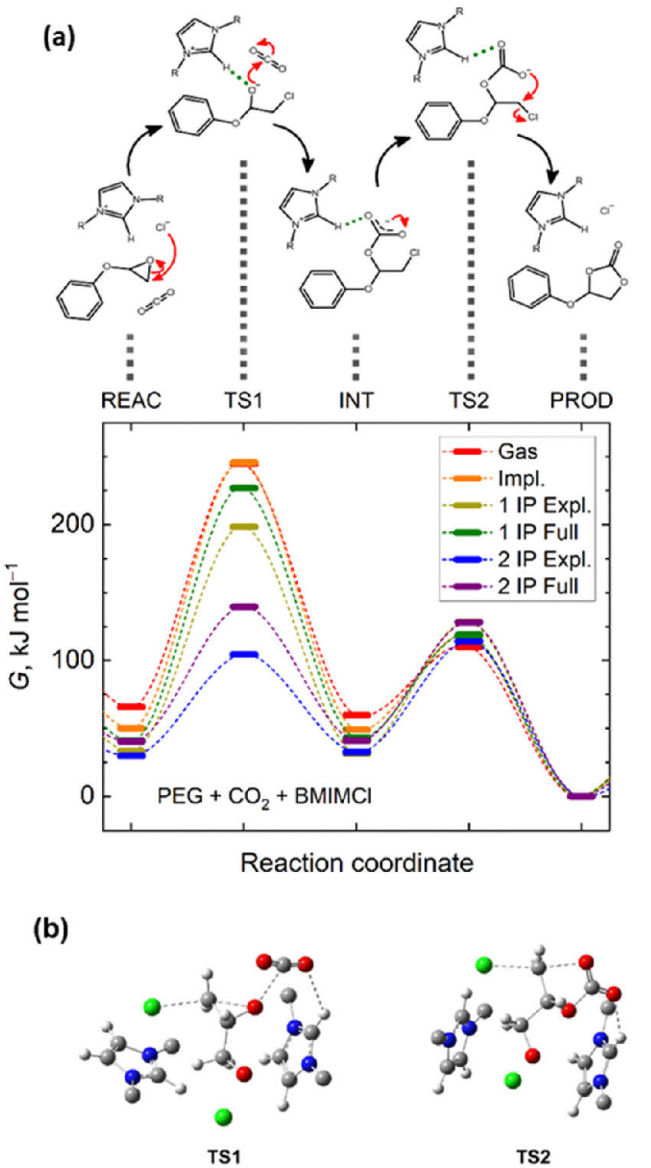

Fig. 3 (a) Important points of the Gibbs energy profiles along the suggested reaction path modelled at the B3LYP-D3/6-311+G(d,p) level of theory. Energies of the reactants (REAC), intermediates (INT), products (PROD), and both transition states (TS) are compared for multiple solvation models: no solvation (Gas); implicit solvation in BMIMCl (Impl.); explicit solvation (Expl.) departing from reactants solvated by either a single ion pair (1 IP) or two ion pairs (2IP); and full solvation as a combination of the implicit and explicit models. Lines tentatively interconnecting Gibbs energies of individual states are only a guide-for-the-eye to illustrate what the whole Gibbs energy profile along the reaction coordinate could look like (the reaction coordinate scale is only schematic). Grey dashed lines relate the Gibbs energy profiles with particular chemical entities while the reaction mechanism among those is marked by black arrows, (b) 3D images of the key molecular fragments representing transition states TS1 and TS2 visualizing the spatial arrangement of the reacting species.

Owing to the polar or ionic nature of the reacting species, solvation effects can severely affect the optimum structures along the reaction path or its energetics. Fig. S6 (ESI†) depicts analogous structures corresponding to the localized minima and maxima along the studied reaction pathway, as shown in Fig. S5 (ESI†), in the explicit presence of a $[BMIM]^+$ cation. Notably, the key molecular contacts of the reactants were not altered upon the inclusion of an explicit cation solvating the reacting species; however, new interactions of the reacting species with the explicit cations stabilize the transition states, leading to a lowering of the energy barriers. Both transition states again exhibited a single imaginary mode, with eigenvectors always corresponding to the desired conversions, as depicted in Fig. S6 (ESI†). Turning on both implicit and explicit solvation models, the first transition state is predicted to exhibit distances of 2.10 Å and 2.60 Å from the terminal carbon atom to the epoxide oxygen and chloride anion, respectively, while the carbon atom of CO_2 is separated from the epoxide oxygen atom by 2.60 Å. For the latter transition state, the key atomic distances amount to 2.39 Å and 2.34 Å for the separation of the terminal carbon atom from the carbonate oxygen atom and chloride, respectively.

Importantly, DFT calculations predicted the existence of a strong hydrogen bond between the –CH– imidazolium bridge and any of the relevant oxygen-anion species. The corresponding O···H distances are of 1.95 Å for the first alcoholate transition state and 2.18 Å for the latter carboxylate transition state. Since halide anions are not particularly active in forming hydrogen bonds with imidazolium cations,[55,77] this observation is crucial for interpreting the mechanism by which the given IL can facilitate the course of this reaction pathway. Hydrogen bonding of the otherwise labile and high-energy transition state geometry to the solvent cation lowers its energy as well as the activation energy barrier for the entire CO_2 fixation pathway.

A comparison of the Gibbs energies of the key states along the reaction path, as well as the results of the individual solvation models, is presented (Fig. 3a). It is obvious that in the gas phase, the primary fixation of CO_2 into a carbonate intermediate is hindered by a substantially larger energy barrier than the mere cyclization of the carbonate intermediate into the cyclic carbonate product. The explicit presence of a single BMIMCl ionic pair stabilizes the first transition state. Nevertheless, the explicit presence of two BMIMCl ionic pairs in the computational model brings a game-changing stabilization of the first transition state. Both the chlorine and epoxide oxygen atoms possess a negative charge but are located on the opposite sides of the epoxide moiety. As such, they can beneficially interact with an individual cation at the respective sides of the reacting PGE molecule. Explicitly two BMIMCl entities lower the first reaction-free energy barrier below 75 kJ mol^{-1}, representing less than a third of the energy barrier for the same process to occur in a vacuum (Table S1, ESI†). Thus, these DFT calculations contribute to proving that the initial epoxide ring opening is the rate-determining step of the overall process in the absence of a catalyst.

Concerning the latter energy barrier, the variation in height observed among the individual models is not significant. In this case, the presence of explicit ions near the carbonate intermediate renders its cyclization more energy-demanding,

as the hydrogen bond of the carbonate to the cation has to be disrupted upon the carbonate torsion that is required for the cyclization. However, since the former barrier is the rate-determining bottleneck, an unfavorable alteration of the latter barrier by ILs is not important.

Interestingly, applying the implicit solvation model mimicking BMIMCl as a polarizable continuum around the reactant molecules and two explicit BMIMCl species led to a 25 kJ mol^{-1} increase in the first energy barrier. This can be understood as an adverse effect of the polar environment, which screens out the otherwise beneficial electrostatic stabilization of the alcoholate transition state. The overall positive impact of BMIMCl on the reaction course can be understood as an interplay between the beneficial interference of the reactants with explicit ions and the somewhat adverse effect of the moderately polar solvent. Current DFT calculations thus suggest that the given CO_2 fixation pathway should be performed in a less polar solvent that is, however, capable of formation of strong hydrogen bonds, stabilizing the key transition states.

While the first barrier is more than two times higher than the second one in the gas phase, concurrent application of the implicit solvation and the explicit presence of BMIMCl brings both energy barriers to a comparable magnitude of approximately 87–99 kJ mol^{-1}, greatly facilitating the reaction to proceed. All the Gibbs energy barriers modelled for the reaction of PGE with CO_2 in BMIMCl are summarized in Table S1 (ESI†).

Concurrent interpretation of our DFT and NMR results, and corroborating with previous reports,[31,36,56,57,78,79] the proposed reaction mechanism steps for the BMIMCl-catalyzed cyclic carbonate formation is herein presented (Fig. 3a). The strong hydrogen bonding between the –CH– imidazolium bridge and the oxygen-anion species (–O···H–, see DFT discussion) enables the nucleophilic attack of the chloride anion on the terminal least hindered carbon of the epoxy ring of the PGE monomer (TS1, in Fig. 3a). Thus, this forms the first chlorinated alcoholate transition state and enables a quick CO_2 fixation resulting in the formation of a stable chloro-carbonate intermediate (INT, in Fig. 3a). Then, the oxygen atom approaches the terminal carbon atom bearing the chlorine substituent, forming the second transition state consisting of the terminal methylene moiety in a planar arrangement surrounded by the chloride and carbonate moieties (TS2, in Fig. 3a). Finally, this transition state decays to a cyclic carbonate upon releasing a chloride anion, as confirmed by ^{1}H NMR analysis (Fig. 2b).

Analogous DFT calculations of the reaction mechanism in MILs could not be performed to the same extent using the PCM model due to the unavailability of properties (mainly the dielectric constant) required by the PCM model for these novel MILs. To compare the potential energy profile of the reaction occurring in various solvents, we created a computational model of the reaction in $(BMIM)_2ZnCl_4$, assuming the explicit presence of a single $(BMIM)_2ZnCl_4$ entity interacting with the reactants, without any implicit solvation model. This analysis revealed that the reaction of PGE with CO_2 in $(BMIM)_2ZnCl_4$ proceeds *via* a mechanism similar to that of BMIMCl. Fig. S7 (ESI†) depicts the geometries of the two transition states and intermediate entities. The first transition state corresponds to the ring-opening of the epoxide and a nucleophilic attack on it by the $[ZnCl_4]^{2-}$ anion, and the other corresponds to a nucleophilic attack by the carbonate oxygen on the terminal PGE carbon atom bearing a chlorine substituent at that time. Interestingly, DFT calculations suggest that the stable intermediate species is a chlorinated carbonate coordinated *via* a chlorine substituent to a nearly planar $[ZnCl_3]^-$ residue.

The comparison of the Gibbs energy profiles for the reaction proceeding in either BMIMCl or $(BMIM)_2ZnCl_4$ suggests that the explicit presence of the latter IL has a beneficial effect on lowering the principal reaction energy barrier (Fig. S8, ESI†). This may be due to the higher flexibility of the first solvation shell around the reacting PGE and CO_2 molecules, enabling additional structural relaxation of the reaction center and thus an improved energetic stabilization of the transition state species. The microscopic explanation for this larger flexibility can be twofold: (i) the larger size of the $[ZnCl_4]^{2-}$ anion compared to Cl^- which contributes to a larger inter-cationic spatial separation, imparting less electrostatic repulsion; and (ii) unlike when using Cl^-, an additional $[ZnCl_3]^-$ anionic entity remains in the solution after the nucleophilic attack by the $[ZnCl_4]^{2-}$ anion, which enables more beneficial configurations in terms of electrostatic interactions. Most likely, these phenomena contributed to the higher catalytic efficiency of MILs for CO_2 fixation. Furthermore, the reaction intermediate predicted to occur in the $(BMIM)_2ZnCl_4$ catalyzed system appears to be significantly destabilized with respect to the mere chloro-carbonate occurring in the case of BMIMCl catalysis, which decreases the activation energy for the second reaction step in turn.

The DFT results and the proposed mechanism correspond well to the other studies showing the key role of the hydrogen bonding of the epoxide oxygen atom when the IL-functionalized MOFs were used for catalysis of the CO_2-epoxide cycloaddition.[80,81] Our calculations show that the IL anions directly participate in the CO_2 fixation process and the cations play a highly important role in terms of supporting the reaction. These computed results agree well with the experimentally observed trend where too low a concentration of the IL hinders the reaction and leads to an incomplete conversion whereas a high enough concentration accelerates the process.

It is worth mentioning that there are two limitations to our computational methodology that are related to our efforts to rationalize the cost and complexity of the current computational model. First, it includes only two explicit ion pairs around the active reaction site to mimic the solvent effects, while the solvated cluster of the reaction center is probably larger in reality. Nevertheless, our models were sufficient to demonstrate the beneficial presence of the hydrogen bonding from the cation near the active reaction site. Sterically, there is only little space for additional IL cations to closely interact with the active reaction site directly. We thus expect the impact of the explicit presence of additional cations on the reaction Gibbs

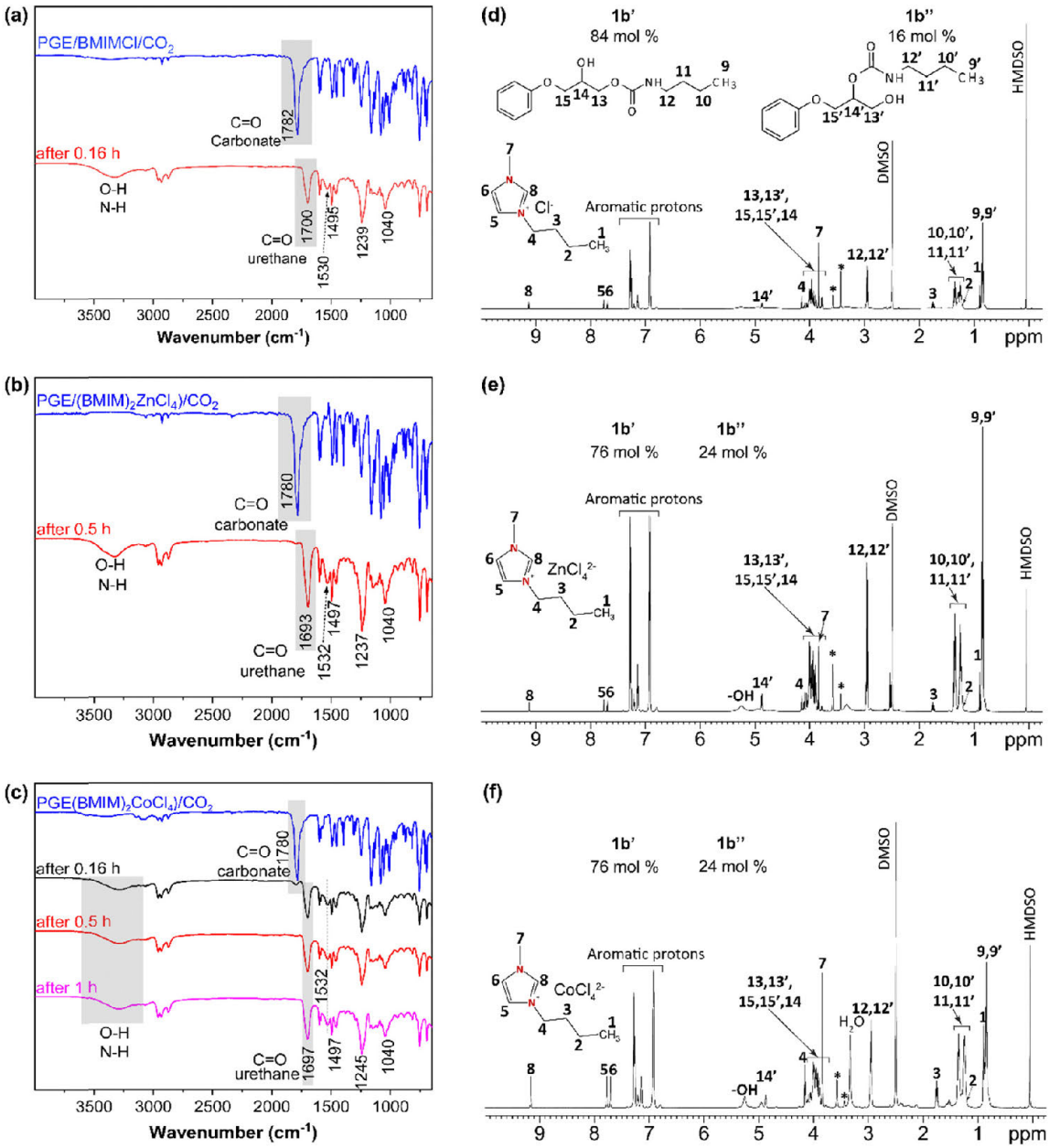

Fig. 4 FTIR spectra of obtained β-hydroxyurethanes *via* reaction of cyclic carbonates from PGE and (a) BMIMCl, (b) $(BMIM)_2ZnCl_4$, (c) $(BMIM)_2CoCl_4$, and NMR spectra of β-hydroxyurethanes isomers (1b′ and 1b″) from PGE cyclic carbonates using (d) BMIMCl, (e) $(BMIM)_2ZnCl_4$, and (f) $(BMIM)_2CoCl_4$. Impurities are denoted by an asterisk (*).

energy profiles to be rather minor. Also, our model relies on a single, presumably the most stable conformation of each significant state along the reaction pathway. These findings are based on the initial simulated annealing procedure and are verified further by additional scans of the potential energy related to conformational variations. Both aspects could be captured in significantly more costly *ab initio* molecular dynamics simulations. Since our aim was a qualitative interpretation of the reaction mechanism and identification of the key states herein, our model proved to be sufficient and other costly simulations remain out of our current scope.

From cyclic carbonates to non-isocyanate urethanes

Conventional PUs represent a market value of 51.2 Billion €, and they are usually processed from a polyol, an isocyanate and a chain extender. The synthesis and use of isocyanates such as methylene diphenyl 4,4′-diisocyanate (MDI) and toluene diisocyanate (TDI) are well-known to be harmful to human health. Therefore, cyclic carbonates are more environmentally friendly alternatives to standard monomers for NIPU production.[82] Among the reported NIPUs, polyhydroxyurethanes (PHUs)

synthesized by ROP of polyfunctional cyclic carbonate monomers with di- or polyamines represent a promising alternative to replace conventional PUs.[83,84] For this reason, as a proof-of-concept for the preparation of potential NIPUs, or a pre-polymer for a NIPU network, the corresponding cyclic carbonates (**1b**) allowed easy mixing with a monofunctional amine at a low reaction temperature (55 °C). Butylamine (BA) was used, as it is a commercially available amine, and in the liquid state at room temperature to study the formation of urethane linkages (Fig. 1). Cyclic carbonates generally present low reactivity to aliphatic amines, and the reaction requires the addition of organic solvents and catalysts.[84–86] However, as observed by FTIR spectra after 0.5 h, the reactions of BA towards the monocyclic carbonate **1b** containing BMIMCl, $(BMIM)_2ZnCl_4$, and $(BMIM)_2CoCl_4$, display a wide band between 3100–3500 cm^{-1} attributed to O–H and N–H stretching vibrations, as result of cyclic carbonates ring opening (Fig. 4a–c).[82,86] The reactions show a rapid opening of cyclic carbonates by aliphatic amine to form β-hydroxyurethanes without the addition of a (co)catalyst or (co)solvent, indicating the universal catalytic abilities of the selected and designed ILs. This is proved by the disappearance of the carbonyl group band from cyclic carbonate at 1780 cm^{-1} with time, proving the reaction between cyclic carbonates and amine groups (Fig. 4a–c). This was further confirmed by the appearance of the new strong band at approximately 1700 cm^{-1} corresponding to the carbonyl of the urethane group.[86,87] The presence of other bands is also indicative of the formation of urethane bonds, such as the bands at 1532, 1245, and 1040 cm^{-1} corresponding to N–H (in the plane bend), C–N (stretch), and C–O (stretch) bonds, respectively.[88,89]

The ^1H NMR analysis has supported these results by showing the urethane groups' formation and complete conversion of cyclic carbonate groups confirmed by the presence of the respective signals corresponding to $-CH_2-$ protons adjacent to –NH–(C—O)– (marked as 12 and 12′, Fig. 4d–f) at around 2.95 ppm and the absence of the NMR signals corresponding to cyclic carbonate at 4.38 ppm, 4.62 ppm and 5.15 ppm.[21,90,91]

Importantly, ^1H NMR spectroscopy allowed the distinction of two formed β-hydroxyurethane isomers: one with a secondary hydroxyl group (denoted as **1b′**, in Scheme 1) and one with a primary hydroxyl group (denoted as **1b″**, in Scheme 1) and calculating their corresponding yields. According to the NMR analysis, the isomer with a secondary hydroxyl constitutes the majority of the product, which is in accordance with previous studies suggesting that the reaction between 5-membered ring cyclic carbonates and amines preferentially gives secondary hydroxyl groups.[92] In the presence of BMIMCl, the obtained isomers **1b′** and **1b″** exhibited yields of 84 and 16%, respectively (Fig. 4d). On the other hand, $(BMIM)_2ZnCl_4$ or $(BMIM)_2CoCl_4$, yielded 76% for the isomer **1b′** and 24% of the isomer **1b″** (Fig. 4e and f). Thus, it seems that the type of ILs initially present in the cyclic carbonate influences the ratio of the formed hydroxyurethane isomers. This impact is probably caused by the high Lewis acidity character[73,93] of MILs and by the coordination effect of MIL anions which further promotes the formation of primary hydroxyl groups (the isomer **1b″**). Previous studies have also reported the influence of catalyst type on the ratio of β-hydroxyurethane isomers.[94–96] In contrast to other studies requiring the addition of specific catalyst promoting cyclic carbonate ring-opening, herein we have shown that MILs may act as dual catalysts for the CO_2 cycloaddition reaction as well as for the aminolysis of cyclic carbonates in bulk (Scheme 1(b)). Due to the catalytic effect of the IL present in cyclic carbonate, the reactivity of BA is increased, and a Lewis acid-activated cyclic carbonate intermediate is formed. The presence of the inductive effect of the substituent (phenyl group) increased the acidity of the negatively charged oxygen and stabilized the transition state.[92] Then, the reaction proceeds by cleavage of the cyclic carbonate ring leading to a deprotonated amine and formation of two types of β-hydroxyurethane isomers, **1b′** (favorable, with secondary hydroxyl group), and **1b″** (less probable, with primary hydroxyl group) (Scheme 1(b)).[92]

Conclusions

In this study, we successfully used a metal-free imidazolium IL (1-butyl-2-methylimidazolium chloride, BMIMCl) and two imidazolium MILs bearing $[ZnCl_4]^{2-}$ and $[CoCl_4]^{2-}$ anions as all-in-one catalysts for two-step conversion of carbon dioxide into β-hydroxyurethanes. For the first step of the supercritical CO_2-epoxy cycloaddition of monofunctional phenyl glycidyl ether (PGE) to cyclic carbonates, the concentration of ILs was optimized (10 mol%) producing the cyclic carbonates with a high yield of ca 98% within 1 h at 80 °C. A feasible mechanism for the CO_2-epoxy cycloaddition catalyzed by ILs was proposed using DFT model calculations. The DFT calculations clearly identified the epoxide ring opening as the rate-determining step and formation of the chlorinated carbonate species as the stable intermediate, which proves the direct participation of the chloride-based anion in the cycloaddition.

In the second step, the formed cyclic carbonates, containing the used ILs as catalysts, exhibited high reactivity towards a monofunctional butylamine. Under solvent-free and co-catalyst-free mild conditions (35 min at 55 °C), the reaction yielded β-hydroxyurethane isomers, with the dominant one bearing the secondary OH groups (76–84%). Moreover, the results further showed that the different structure of the IL-anion affects the formation of individual isomers. Due to the high variability and facile tunability of the IL structure, this effect may be further elaborated for the tailor-made preparation of NIPU networks with variable architecture and properties, which will be the subject of further research studies in the future.

Altogether, the tested ILs can be beneficially considered as promising all-in-one catalysts for CO_2 conversion into NIPUs through cyclic carbonate intermediates. On the other hand, the challenge seems to be the scale-up of the process involving the use of supercritical CO_2, which would allow the transfer of the technology to an industrial scale.

Authors' contributions

Marwa Rebei contributed to the project conceptualization, performed all reaction experiments and characterizations, and wrote the original manuscript. Ctirad Červinka performed the DFT calculations and interpreted the results. Andrii Mahun performed and interpreted the NMR data. Petra Ecorchard and Jan Honzíček synthesized the metal-based ionic liquids and characterized them *via* FTIR and NMR spectroscopy and TGA. Sébastien Livi supervised supercritical CO_2 experiments. Ricardo K. Donato contributed to the conceptualization of the project. Hynek Beneš conceptualized and supervised the project and performed editing of the manuscript.

Conflicts of interest

There are no conflicts to declare.

Acknowledgements

The authors acknowledge the financial support from the Czech Science Foundation (GACR No. 22-05244S). M.R. acknowledges the Grant Agency of Charles University (GAUK No. 413022). Computational resources were provided by the e-INFRA CZ project (ID:90254), supported by the Ministry of Education, Youth and Sports of the Czech Republic. C. Č. acknowledges the support of the project "The Energy Conversion and Storage", funded as project No. CZ.02.01.01/00/22_008/0004617 by Programme Johannes Amos Commenius, call Excellent Research.

References

1 M. Aresta, *Michele Aresta-Carbon Dioxide as Chemical Feedstock*, 2010.
2 A. Ballamine, *Sci. Technol. Energy Transition*, 2022, **1**, 2–6.
3 L. Plasseraud, *ChemSusChem*, 2010, **3**, 631–632.
4 R. Ghanbaralizadeh, H. Bouhendi, K. Kabiri and M. Vafayan, *J. CO2 Util.*, 2016, **16**, 225–235.
5 Y. Qin, X. Sheng, S. Liu, G. Ren, X. Wang and F. Wang, *J. CO2 Util.*, 2015, **11**, 3–9.
6 Y. Li, Y. Y. Zhang, L. F. Hu, X. H. Zhang, B. Y. Du and J. T. Xu, *Prog. Polym. Sci.*, 2018, **82**, 120–157.
7 A. J. Hunt, E. H. K. Sin, R. Marriott and J. H. Clark, *ChemSusChem*, 2010, **3**, 306–322.
8 K. Kiatkittipong, M. A. A. M. Shukri, W. Kiatkittipong, J. W. Lim, P. L. Show, M. K. Lam and S. Assabumrungrat, *Processes*, 2020, **8**, 548.
9 Z. Qin, C. M. Thomas, S. Lee and G. W. Coates, *Angew. Chem., Int. Ed.*, 2003, **42**, 5484–5487.
10 S. D. Thorat, P. J. Phillips, V. Semenov and A. Gakh, *J. Appl. Polym. Sci.*, 2003, **89**, 1163–1176.
11 Q. Liu, L. Wu, R. Jackstell and M. Beller, *Nat. Commun.*, 2015, **6**, 5933.
12 A. Steblyanko, W. Choi, F. Sanda and T. Endo, *J. Polym. Sci., Part A: Polym. Chem.*, 2000, **38**, 2375–2380.
13 T. S. Anderson and C. M. Kozak, *Eur. Polym. J.*, 2019, **120**, 109237.
14 C. Yang, Y. Chen, P. Xu, L. Yang, J. Zhang and J. Sun, *Mol. Catal.*, 2020, **480**, 110637.
15 L. Qin, Y. Li, F. Liang, L. Li, Y. Lan, Z. Li, X. Lu, M. Yang and D. Ma, *Microporous Mesoporous Mater.*, 2022, **341**, 112098.
16 X. Liu, X. Yang, S. Wang, S. Wang, Z. Wang, S. Liu, X. Xu, H. Liu and Z. Song, *ACS Sustainable Chem. Eng.*, 2021, **9**, 4175–4184.
17 G. Beniah, D. J. Fortman, W. H. Heath, W. R. Dichtel and J. M. Torkelson, *Macromolecules*, 2017, **50**, 4425–4434.
18 Z. Karami, K. Kabiri and M. J. Zohuriaan-Mehr, *J. CO2 Util.*, 2019, **34**, 558–567.
19 R. H. Lambeth and T. J. Henderson, *Polymer*, 2013, **54**, 5568–5573.
20 J. Ke, X. Li, S. Jiang, C. Liang, J. Wang, M. Kang, Q. Li and Y. Zhao, *Polym. Int.*, 2019, **68**, 651–660.
21 O. Lamarzelle, P. L. Durand, A. L. Wirotius, G. Chollet, E. Grau and H. Cramail, *Polym. Chem.*, 2016, **7**, 1439–1451.
22 M. Malik and R. Kaur, *Polym. Adv. Technol.*, 2018, **29**, 1078–1085.
23 J. J. Santos, J. H. Lopes, K. M. F. R. De Aguiar, M. B. Simões, J. C. Mpeko, R. G. Jasinevicius, E. T. Cavalheiro, H. Imasato and U. P. Rodrigues-Filho, *J. CO2 Util.*, 2023, **27**, 102303.
24 S. Yue, P. Wang and X. Hao, *Fuel*, 2019, **251**, 233–241.
25 J. Peng, S. Wang, H. J. Yang, B. Ban, Z. Wei, L. Wang and B. Lei, *Fuel*, 2018, **224**, 481–488.
26 X. Yang, Q. Zou, T. Zhao, P. Chen, Z. Liu, F. Liu and Q. Lin, *ACS Sustainable Chem. Eng.*, 2021, **9**, 10437–10443.
27 A. G. Zazybin, K. Rafikova, V. Yu, D. Zolotareva, V. M. Dembitsky and T. Sasaki, *Russ. Chem. Rev.*, 2017, **86**, 1254–1270.
28 T. Wang, C. Shen, G. Yu and X. Chen, *Polym. Degrad. Stab.*, 2021, **194**, 109751.
29 I. A. Berezianko, I. V. Vasilenko and S. V. Kostjuk, *Eur. Polym. J.*, 2019, **121**, 109307.
30 A. Bouyahya, S. Balieu, R. Beniazza, M. Raihane, A. El Kadib, D. Le Cerf, P. Thébault, G. Gouhier and M. Lahcini, *New J. Chem.*, 2019, **43**, 5872–5878.
31 R. R. Henriques, C. P. De Oliveira, R. Stein, K. Pontes, A. A. Silva and B. G. Soares, *ACS Appl. Polym. Mater.*, 2022, **4**, 1207–1217.
32 D. Liu, G. Li and H. Liu, *Appl. Surf. Sci.*, 2018, **428**, 218–225.
33 J. Liang, Y. Q. Xie, Q. Wu, X. Y. Wang, T. T. Liu, H. F. Li, Y. B. Huang and R. Cao, *Inorg. Chem.*, 2018, **57**, 2584–2593.
34 M. Ding and H. L. Jiang, *ACS Catal.*, 2018, **8**, 3194–3201.
35 J. Liang, Y. Q. Xie, X. S. Wang, Q. Wang, T. T. Liu, Y. B. Huang and R. Cao, *Chem. Commun.*, 2018, **54**, 342–345.
36 M. Rebei, A. Mahun, Z. Walterová, O. Trhlíková, R. K. Donato and H. Beneš, *Polym. Chem.*, 2022, **13**, 5380–5388.
37 G. P. Wu, D. J. Darensbourg and X. B. Lu, *J. Am. Chem. Soc.*, 2012, **134**, 17739–17745.
38 D. J. Darensbourg, *J. Chem. Educ.*, 2017, **94**, 1691–1695.
39 X. Wu, C. Chen, Z. Guo, M. North and A. C. Whitwood, *ACS Catal.*, 2019, **9**, 1895–1906.

40 N. A. Noorhisham, D. Amri, A. H. Mohamed, N. Yahaya, N. M. Ahmad, S. Mohamad, S. Kamaruzaman and H. Osman, *J. Mol. Liq.*, 2021, **326**, 115340.
41 C. Červinka, M. Klajmon and V. Štejfa, *J. Chem. Theory Comput.*, 2019, **15**, 5563–5578.
42 A. P. Thompson, H. M. Aktulga, R. Berger, D. S. Bolintineanu, W. M. Brown, P. S. Crozier, P. J. in't Veld, A. Kohlmeyer, S. G. Moore, T. D. Nguyen, R. Shan, M. J. Stevens, J. Tranchida, C. Trott and S. J. Plimpton, *Comput. Phys. Commun.*, 2022, **271**, 108171.
43 J. N. Canongia Lopes and A. A. H. Pádua, *Theor. Chem. Acc.*, 2012, **131**, 1–11.
44 R. T. Cygan, V. N. Romanov and E. M. Myshakin, *J. Phys. Chem. C*, 2012, **116**, 13079–13091.
45 L. S. Dodda, I. C. De Vaca, J. Tirado-Rives and W. L. Jorgensen, *Nucleic Acids Res.*, 2017, **45**, W331–W336.
46 W. L. Jorgensen and J. Tirado-Rives, *Proc. Natl. Acad. Sci. U. S. A.*, 2005, **102**, 6665–6670.
47 L. S. Dodda, J. Z. Vilseck, J. Tirado-Rives and W. L. Jorgensen, *J. Phys. Chem. B*, 2017, **121**, 3864–3870.
48 M. J. Frisch, G. W. Trucks, H. B. Schlegel *et al.*, *Gaussian 16, Revision C. 01*, Gaussian, Inc., Wallingford CT, 2016.
49 A. D. Becke, *J. Chem. Phys.*, 1992, **96**, 2155–2160.
50 L. G. Stefan Grimme and S. Ehrlich, *J. Comput. Chem.*, 2011, **32**, 1456–1465.
51 C. Peng, P. Y. Ayala, H. B. Schlegel and M. J. Frisch, *J. Comput. Chem.*, 1996, **17**, 49–56.
52 C. Červinka, M. Fulem and K. Růžička, *J. Chem. Eng. Data*, 2012, **57**, 227–232.
53 J. Tomasi, B. Mennucci and R. Cammi, *Chem. Rev.*, 2005, **105**, 2999–3093.
54 E. L. Bennett, C. Song, Y. Huang and J. Xiao, *J. Mol. Liq.*, 2019, **294**, 111571.
55 M. M. Huang, Y. Jiang, P. Sasisanker, G. W. Driver and H. Weingärtner, *J. Chem. Eng. Data*, 2011, **56**, 1494–1499.
56 M. Součková, J. Klomfar and J. Pátek, *Fluid Phase Equilib.*, 2017, **454**, 43–56.
57 T. K. L. Nguyen, S. Livi, B. G. Soares, S. Pruvost, J. Duchet-Rumeau and J. F. Gérard, *ACS Sustainable Chem. Eng.*, 2016, **4**, 481–490.
58 T. K. L. Nguyen, S. Livi, S. Pruvost, B. G. Soares and J. Duchet-Rumeau, *J. Polym. Sci., Part A: Polym. Chem.*, 2014, **52**, 3463–3471.
59 J. Byun and K. A. I. Zhang, *ChemCatChem*, 2018, **10**, 4610–4616.
60 K. Błażek, H. Beneš, Z. Walterová, S. Abbrent, A. Eceiza, T. Calvo-Correas and J. Datta, *Polym. Chem.*, 2021, **12**, 1643–1652.
61 A. Ghosh, G. N. Reddy, M. Siddhique, P. K. S. Chatterjee, S. Bhattacharjee, R. Maitra, S. E. Lyubimov, A. V. Arzumanyan, A. Naumkin, A. Bhaumik and B. Chowdhury, *Green Chem.*, 2022, **24**, 1673–1692.
62 C. Pronoitis, M. Hakkarainen and K. Odelius, *ACS Sustainable Chem. Eng.*, 2022, **10**, 2522–2531.
63 E. I. Privalova, E. Karjalainen, M. Nurmi, P. Mäki-Arvela, K. Eränen, H. Tenhu, D. Y. Murzin and J. P. Mikkola, *ChemSusChem*, 2013, **6**, 1500–1509.
64 J. Avila, L. F. Lepre, C. C. Santini, M. Tiano, S. Denis-Quanquin, K. Chung Szeto, A. A. H. Padua and M. Costa Gomes, *Angew. Chem., Int. Ed.*, 2021, **60**, 12876–12882.
65 Y. Li, B. Dominelli, R. M. Reich, B. Liu and F. E. Kühn, *Catal. Commun.*, 2019, **124**, 118–122.
66 Z. Zhang, F. Fan, H. Xing, Q. Yang, Z. Bao and Q. Ren, Innovations of Green Process Engineering for Sustainable Energy Environment, 2017 - Top. Conf. 2017 AIChE Annu. Meet., 2017, 24–29.
67 A. Comès, R. Poncelet, P. P. Pescarmona and C. Aprile, *J. CO2 Util.*, 2021, **48**, 101529.
68 W. de Almeida, J. L. S. Milani, C. H. de J. Franco, F. T. Martins, A. de Fatima, A. F. A. da Mata and R. P. das Chagas, *Mol. Catal.*, 2022, **530**, 112632.
69 M. H. Anthofer, M. E. Wilhelm, M. Cokoja, M. Drees, W. A. Herrmann and F. E. Kühn, *ChemCatChem*, 2015, **7**, 94–98.
70 B. C. Smith, *Spectroscopy*, 2016, **31**, 34–37.
71 A. J. Kamphuis, F. Picchioni and P. P. Pescarmona, *Green Chem.*, 2019, **21**, 406–448.
72 G. Chen, J. Zhang, X. Cheng, X. Tan, J. Shi, D. Tan, B. Zhang, Q. Wan, F. Zhang, L. Liu, B. Han and G. Yang, *ChemCatChem*, 2020, **12**, 1963–1967.
73 J. Estager, J. D. Holbrey and M. Swadźba-Kwaśny, *Chem. Soc. Rev.*, 2014, **43**, 847–886.
74 A. L. Girard, N. Simon, M. Zanatta, S. Marmitt, P. Gonçalves and J. Dupont, *Green Chem.*, 2014, **16**, 2815–2825.
75 A. Sibaouih, P. Ryan, M. Leskelä, B. Rieger and T. Repo, *Appl. Catal. A Gen.*, 2009, **365**, 194–198.
76 R. Yuan and H. He, *Inorg. Chem. Commun.*, 2020, **121**, 108235.
77 C. Červinka and V. Štejfa, *Phys. Chem. Chem. Phys.*, 2021, **23**, 4951–4962.
78 F. D. Bobbink, W. Gruszka, M. Hulla, S. Das and P. J. Dyson, *Chem. Commun.*, 2016, **52**, 10787–10790.
79 F. Siragusa, E. Van Den Broeck, C. Ocando, A. J. Muller, G. De Smet, B. U. W. Maes, J. De Winter, V. Van Speybroeck, B. Grignard and C. Detrembleur, *ACS Sustainable Chem. Eng.*, 2021, **9**, 1714–1728.
80 L. J. Zhou, W. Sun, N. N. Yang, P. Li, T. Gong, W. J. Sun, Q. Sui and E. Q. Gao, *ChemSusChem*, 2019, **12**, 2202–2210.
81 S. M. Masoom Nataj, S. Kaliaguine and F. G. Fontaine, *ChemCatChem*, 2023, **15**, e202300079.
82 J. Ke, X. Li, F. Wang, M. Kang, Y. Feng, Y. Zhao and J. Wang, *J. CO_2 Util.*, 2016, **16**, 474–485.
83 F. Camara, S. Benyahya, V. Besse, G. Boutevin, R. Auvergne, B. Boutevin and S. Caillol, *Eur. Polym. J.*, 2014, **55**, 17–26.
84 A. Gomez-Lopez, F. Elizalde, I. Calvo and H. Sardon, *Chem. Commun.*, 2021, **57**, 12254–12265.
85 X. Sheng, Y. Wang, Y. Qin, X. Wang and F. Wang, *RSC Adv.*, 2014, **4**, 54043–54050.
86 C. Carré, H. Zoccheddu, S. Delalande, P. Pichon and L. Avérous, *Eur. Polym. J.*, 2016, **84**, 759–769.
87 A. Gomez-Lopez, B. Grignard, I. Calvo, C. Detrembleur and H. Sardon, *ACS Appl. Polym. Mater.*, 2020, **2**, 1839–1847.
88 Brian C. Smith, *Spectroscopy*, 2023, **38**, 14–16.

89 Brian C. Smith, *Spectroscopy*, 2023, **38**, 14–18.
90 A. Cornille, M. Blain, R. Auvergne, B. Andrioletti, B. Boutevin and S. Caillol, *Polym. Chem.*, 2017, **8**, 592–604.
91 T. Quérette, E. Fleury and N. Sintes-Zydowicz, *Eur. Polym. J.*, 2019, **114**, 434–445.
92 L. Maisonneuve, O. Lamarzelle, E. Rix, E. Grau and H. Cramail, *Chem. Rev.*, 2015, **115**, 12407–12439.
93 W. Wu, Y. Lu, H. Ding, C. Peng and H. Liu, *Phys. Chem. Chem. Phys.*, 2015, **17**, 1339–1346.
94 C. D. Diakoumakos and D. L. Kotzev, *Macromol. Symp.*, 2004, **216**, 37–46.
95 S. Benyahya, M. Desroches, R. Auvergne, S. Carlotti, S. Caillol and B. Boutevin, *Polym. Chem.*, 2011, **2**, 2661–2667.
96 B. Ochiai, S. Inoue and T. Endo, *J. Polym. Sci., Part A: Polym. Chem.*, 2005, **43**, 6613–6618.

Supporting information

Fast carbon dioxide–epoxide cycloaddition catalyzed by metal and metal-free ionic liquids for designing non-isocyanate polyurethanes

Marwa Rebei,[a,b] Ctirad Červinka,[c] Andrii Mahun,[a,b] Petra Ecorchard,[d] Jan Honzíček,[e] Sébastien Livi,[f] Ricardo K. Donato,[g] Hynek Beneš[a,*]

[a] *Institute of Macromolecular Chemistry of the Czech Academy of Sciences, Heyrovského nám.2, Prague 6, 162 00, Czech Republic*

[b] *Department of Physical and Macromolecular Chemistry, Faculty of Science, Charles University, Hlavova 8, 12843 Prague, Czech Republic*

[c] *Department of Physical Chemistry, University of Chemistry and Technology Prague Technická 5, CZ-166 28 Prague 6, Czech Republic*

[d] *Institute of Inorganic Chemistry of the Czech Academy of Sciences, Husinec-Řež 1001, 250 68 Řež, Czech Republic*

[e] *Institute of Chemistry and Technology of Macromolecular Materials, Faculty of Chemical Technology, University of Pardubice, Studentská 573, 532 10, Pardubice, Czech Republic*

[f] *Université de Lyon, CNRS, Université Claude Bernard Lyon 1, INSA Lyon, Université Jean Monnet, UMR 5223, Ingénierie des Matériaux Polymères, F-69621 Cédex, France*

[g] *National University of Singapore, Center for Advanced 2D Materials, Singapore 117546, Singapore*

E-mail: benesh@imc.cas.cz

Metal-based ionic liquids (MILs)

Firstly, the synthesized MILs, $(BMIM)_2ZnCl_4$ and $(BMIM)_2CoCl_4$, were characterized to prove the IL structure. The ^1H and ^{13}C NMR spectra of $(BMIM)_2ZnCl_4$ are shown in Fig. S1 and S2 and compared to BMIMCl.

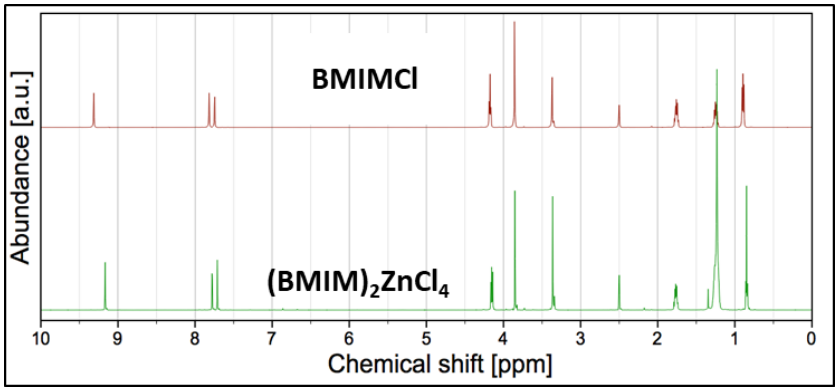

Fig. S1. ^1H NMR (DMSO-D6) of BMIMCl and $(BMIM)_2ZnCl_4$. BMIMCl: δ 0.893 (t, H_3C-) 1.247 (m, -CH_2-CH_3) 1.758 (p, -CH_2-CH_2-CH_3) 3.371 (s, H_2O) 3.856 (s, H_3C-N) 4.174 (t, -CH_2-CH_2- CH_2-CH_3) 7.746 (s, H_2C=CH_2-N-R) 7.817 (s, H_2C=CH_2-N-CH_3) 9.314 (s, N-C*H*-N). $(BMIM)_2ZnCl_4$: δ 0.848 (t, H_3C-) 1.232 (m, -CH_2-CH_3) 1.776 (p, -CH_2-CH_2-CH_3) 3.363 (s, H_2O) 3.851 (s, H_3C-N) 4.152 (t, -CH_2-CH_2- CH_2-CH_3) 7.711 (s, H_2C=CH_2-N-R) 7.779 (s, H_2C=CH_2-N-CH_3) 9.314 (s, N-C*H*-N).

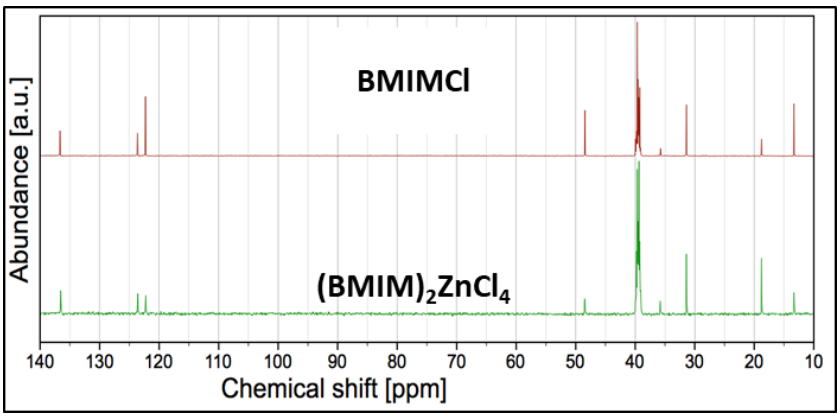

Fig. S2. ^{13}C NMR (DMSO-D6): of BMIMCl and $(BMIM)_2ZnCl_4$. BMIMCl: δ 13.321 (1C, -*C*H_3) 18.793 (1C, -*C*H_2-CH_3) 31.391 (1C, -*C*H_2- CH_2-CH_3) 35.748 (1C, H_3C-N) 48.446 (1C, *C*H_2-CH_2- CH_2-CH_3) 122.287 (1C, H_2C=*C*H_2-N-R) 123.621 (1C, H_2C=*C*H_2-N-CH_3) 136.642 (1C, N-*C*H-N). $(BMIM)_2ZnCl_4$: δ 13.321 (1C, -*C*H_3) 18.793 (1C, -*C*H_2-CH_3) 31.401 (1C, -*C*H_2-CH_2-CH_3) 35.827 (1C, H_3C-N) 48.501 (1C, *C*H_2-CH_2- CH_2-CH_3) 122.269 (1C, H_2C=*C*H_2-N-R) 123.615 (1C, H_2C=*C*H_2-N-CH_3) 136.530 (1C, N-*C*H-N).

The ^{1}H NMR spectra proved the formation of a typical imidazolium ring in $(BMIM)_2ZnCl_4$ by the presence of signals at δ =3.85 (s, H_3C-N), 7.71 (s, H_2C=CH_2-N-R), and 9.166 (s, N-C*H*-N).[1] The metal contents (%) in $(BMIM)_2ZnCl_4$ and $(BMIM)_2CoCl_4$ were calculated using elemental analysis (AAS). The results showed that the experimental metal content values Zn (11.04%) and Co (12.74%) are very close to the theoretical values, 11.03 and 12.30 %, respectively [2,3], suggesting the effective insertion of the metal centre (Zn and Co) in the imidazolium IL. When comparing FTIR spectra and thermogravimetric analyses (TGA) of BMIMCl with $(BMIM)_2CoCl_4$, and $(BMIM)_2ZnCl_4$, the MILs showed a low level of absorbed water (approximately 1 wt%) (Fig. S3).

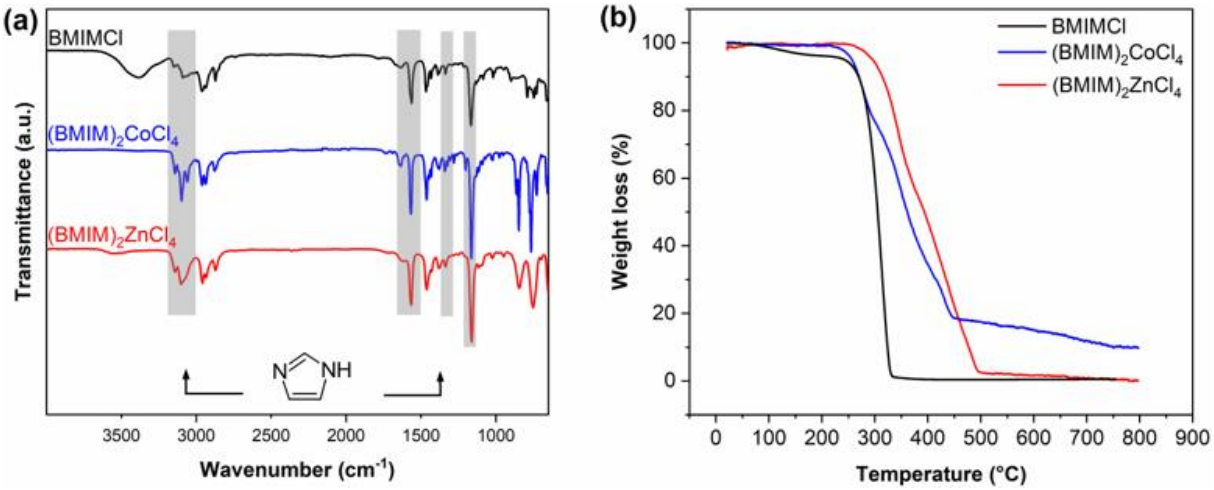

Fig. S3. (a) FTIR spectra and (b) TGA curves of BMIMCl, $(BMIM)_2CoCl_4$ and $(BMIM)_2ZnCl_4$.

FTIR spectra of $(BMIM)_2CoCl_4$, and $(BMIM)_2ZnCl_4$ exhibited typical characteristic bands from the imidazolium ring proved by the presence of bands at 3090 - 3142, 1563 - 1640, and 1163 cm^{-1}, respectively attributed to the alkyl stretching in imidazole ring (C-H), imidazole ring stretching, and bending of H-C-C and H-C-N bonds (Fig. S3a).[4,5] The formation of aliphatic (C-H) alkyl chains were also confirmed by the peaks at 2690, 2877, and 2933 cm^{-1}.[5] Thermograms of $(BMIM)_2CoCl_4$ and $(BMIM)_2ZnCl_4$ showed four decomposition steps, unlike BMIMCl which showed only two steps (Fig. S3b). This proves the presence of the inorganic material, anionic metal centre into the IL, which starts decomposing at the final stage of the TGA analysis at temperature after 430 to 547 °C. Moreover, these MILs showed to be thermally stable at *T* lower than 100 °C, as the first decomposition step starts at onset *T* of approximately 240 °C, which means that the metal salts do not decompose at the reaction temperature selected in this study (80 °C), and their catalytic activity will not be compromised. The high thermal

stability of the compound is also due to the imidazolium cation that proved to be more thermally and chemically stable than other cations of ILs, such as pyridinium, or phosphonium salts.[6] The addition of the metal anionic centre was proved to enhance the Lewis acidity of the ionic liquid, hence increasing its nucleophilic character and therefore catalytic activity.[7] These properties provided by the MILs offer the opportunity to use them as new catalytic tools for the CO_2 cycloaddition reaction.

Synthesis of cyclic carbonates

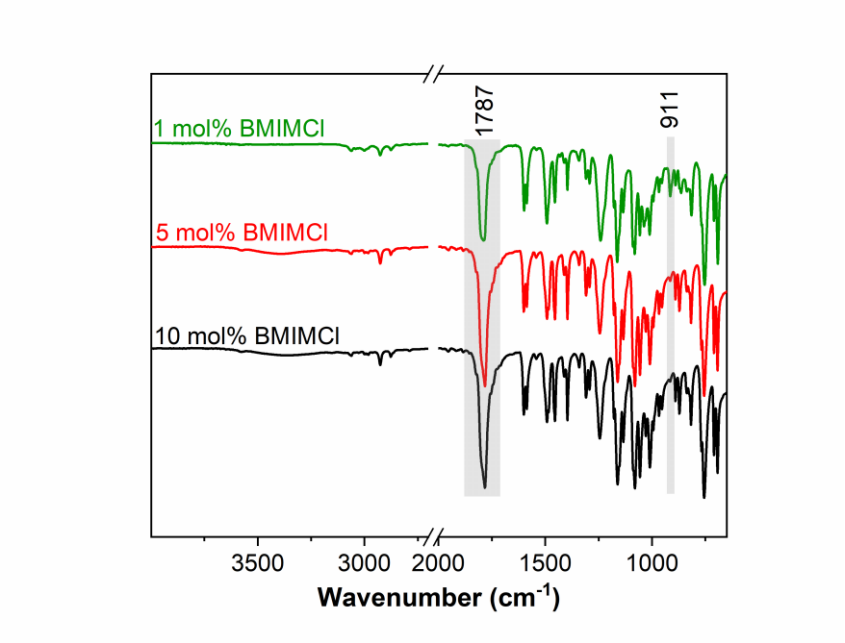

Fig. S4. FTIR spectra of PGE/CO_2/BMIMCl reaction products at different concentrations of IL (1, 5 and 10 mol%), and at reaction conditions (T=80 °C, P(CO_2)=7.7 MPa).

Computational investigation of the mechanism

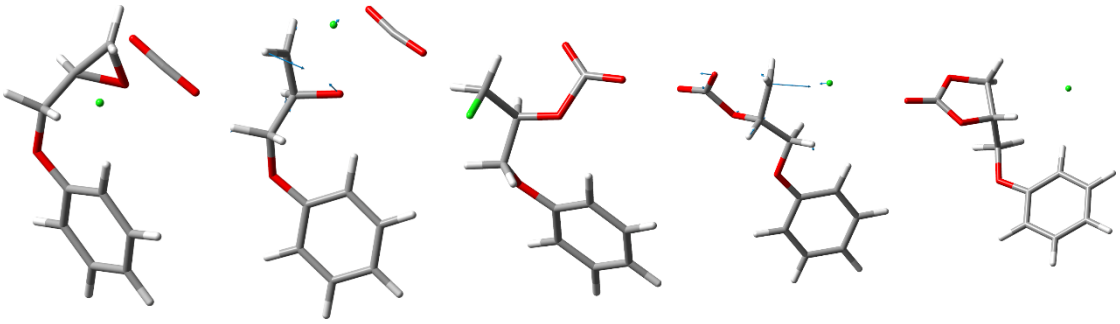

Fig. S5. Geometries of the important points along the overall reaction mechanism in the minimum representation departing from a 1:1 mixture of reactants catalyzed by a chloride anion. From left to right: reactants in an optimum mutual configuration, transition state for CO_2 fixation, chloro-carbonate intermediate, transition state for carbonate cyclisation, and cyclic carbonate product. Eigenvectors of the single internal mode exhibiting an imaginary vibrational frequency are depicted for both transition states.

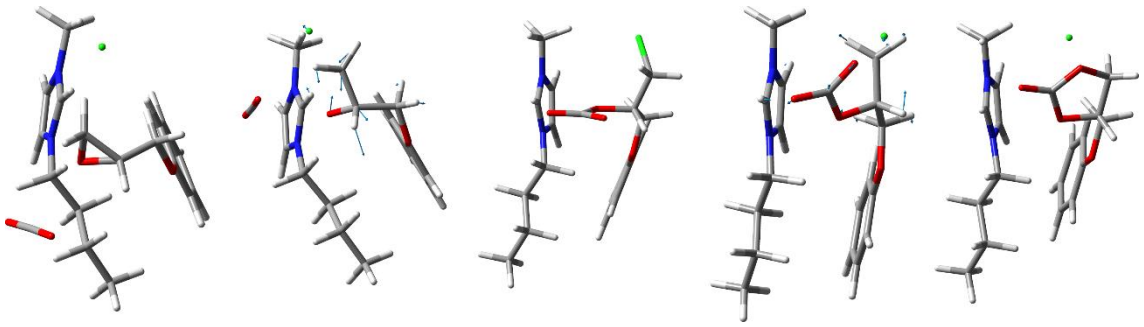

Fig. S6. Geometries of the important points along the overall reaction mechanism in the explicitly solvated representation including one whole BMIMCl ion pair in excess to the 1:1 mixture of reactants. From left to right: reactants in an optimum mutual configuration, transition state for CO_2 fixation, chloro-carbonate intermediate, transition state for carbonate cyclisation, and cyclic carbonate product. Eigenvectors of the single internal mode exhibiting an imaginary vibrational frequency are depicted for both transition states.

Table S1. Relative Gibbs energies (at 298 K, in kJ mol^{-1}) of important entities along the reaction of PGE with CO_2 in BMIMCl, as obtained from B3LYP-D3(BJ)/6-311+G(d,p) level of theory and for various solvation models of implicit (PCM), explicit (including 1 or 2 ionic pairs), and full (combining implicit and explicit) solvation. Explicit solvent particles are noted in brackets.

Solvation model	REAC	TS1	INT	TS2	PROD	BAR1	BAR2
Vacuum (1 Cl^-)	66.0	244.8	60.1	110.0	0.0	178.8	49.9
PCM (1 Cl^-)	50.1	245.7	49.1	118.2	0.0	195.6	69.1
Vacuum (1 $BMIM^+$ & 1 Cl^-)	33.4	198.5	31.6	128.4	0.0	165.2	96.8
PCM (1 $BMIM^+$ & 1 Cl^-)	40.9	226.7	43.0	118.9	0.0	185.9	76.0
Vacuum (2 $BMIM^+$ & 2 Cl^-)	29.9	104.6	32.5	114.1	0.0	74.7	81.5
PCM (2 $BMIM^+$ & 2 Cl^-)	40.5	139.5	40.9	128.1	0.0	99.0	87.2

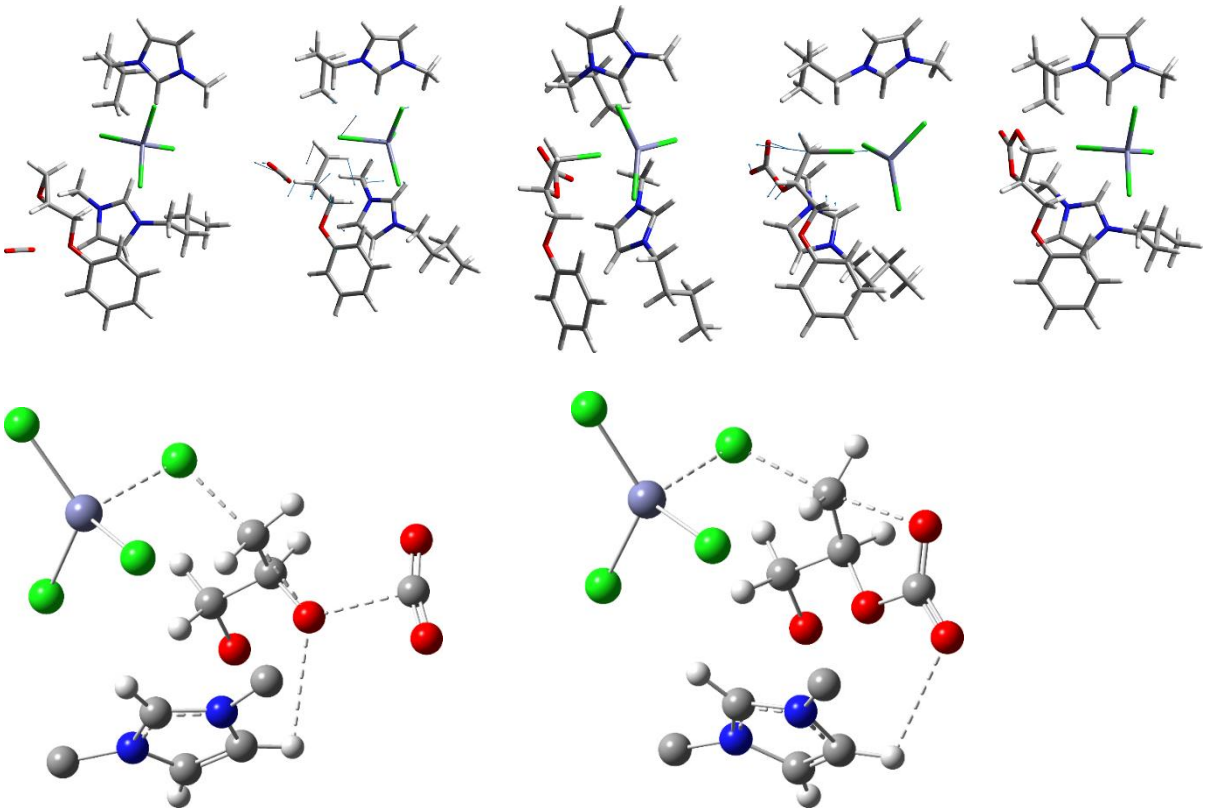

Fig. S7. Geometries of the important points along the overall reaction mechanism in the explicitly solvated representation including one explicit $(BMIM)_2ZnCl_4$ entity in excess of the 1:1 mixture of reactants. First row, from left to right: reactants in an optimum mutual configuration, transition state for CO_2 fixation, chloro-carbonate intermediate, transition state for carbonate cyclisation, and cyclic carbonate product. Eigenvectors of the single internal mode exhibiting an imaginary vibrational frequency are depicted for both transition states. Second row: a detailed view of the most important fragments of the reacting species representing TS1 and TS2 clusters.

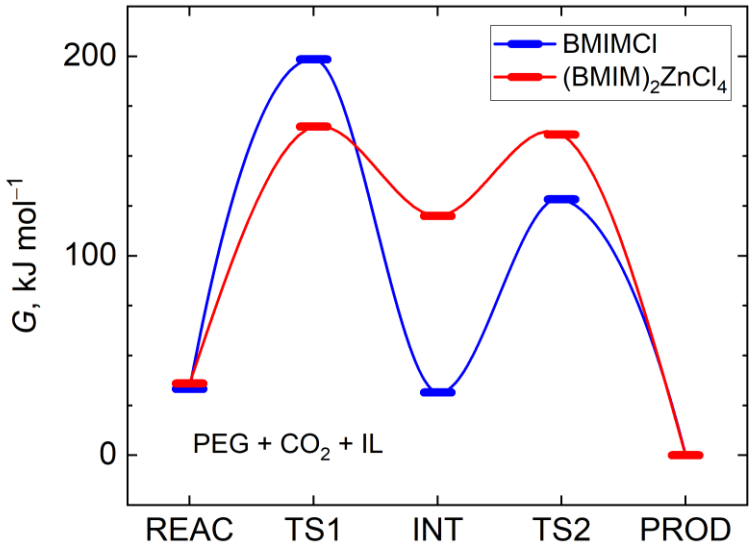

Fig. S8. Gibbs energy profiles along the suggested reaction paths as modelled at the B3LYP-D3/6-311+G(d,p) level of theory. Energies of the reactants, intermediate entities, products, and transition states are compared for the reactions occurring in a vacuum in the explicit presence of a single stoichiometric entity of BMIMCl or $(BMIM)_2ZnCl_4$. Lines interconnecting individual states are only for guide-the-eye.

References

1 H. S. Kim, J. J. Kim, H. Kim and H. G. Jang, *J. Catal.*, 2003, **220**, 44–46.

2 J. Palgunadi, O. S. Kwon, H. Lee, J. Y. Bae, B. S. Ahn, N. Y. Min and H. S. Kim, *Catal. Today*, 2004, **98**, 511–514.

3 C. Zhong, T. Sasaki, A. Jimbo-Kobayeshi, E. Fujiwara, A. Kobayashi, M. Tada and Y. Iwasawa, *Bull. Chem. Soc. Jpn.*, 2007, **80**, 2365–2374.

4 D. Liu, G. Li and H. Liu, *Appl. Surf. Sci.*, 2018, **428**, 218–225.

5 T. Rajkumar and G. Ranga Rao, *Mater. Chem. Phys.*, 2008, **112**, 853–857.

6 P. Migowski, P. Lozano and J. Dupont, *Green Chem.*, 2023, 1237–1260.

7 J. Estager, J. D. Holbrey and M. Swadźba-Kwaśny, *Chem. Soc. Rev.*, 2014, **43**, 847–886.